REPORT DOCUMENTATION PAGE

Public reporting burden for this collection of information is estimated to average 1 hour per response, including the time for reviewing instructions, searching existing data sources, gathering and maintaining the data needed, and completing and reviewing the collection of information. Send comments regarding this burden estimate or any other aspect of this collection of information, including suggestions for reducing this burden to Washington Headquarters Services, Directorate for Information Operations and Reports, 1215 Jefferson Davis Highway, Suite 1204, Arlington, VA 22202-4302, and to the Office of Management and Budget, Paperwork Reduction Project (0704-0188), Washington, DC 20503

1. AGENCY USE ONLY (Leave Blank)	2. REPORT DATE Dec. 1, 1996	3. REPORT TYPE AND DATES COVERED Progress Report: Aug. 1, 1995 – July 31, 1996

4. TITLE AND SUBTITLE
Mechanics of Wide-Spread Fatigue Damage
and Life-Enhancement Methodologies

5. FUNDING NUMBERS
F49620-93-1-0345

6. AUTHOR(S)
Dr. S. N. Atluri

AFOSR-TR-97
0096

7. PERFORMING ORGANIZATION NAME(S) AND ADDRESS(ES)

Computational Mechanics Center
Georgia Institute of Technology
Atlanta GA 30332-0356

9. SPONSORING/MONITORING AGENCY NAME(S) AND ADDRESS(ES)

Air Force Office of Scientific Research
110 Duncan Ave., Suite B115
Bolling Air Force Base DC 20332

N/A

10. SPONSORING/MONITORING AGENCY REPORT NUMBER
93-1-0345

11. SUPPLEMENTARY NOTES COR:

12a. DISTRIBUTION/AVAILABILITY STATEMENT
No restrictions

12b. DISTRIBUTION CODE

13. ABSTRACT (Maximum 200 words)

DTIC QUALITY INSPECTED 2

This project emphasizes the development and evaluation of analytic methods for the solution of fracture mechanics problems as related to aircraft structures. Some of these methods are: finite and boundary element methods, singular/hybrid finite elements, alternating method, and path-independent and domain-independent integrals. When these methods are applied to various cases of aircraft structural problems, predictions of crack growth and fatigue life can be made. The final report describes these analytical methods as applied to various cases of aircraft structural problems, including the evaluation of composite patch repairs to existing cracks.

14. SUBJECT TERMS Fracture Mechanics; Finite Element Methods; Fatigue of Metal

15. NUMBER OF PAGES
175

16. PRICE CODE

17. SECURITY CLASSIFICATION OF REPORT	18. SECURITY CLASSIFICATION OF THIS PAGE	19. SECURITY CLASSIFICATION OF ABSTRACT	20. LIMITATION OF ABSTRACT
Unclassified	Unclassified	Unclassified	Unlimited: UL

NSN 7540-01-280-5500

Standard Form 298 (Rev 2-89)
Prescribed by ANSI Std 239-18 298-102

Final Technical Report

United States Air Force Contract F49620-93-1-0345

Computational Mechanics Center
Georgia Institute of Technology
Project Numbers B-15-F47/E-15-632

Title: AASERT-Structural Integrity of Aging of Aerospace
Structures and Repairs

By: S. N. Atluri, Principal Investigator

November 19, 1996

Final Report
USAF Contract F49620-93-1-0345
AASERT-Structural Integrity of Aging of Aerospace Structures and Repairs

I. Introduction

In 1993, the US Department of Defense announced the FY94 competition for the Augmentation Awards for Science and Engineering Research Training program. In order to be eligible for one of these awards, a faculty investigator must have had an existing DOD-funded research grant or contract. In the case of this particular award, the linked DOD-funded research grant was USAF Grant No. F49620-93-1-0270 entitled "Mechanics of Wide-Spread Fatigue Damage and Life-Enhancement Methodologies for Aging Aerospace Structures." Both this grant and the linked grant are under sponsorship of the Air Force Office of Scientific Research.

The distinction between this grant and the linked grant is that funds provided under this grant could be used only for salaries for graduate and undergraduate students, tuition/fees for graduate students only, and incidental costs associated with the activities of the students supported under this grant. Students supported under this grant must be U.S. citizens or nationals of the United States whose research activity was directly related to the linked grant, and who are in addition to students who were normally accommodated by the linked grant.

II. Students Supported under this Grant

During the course of this grant, three students were supported from funds provided by it. These students were:

a. <u>Cummings, Robert</u>; period of support: 1/3/95-6/9/95. Mr. Cummings was a Ph.D. student in Materials Engineering. At the time of his entry into that program, and the beginning of support under this grant, Mr. Cummings was employed as Materials Engineer, Warner Robins Air Logistics Center, Georgia. Mr. Cummings did not prepare any technical publications while supported.

b. <u>Jansen, Randy</u>; period of support: 3/28/94-10/27/94. Mr. Jensen was a Ph.D. student in Aerospace Engineering. At the time of his entry into that program, and the beginning of his support under this grant, Mr. Jensen was employed as a structural engineer at the Warner Robins Air Logistics Center, Georgia. Mr Jansen participated in the research described in the enclosed report, "Composite Patch Repairs of Cracked Metallic Structures," and the Progress Report, "Mechanics of Widespread Fatigue Damage and Life-Enhancement Methodologies for Aging Aircraft Structures," which was submitted in connection with grant no. F49620-93-1-0270, described above, also enclosed.

c. Visser, Bradley; period of support: 6/21/93-12/9/94. At the time Mr. Visser received initial support under this grant, he was a graduate student (MS level) in the School of Aerospace Engineering at Georgia Tech. He received his Master of Science degree in June 1994 and entered the Ph.D. program in Aerospace Engineering. While employed under this grant, Mr. Visser prepared the enclosed report "Summary of Research: Alternating Method for Bending of Plates." Mr. Visser also participated in the research described in the enclosed report, "Composite Patch Repairs of Cracked Metallic Structures," and the Progress Report, "Mechanics of Widespread Fatigue Damage and Life-Enhancement Methodologies for Aging Aircraft Structures," which was submitted in connection with grant no. F49620-93-1-0270, described above, also enclosed.

III. Report: "Composite Patch Repairs of Cracked Metallic Structures"

This report appears on the following pages numbered 1-57.

IV. Progress Report - "Mechanics of Widespread Fatigue Damage and Life Enhancement Methodologies for Aging Aerospace Structures."

This two-page report follows Part III.

V. Report - "Summary of Research - Alternating Method for Bending of Plates."

This section is last.

TABLE OF CONTENTS

CHAPTER III

COMPOSITE PATCH REPAIRS OF CRACKED METALLIC STRUCTURES

3.1 Introduction

In order to enhance the life of cracked structures, the repair technique which uses adhesively bonded composite patches is being considered as a cost-effective and reliable method[Baker and Jones (1988)]. To study the effect of the design parameters (including the size, thickness, and material properties of the composite patch, and the mechanical properties and thickness of the adhesive layer) on the crack-tip stress intensity factors, finite element alternating method has been developed for the studies of composite patching problems. The section summaries the procedure used for the analyses of composite patching problems with numerical examples which illustrate the effect of patching.

The traction in the adhesive layer must be solved for first in order to solve the patching problem. Consider the following two problems. The first problem is the cracked structure. The patch is replaced by the undermined adhesive traction that are applied on the area where the patch is applied. The second problem is the composite patch itself with the adhesive traction applied on it. Together with the finite element alternating method for the cracked structures, two different approaches had been used to solve for the adhesive traction, one implicit method [see Park, Ogiso, and Atluri (1992)] and one explicit method [see Nagaswamy, Pipkins, and Atluri (1995)]. In the implicit method, the stiffness of the cracked structure, at the given external loading, with respect to the traction loading is determined using the finite element alternating method. A linear equation system can be obtained for the adhesive traction by using the compatibility condition between the sheet and the patch. After solve for the adhesive traction, the stress intensity factors can be easily determined through the analytical solutions used in the finite element alternating methods for the cracked structure. More details about the implicit method can be found in Park, Ogiso, and Atluri (1992). In the alternative explicit method, the adhesive traction is solved by solving the patched structure using an ordinary finite element method, with the crack being modeled explicitly. However, the crack tip is not modeled in detail since the objective is only to obtain the adhesive traction. Once the adhesive traction is obtained, the stress intensity factors can be determined accurately by analyzing the unpatched cracked structure with adhesive traction applied at the location of the patch, using the finite element alternating method.

3.1.1 Analysis of repaired cracks

In this section, the problems of composite-patch repair of (i) center and edge-cracked panels loaded in the far field; and (ii) cracks emanating from pin-loaded fastener holes (the so-called "multiple-site-damage" (MSD)), are examined in thorough detail. The effects of various non-dimensional design parameters on the reduction in the stress-intensity factors near the crack-tip are determined, and are presented in the form of design charts. Both analytical and numerical methods are employed in this study. In the analytical method, the cracked metallic plate was considered to he infinitely large and the composite patch was modeled as a long orthotropic strip of finite height (in the direction perpendicular to the crack axis). Next, by using the FEAM, a more general analysis capability that can treat arbitrary shapes of the cracked metallic sheet as
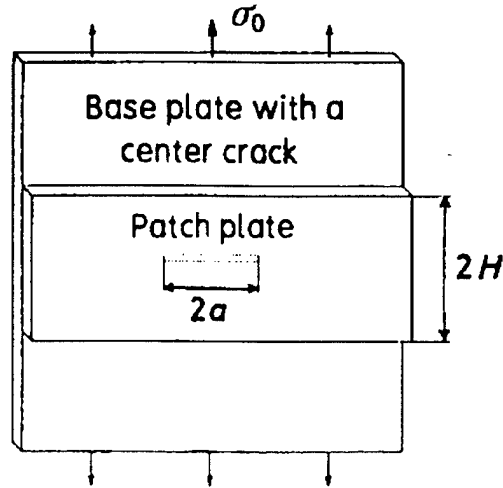
Figure 3.1: Schematic of a cracked metallic sheet repaired with a composite patch

well as the composite patches, is developed. This general FEAM is applied to: (i) composite patch repairs of cracks emanating from loaded fastener holes (the MSD problem); (ii) composite patch repairs of semi-elliptical shaped surface flaws in thick-section plates; and (iii) composite patch repairs of quarter-elliptical shaped surface flaws emanating from fastener holes. The problem (i) is two-dimensional in nature, while problems (ii) and (iii) are fully three-dimensional. In all these cases, the effects of various design parameters on the reduction of the crack-tip (front) stress-intensity, due to repair, are fully discussed.

Repair of center or edge cracks in unstiffened panels

Due to the fact that, in general, an analytical (as opposed to purely numerical) approach is more conveniently employed to examine the effects of each design parameter on the mechanical behavior of a repaired crack, a model problem of a repaired crack is first analyzed. Fig. 3.2 depicts the problem of an infinite isotropic (metal) sheet containing a crack of length $2a$, repaired by an adhesively bonded infinitely long orthotropic (composite) patch of height $2H$ (height is measured normal to the crack-axis). It is assumed that the crack lies along the it-axis and that the principal material directions of the patch coincide with the geometric it and y axes. Let the thickness of the metal plate, the composite patch and the adhesive layer, be, respectively, h_s, h_p and h_a.

The metal sheet is subjected to a hoop stress of σ_0 as in Fig. 3.1. This mode I symmetric problem can be solved by a superposition of the two following problems:

Problem A: Determine the stress field in an isotropic metal sheet without a crack, to which is bonded an orthotropic patch as in Fig. 3.2a.

Problem B: When the tractions at the location of the crack, as determined from the solution of Problem A above, are erased, determine the stress-intensity factors at the crack-tips. This problem is sketched in Fig. 3.2b.

The relevant material and geometric parameters from Problems A and B are as follows:

1. The Young's modulus E_s, and Poisson's ratio v_s for the isotropic sheet.
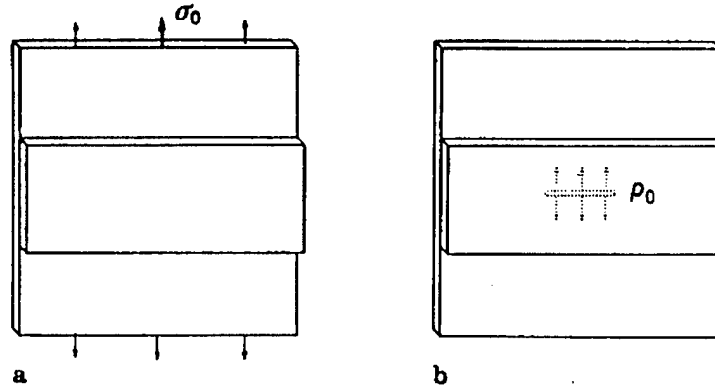
Figure 3.2: Linear superposition of problem A and problem B to solve the problem in Fig. 3.1

2. Thickness h_s of the isotropic sheet.

3. The Young's modulus E_x and E_y of the orthotropic patch; the Poisson ratio v_y and the shear modulus G_{xy} of the orthotropic patch.

4. The height H; and thickness h_p of the orthotropic patch; and

5. The thickness h_a, and the shear modulus G_a of the adhesive layer.

By using the Buckingham's $\prod$ theorem, the grouping of non-dimensional parameters that arise from the above geometric and material data is determined to be:

$$\left(\frac{G_s F}{h_s}\right), \left(\frac{a}{h_s}\right), \left(\frac{h_p E_y}{h_s G_s}\right), (v_s), \left(\frac{E_y}{E_x}\right), \left(\frac{E_x}{G_{xy}}\right), (v_y), \left(\frac{H}{a}\right). \tag{3.1}$$

It is the objective of the present analysis to determine the stress-intensity factor as a function of the above 8 non-dimensional parameters. This ensemble of curves would then lead to a design procedure to select the appropriate composite patch, and adhesive, for a given crack in a metallic sheet. This is the first comprehensive treatment of this problem in the literature.

Problem A (Fig. 3.2a)

Since the base plate and the patch have infinite lengths in the x-direction and since there is no crack, we can treat this problem as a one-dimensional patch problem. Here it is assumed that the shear stresses in the adhesive layer are only in the y-direction (i.e.,$\tau_{xz} = 0$), the base plate and the patch are in states of plane stress, and that the shear stresses in the adhesive layer are applied on the base plate and the patch as body forces (Fig. 3.3).

The equilibrium equations for a metal sheet and the composite patch are, respectively:

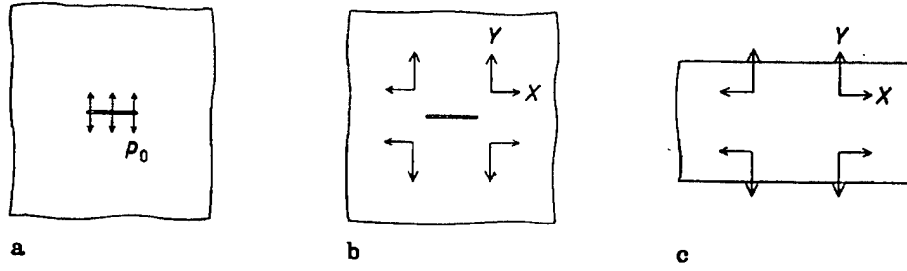$$\frac{d\sigma_{yy}^s}{dy} = \frac{\tau_{yz}}{h_s}, \tag{3.2}$$

Figure 3.3: Basic problems needed in solving the problems of Fig. 3.2b

$$\frac{d\sigma_{yy}^p}{dy} = -\frac{\tau_{yz}}{h_p}.\tag{3.3}$$

Here σ_{yy}^s and σ_{yy}^p are the normal stresses in the y direction in the base sheet and in the patch respectively, and τ_{yz} is the shear stress in the adhesive layer.

The stress-strain relations of the base sheet and the patch are given by:

$$\varepsilon_{xx}^s = \frac{1}{E_s}\left(\sigma_{xx}^s - v_s\sigma_{yy}^s\right),\tag{3.4}$$

$$\varepsilon_{yy}^s = \frac{1}{E_s}\left(\sigma_{yy}^s - v_s\sigma_{xx}^s\right),\tag{3.5}$$

$$\varepsilon_{xx}^p = \frac{1}{E_x}\left(\sigma_{xx}^p - v_x\sigma_{yy}^p\right),\tag{3.6}$$

$$\varepsilon_{yy}^p = \frac{1}{E_y}\left(\sigma_{yy}^p - v_y\sigma_{xx}^p\right).\tag{3.7}$$

Here E_s and v_s are Young's modulus and Poisson's ratio of a base sheet respectively; and E_x, E_y and v_x, v_y are the moduli and Poisson's ratios of an orthotropic patch. Among these variables, the relation $v_x/E_x = v_y/E_y$ is satisfied.

As a compatibility condition between the metal sheet and the composite patch, the following relations proposed by Mitchell, Wooley, and Chivirut (1975), Jones and Callinan (1979) were used

$$\tau_{yz} = \frac{v^s - v^p}{F}\tag{3.8}$$

Here

$$F = \frac{h_a}{G_a} + \frac{3h_s}{8G_s} - \frac{3h_p}{8G_p}.\tag{3.9}$$

v_s and v^p are the y displacements in the sheet and the plate respectively, and G_a, G_s and G_p are the shear moduli of the adhesive, the base sheet and the patch, respectively. We assume that G_p has the same value as G_{xy} in the patch plate. From the elaborate numerical results presented later, it will be seen that this assumption has little effect on the stress intensity factors.

By using Eq. 3.8 and the following boundary conditions:

$$\sigma_{yy}^s = \sigma_0 \text{ at } y = H, \quad \sigma_{yy}^p = 0 \text{ at } y = H, \tag{3.10}$$

we can solve Eqs. 3.2 and 3.3 easily. The stresses are obtained as

$$\sigma_{yy}^s = \sigma_0 - \frac{\left(1 - v_s^2\right)\sigma_0}{FE_s h_s A^2 \cosh AH}\left(\cosh AH - \cosh Ay\right), \tag{3.11}$$

$$\sigma_{yy}^p = \frac{\left(1 - v_s^2\right)\sigma_0}{FE_s h_p A^2 \cosh AH}\left(\cosh AH - \cosh Ay\right), \tag{3.12}$$

$$\tau_{yz} = \frac{\left(1 - v_s^2\right)\sigma_0}{FE_s A \cosh AH}\sinh Ay. \tag{3.13}$$

Here, to simplify the problem, the additional assumptions $\varepsilon_{xx}^s = 0$ and $\varepsilon_{xx}^p = 0$ were used. A^2 is defined as

$$A^2 = \frac{1}{F}\left(\frac{1 - v_s^2}{E_s h_s} + \frac{1 - v_x v_y}{E_y h_p}\right). \tag{3.14}$$

From Eqs. (3.11-3.13), we can notice that σ_{yy}^s and τ_{yz} have their maximum values at $y = H$, and decrease exponentially as $(H - y)$ becomes larger than zero. On the other hand, σ_{yy}^p is zero at $y = H$, but it increases exponentially as $(H - y)$ becomes larger than zero.

When $\cosh AH \gg 1$, the stresses near $y = 0$ can be expressed as

$$\sigma_{yy}^s = \sigma_0 - \frac{\left(1 - v_s^2\right)}{FE_s h_s A^2}\sigma_0, \tag{3.15}$$

$$\sigma_{yy}^p = \frac{\left(1 - v_s^2\right)}{FE_s h_p A^2}\sigma_0, \tag{3.16}$$

$$\tau_{yz} = 0. \tag{3.17}$$

These stresses are the same as those when the patch is considered to be of an infinite height. Thus, when the value of $\cosh AH$ is much greater than 1, we can assume that the patch has an infinite height, because this assumption gives nearly the same values for the stress intensity factors at the cracktip, and induced stresses near $y = 0$.

Problem B (Fig. 3.2b)

In order to solve this problem, a superposition of the basic problems shown in Fig. 3.3a, b and c may be used.

Fig. 3.3a is the case where uniform surface pressure p_0 is applied on the crack surface in a metal sheet of infinite size. Its solution is well known [Gladwell and England (1977)]. Let the displacement field of this problem be $u^{sA} = f_1(x,y)$, $v^{sA} = f_2(x,y)$. Here u^s is the displacement in the x direction and v^s is the displacement in the y direction, in the sheet.

Fig. 3.3b is the problem wherein point loads X, Y are applied symmetrically at the points (x_0, y_0), $(-x_0, y_0)$, $(x_0, -y_0)$ and $(-x_0, -y_0)$ on an infinite isotropic plate with a central crack. Let this solution be u^{sB} and $v^{sB}(x, y)$. The solutions can be found in Erdogan and Arin (1972) and Roderick (1980). By using the solution in Roderick (1980), the displacements at a point (x, y) for this problem can be expressed as:
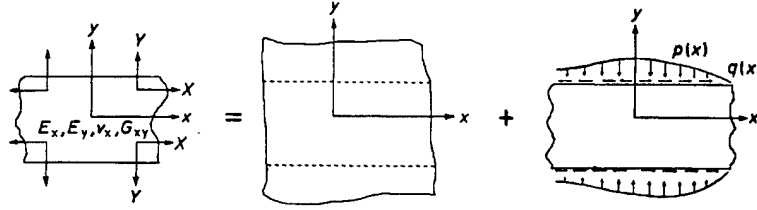
Figure 3.4: Green's function solution for a finite orthotropic plate, through superposition

$$u^{sB}(x,y) = H_{11}(x,y;x_0,y_0)X + H_{12}(x,y;x_0,y_0)Y \tag{3.18}$$

$$v^{sB}(x,y) = H_{21}(x,y;x_0,y_0)X + H_{22}(x,y;x_0,y_0)Y \tag{3.19}$$

The problem of Fig. 3.3c is where the point loads X,Y are applied symmetrically at the points (x_0,y_0), $(-x_0,y_0)$, $(x_0,-y_0)$ and $(-x_0,-y_0)$ on an orthotropic patch of height $2H$. The problem of Fig. 3.3c can again be solved through a linear superposition of two other problems as in Fig. 3.4b and c. Fig. 3.4b is of the problem of an infinite orthotropic sheet; and 16c is of a finite height composite patch with residual tractions, from the solution of the problem in Fig. 3.4b, acting on the edges $y = \pm H$. The displacement field for the problem in Fig. 3.4b can be found in Leknitskiic (1968). Now we consider the problem of Fig. 3.4c. Here, $-p(x)$ and $-q(x)$ are the normal and shear stresses acting on the $y = H$ plane. Since, for the problem in Fig. 3.4c, the displacements $u^{pc}(x,y)$ and $v^{pc}(x,y)$ are odd and even functions, respectively, with respect to x, we may define:

$$u^{pc}(x,y) = \frac{2}{\pi}\int_0^\infty \phi(\alpha,y)\sin\alpha x\,d\alpha, \tag{3.20}$$

$$v^{pc}(x,y) = \frac{2}{\pi}\int_0^\infty \psi(\alpha,y)\cos\alpha x\,d\alpha, \tag{3.21}$$

where $\phi(\alpha,y)$ and $\psi(\alpha,y)$ are the Fourier transforms of $u^{pc}(x,y)$ and $v^{pc}(x,y)$ respectively. Since there are no further body forces, the equilibrium equations for the patch in Fig. 3.4c are written in terms of u^{pc} and v^{pc} for this component problem of Fig. 3.4c, as:

$$\left(\frac{v_x E_y}{1-v_x v_y}\right)\frac{\partial^2 u^{pc}}{\partial x\partial y} + \left(\frac{E_y}{1-v_x v_y}\right)\frac{\partial^2 v^{pc}}{\partial y^2} - G_{xy}\left(\frac{\partial^2 u^{pc}}{\partial x\partial y} + \frac{\partial^2 v^{pc}}{\partial x^2}\right) = 0 \tag{3.22}$$

and

$$\left(\frac{E_x}{1-v_x v_y}\right)\frac{\partial^2 u^{pc}}{\partial x^2} + \left(\frac{v_y E_y}{1-v_x v_y}\right)\frac{\partial^2 v^{pc}}{\partial x\partial y} + G_{xy}\left(\frac{\partial^2 u^{pc}}{\partial y^2} + \frac{\partial^2 v^{pc}}{\partial x\partial y}\right) = 0. \tag{3.23}$$

Substituting Eq.3.20-3.21 into Eq.3.22-3.23, we obtain:

$$\frac{\partial^4\phi}{\partial y^4} + \alpha^2\left(-\frac{E_x}{G_{xy}}+2v_x\right)\frac{\partial^2\phi}{\partial y^2} + \alpha^4\frac{E_x}{E_y}\phi = 0, \tag{3.24}$$

$$\frac{\partial^4\psi}{\partial y^4} + \alpha^2\left(-\frac{E_x}{G_{xy}}+2v_x\right)\frac{\partial^2\psi}{\partial y^2} + \alpha^4\frac{E_x}{E_y}\psi = 0, \tag{3.25}$$

The general solutions of Eqs. 3.24-3.25 are:

$$\phi = e_1 A_1 \cosh\beta_1 y + e_2 A_2 \cosh\beta_2 y + e_1 A_3 \sinh\beta_1 y + e_2 A_4 \sinh\beta_2 y, \tag{3.26}$$

$$\psi = A_1 \sinh\beta_1 y + A_2 \sinh\beta_2 y + A_3 \cosh\beta_1 y + A_4 \cosh\beta_2 y, \tag{3.27}$$

where

$$e_k = \frac{\alpha\beta_k [\nu_x E_y + G_{xy}(1 - \nu_x\nu_y)]}{G_{xy}\beta_k^2 (1 - \nu_x\nu_y) - \alpha^2 E_x}, \quad k = 1, 2 \tag{3.28}$$

and β_1 and β_2 are roots of

$$\beta^4 - \alpha^2 \left(\frac{E_x}{G_{xy}} - 2\nu_x \right) \beta^2 + \alpha^4 \frac{E_x}{E_y} = 0 \tag{3.29}$$

Considering the symmetry conditions, $u^{pc}(x, y) = u^{pc}(x, -y)$, and $v^{pc}(x, y) = -v^{pc}(x, -y)$, we see that the constants A_3 and A_4 must be zero in Eqs. 3.26-3.27. Using Eqs. 3.26-3.27 in Eq. 3.20-3.21, we obtain the displacements u^{pc} and v^{pc}. From these, the corresponding stresses can be determined as:

$$\sigma_{xx}^{pc} = \frac{2}{\pi} \int_0^\infty [(\alpha M_1 e_1 + M_2\beta_1) A_1 \cosh\beta_1 y + (\alpha M_1 e_2 + M_2\beta_2) A_2 \cosh\beta_2 y] \cos\alpha x d\alpha$$

$$\sigma_{yy}^{pc} = \frac{2}{\pi} \int_0^\infty [(\alpha M_2 e_1 + M_3\beta_1) A_1 \cosh\beta_1 y + (\alpha M_2 e_2 + M_3\beta_2) A_2 \cosh\beta_2 y] \cos\alpha x d\alpha$$

$$\sigma_{xy}^{pc} = \frac{2}{\pi} \int_0^\infty [G_{xy}(e_1\beta_1 - \alpha) A_1 \sinh\beta_1 y + G_{xy}(e_2\beta_2 - \alpha) A_2 \sinh\beta_2 y] \sin\alpha x d\alpha, \tag{3.30}$$

where

$$M_1 = \frac{E_x}{1 - \nu_x\nu_y}, \quad M_2 = \frac{\nu_y E_x}{1 - G\nu_x\nu_y} = \frac{\nu_x E_y}{1 - \nu_x\nu_y}, \quad M_3 = \frac{E_y}{1 - \nu_x\nu_y}.$$

If $P(\alpha)$ and $Q(\alpha)$ are the Fourier transforms of the tractions $p(x)$ and $q(x)$ in Fig. 3.4c, such that

$$p(x) = \frac{2}{\pi} \int_0^\infty P(\alpha) \cos\alpha x dx, \tag{3.31}$$

$$q(x) = \frac{2}{\pi} \int_0^\infty Q(\alpha) \sin\alpha x dx, \tag{3.32}$$

then the boundary conditions at $\sigma_{yy}^{pc}(x, H) = +p(x)$ and $\sigma_{xy}^{pc}(x, H) = +q(x)$ result in the following equations:

$$(\alpha M_2 e_1 + M_3\beta_1)(\cosh\beta_1 H) A_1 + (\alpha M_2 e_2 + M_3\beta_2)(\cosh\beta_2 H) A_2 = P(\alpha) \tag{3.33}$$

and

$$G_{xy}(e_1\beta_1 - \alpha)(\sinh\beta_1 H) A_1 + G_{xy}(e_2\beta_2 - \alpha)(\sinh\beta_2 H) A_2 = Q(\alpha) \tag{3.34}$$

from which A_1 and A_2 are solved for. Thus, the displacement solution $u^{pc}(x, y)$ and $v^{pc}(x, y)$ is obtained for the problem in Fig. 3.4c.

Let the displacement solution for the patch problem of Fig. 3.3c, obtained as a superposition of problems in Fig. 3.4b and c, be written as:

$$u^{pc}(x,y) = \frac{1}{h_p} \int_D [K_{11}(x,y;x_0,y_0)\,\tau_{xz}(x_0,y_0) + K_{12}(x,y;x_0,y_0)\,\tau_{yz}(x_0,y_0)]\,dx_0 dy_0 \qquad (3.35)$$

and

$$v^{pc}(x,y) = \frac{1}{h_p} \int_D [K_{21}(x,y;x_0,y_0)\,\tau_{xz}(x_0,y_0) + K_{22}(x,y;x_0,y_0)\,\tau_{yz}(x_0,y_0)]\,dx_0 dy_0 \qquad (3.36)$$

wherein, the adhesive shear stresses (τ_{xz}/h_p) and (τ_{yz}/h_p) are treated as body forces per unit volume, acting on the composite patch, as in Fig. 3.3c.

The sheet displacements from problems 3.3A and 3.3B may be written as:

$$
\begin{aligned}
u^s(x,y) &= u^{sA}(x,y) + u^{sB}(x,y) \\
&= f_1(x,y) - \frac{1}{h_s} \int_D [H_{11}(x,y;x_0,y_0)\,\tau_{xz}(x_0,y_0) + H_{12}(x,y;x_0,y_0)\,\tau_{yz}(x_0,y_0)]\,dx_0 dy_0 \quad (3.37)
\end{aligned}
$$

and

$$v^s(x,y) = f_2(x,y) - \frac{1}{h_s} \int_D [H_{21}(x,y;x_0,y_0)\,\tau_{xz}(x_0,y_0) + H_{22}(x,y;x_0,y_0)\,\tau_{yz}(x_0,y_0)]\,dx_0 dy_0 \qquad (3.38)$$

where D, the domain of integration, is the size of the composite patch. The body forces on the sheet are $(-\tau_{xz}/h_s)$ and $(-\tau_{yz}/h_s)$ in the x and y directions, respectively.

The compatibility condition between the sheet and the patch is expressed as

$$\tau_{xz} = \left(\frac{u^s - u^p}{F}\right) \text{ and } \tau_{yz} = \left(\frac{v^s - v^p}{F}\right). \qquad (3.39)$$

By substituting Eqs. 3.35-3.36 and Eqs. 3.37-3.38 into Eq. 3.39, one obtains the following integral equations for τ_{xz} and τ_{yz}:

$$F\tau_{xz}(x,y) + \int_D [k_{11}(x,y;x_0,y_0)\,\tau_{xz}(x_0,y_0) + k_{12}(x,y;x_0,y_0)\,\tau_{yz}(x_0,y_0)]\,dx_0 dy_0 = f_1(x,y) \qquad (3.40)$$

and

$$F\tau_{yz}(x,y) + \int_D [k_{21}(x,y;x_0,y_0)\,\tau_{xz}(x_0,y_0) + k_{22}(x,y;x_0,y_0)\,\tau_{yz}(x_0,y_0)]\,dx_0 dy_0 = f_2(x,y)$$

where

$$k_{11} = \left(\frac{H_{11}}{h_s} + \frac{K_{11}}{h_p}\right),\ k_{12} = \left(\frac{H_{12}}{h_s} + \frac{K_{12}}{h_p}\right),\ k_{21} = \left(\frac{H_{21}}{h_s} + \frac{K_{21}}{h_p}\right),\ k_{22} = \left(\frac{H_{22}}{h_s} + \frac{K_{22}}{h_p}\right). \qquad (3.41)$$

In integral Eqs. 3.40 and 3.1.1, the domain of integration D is the size of the orthotropic patch, which is finite in the y direction, but ∞ in the x direction. For numerical purposes, however, the domain D in the x direction is also truncated to some finite value. In order to solve Eqs. 3.40 and 3.1.1, the domain
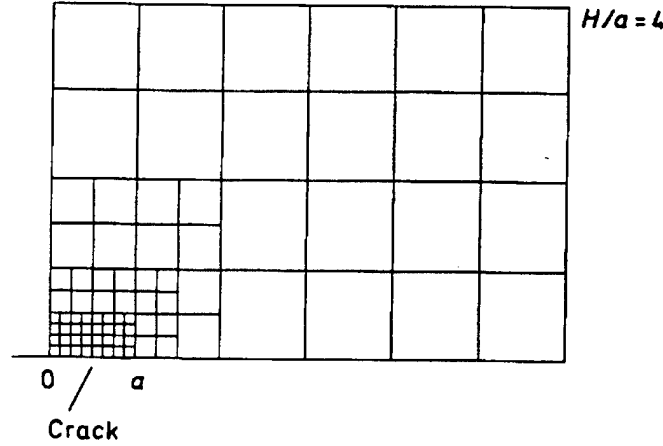
Figure 3.5: A typical finite element mesh of the adhesive layer

D is discretized into a number of small sub-elements. In each subelement, τ_{xz} and τ_{yz} are assumed to be constant. Thus a system of linear equations, for discrete values of τ_{xz} and τ_{yz}, is obtained. By solving these, the shear stresses τ_{xz} and τ_{yz} are determined. Since the stress-state on the sheet, as in Fig. 3.3a and b, is thus completely known, the k-factors can be evaluated from the analytical solutions for problems 3.3A and B.

One example of descritization of D is shown in Fig. 3.5, for the case when $(H/a) = 4$. By varying the size of this D, it was determined that the obtained k-factors are insensitive to the size of D, as long as the dimensions of D are about five times as large as a. Note also the finer mesh near the crack, in Fig. 3.5, as the adhesive shear stresses are expected to be maximum near the crack itself.

Behavior of patched cracks in unstiffened panels

Attention is focused in this study, on the variation of:

1. non-dimensional stress intensity, i.e., $K_I/\sigma_0\sqrt{\pi a}$

2. non-dimensional adhesive shear, $\frac{\tau_{xz}}{\sigma_0}$ and $\frac{\tau_{yz}}{\sigma_0}$

3. non-dimensional patch stress, $[\sigma_{yy}^p h_p]/(\sigma_0 h_s)$

as a function of the non-dimensional parameters:

$$\left(\frac{G_s F}{h_s}\right), \left(\frac{h_p E_y}{h_s G_s}\right), \left(\frac{a}{h_s}\right), \left(\frac{H}{a}\right), (\nu_s), \left(\frac{E_y}{E_x}\right), \left(\frac{E_x}{G_{xy}}\right), (\nu_y).$$

From the computed results, it was found that the more significant parameters are:

1. $\left(\frac{G_s F}{h_s}\right)$: which characterizes the adhesive flexibility. The "smaller" this number is, the "stiffer" is the adhesive.

2. $\left(\frac{h_p E_y}{h_s G_s}\right)$: which characterizes the patch stiffness in the direction normal to the crack axis.
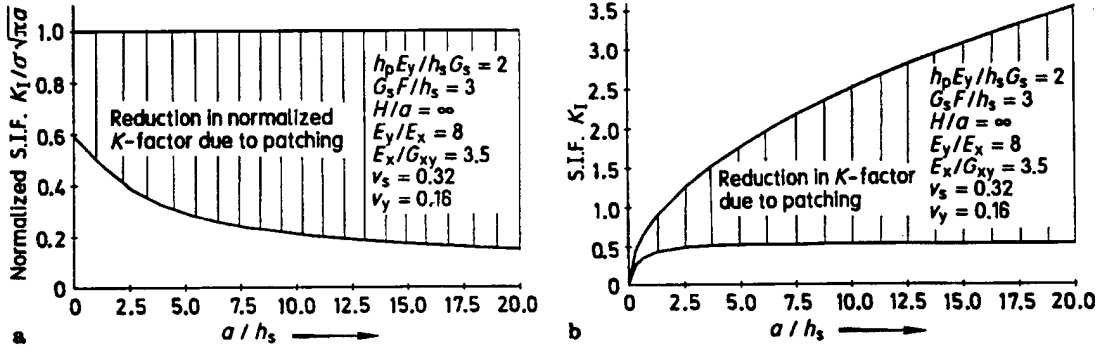
Figure 3.6: (a) Reduction in normalized k-factor due to patching, as a function of the crack length; (b) reduction in the actual k-factor (for $\sigma_o = 1$) due to patching as a function of the crack length

The "larger" this number, the "stiffer" is the patch in the direction normal to the crack-axis.

Fig. 3.6a shows the variation of the normalized stress-intensity factor as the crack-length increases, for the case of a very large composite patch, $(H/a) \to \infty$; $(h_p E_y / h_s G_s) = 2$; and $(G_s F/h_s) = 3.0$. Note that, in the absence of a composite patch, the normalized k-factor, i.e., $[K_I / \sigma \sqrt{\pi a}] = 1.0$. Thus, the vertical distance between the horizontal straight line [normalized k-factor $= 1.0$] for the unpatched crack, and the curve for the repaired crack, indicates the reduction in the normalized k-factor due to patching. Fig. 3.6a clearly shows that more and more reduction in the normalized k-factor results as the crack-length increases.

Also it is seen from Fig. 3.6a that, as $(a/h_s) \ll 1$, the normalized k-factor converges to that in a center-cracked sheet with the crack-face pressure of p_0 (see Fig. 3.3a), which is smaller than the applied far-field stress σ_0 in the sheet (see Fig. 3.2a). Thus, when the crack length in the metal sheet is very small, the reduction in k -factor is achieved by the reduction in the crack-face pressure, p_0, in the metal sheet, due to the pressure of the composite patch. From Eq. 3.11 it is seen that p_0 in Fig. 3.2b is given by

$$p_0 = \sigma_{yy}^s (y = 0) = \sigma_0 - \frac{\left(1 - \nu_s^2\right)\sigma_0}{FE_s h_s A^2 \cosh AH} (\cosh AH - 1) \tag{3.42}$$

Substituting for A^2 from Eq. 3.14 into 3.42, it is seen that p_0 is independent of the adhesive flexibility parameter "F"; for large values of H when $\cosh AH \gg 1$. Thus, for short cracks, the reduction in the normalized k-factor is unaltered by the adhesive flexibility. As the crack becomes longer, the adhesive shear stresses acting on the metal sheet have more dominant effect on the crack-tip k-factor, and the reduction in the k-factor depends on the adhesive flexibility parameter F.

Fig. 3.6b shows the variation of the actual k-factor as the crack grows, with and without the presence of a composite patch. It is seen that without the patch, the k-factor increases as $\sqrt{a}$ as expected, but in the presence of a patch, the k-factor levels off to a constant value as the crack grows. This result has also been noted earlier by Rose (1981) and Atluri and Kathiresan (1978). It should be noted, however, that in the present analysis, the adhesive bond between the metal sheet and the composite patch is assumed to be perfect. However, the shear stress in the adhesive is maximum near the center of the crack, where the crack-opening displacement v^s in the sheet is maximum. Thus, for all adhesives whose maximum shear-strength is a finite value, a disbond can be expected to occur between the metal sheet and the composite patch near the center of the crack at $y = 0$, as well as possibly at $y = H$. When this disbonding is modeled properly, its
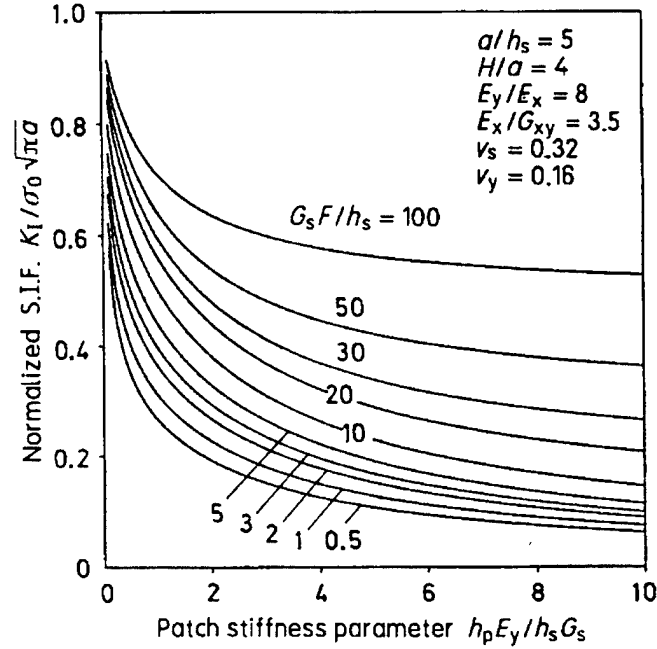
Figure 3.7: Reduction in normalized k-factor for a given crack length, as a function of the patch stiffness and adhesive flexibility

effect is to increase the actual k-factor of the repaired crack, as the crack length increases. This situation of the damage tolerance of the bond is being currently quantified.

Fig. 3.7 shows the effects of the "patch-stiffness" parameter and the "adhesive-flexibility" parameter on the normalized stress-intensity factor of the patched crack, for a given crack length $(a/h_s) = 5.0$, and a given patch-height, $(H/a) = 4.0$.

For a fixed "adhesive-flexibility" value, the stress-intensity factor (S.I.F.) of the patched crack decreases rapidly from its "unpatched" value, as the patch-stiffness increases. This S.I.F. reduction is, however, smaller as the adhesive flexibility increases.

From Fig. 3.7, it is evident that the S.I.F. reduction due to a patch is maximum when one uses a very stiff composite patch, as well as a very stiff adhesive layer.

However, a stiff adhesive layer has a deleterious effect on the integrity of the bond itself as the adhesive shear stresses increase in such a case, as seen from Fig. 3.8 and 3.9.

Fig. 3.8 shows the non-dimensional shear stress (τ_{yz}/σ_0) in the adhesive layer, at the center of the crack, i.e., $x = 0$ and $y = 0$; while Fig. 3.9 shows the corresponding value at the end of the patch, i.e., $x = 0$ and $y = H$. It is noted that in all cases, $\tau_{xz} \ll \tau_{yz}$ and hence τ_{xz} is not shown. It is seen that τ_{yz} at $y = 0$ arises only from the problem in Fig. 3.2b. Since $\tau_{yz} = (v^s - v^p)/F$ and since $(v^s - v^p)$ is maximum at $x = 0$ and $y = 0$ in Fig. 3.2b, the maximum value for the problem in Fig. 3.2b also occurs at $x = 0$ and $y = 0$. Also, the stress τ_{yz} at $x = 0$ and $y = H$ for the problem in Fig. 3.1 are nearly the same as that for the problem in Fig. 3.2a, and given by Eq. 3.13 when $y = H$.

From Fig. 3.8 it is seen that τ_{yz} at $x = 0$ and $y = 0$ increases rapidly as the adhesive becomes stiffer (i.e., as F decreases), especially for moderate values of patch stiffness. For fixed values of F, (τ_{yz}/σ_0) at $x = 0$
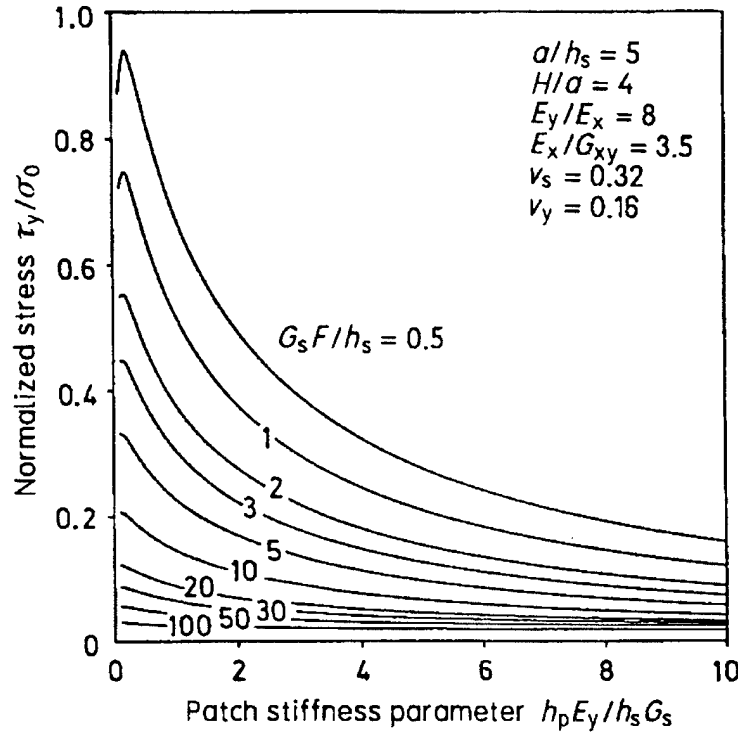
Figure 3.8: Variation of τ_{yz} at $x = 0$, $y = 0$ as a function of the patch-stiffness and adhesive flexibility

and $y = 0$ decreases as the patch stiffness increases. For large values of adhesive flexibility, the maximum shear stress is nearly constant regardless of the value of the patch stiffness.

From Fig. 3.9 it is seen that τ_{yz} at $x = 0$ and $y = H$ also increase as the adhesive layer becomes stiffer. However, for fixed values of F, this shear stress increases as the patch increases.

Thus, we note that when a patch with a low stiffness $((h_p E_p) / (h_s G_s) < 3.0)$ is used, the value of τ_{yz} at $x = y = 0$ is larger than the value of τ_{yz} at $x = 0$ and $y = H$. As the patch becomes stiffer, τ_{yz} at $x = 0 = y$ decreases, while τ_{yz} at $x = 0$ and $y = H$ increases. Thus as the patch becomes very stiff, $\tau_{yz}(x = 0, y = H) > \tau_{yz}(x = 0, y = 0)$.

Thus, in general, depending of the values of the patch stiffness, the likelihood of a disbond between the metal plate and the patch exists both at the locations $(x = 0, y = 0)$ and $(x = 0, y = H)$.

Fig. 3.10 shows the effect of the patch-stiffness and adhesive flexibility on the values of $(\sigma_{yy}^p h_p) / (\sigma_0 h_s)$. The value of $(\sigma_{yy}^p / \sigma_0)$ changes, on the other hand, according to the value of (h_s / h_p). For fixed value of adhesive flexibility, $(\sigma_{yy}^p h_p) / (\sigma_0 h_s)$ increases as the patch-stiffness increases. For fixed patch-stiffness, $(\sigma_{yy}^p h_p) / (\sigma_0 h_s)$ increases as the adhesive stiffness increases.

So far, we have assumed that the metal sheet is infinite, and the composite patch is of a finite height but infinitely long. In reality however, the base sheet as well as the patch are finite in size; moreover, the patch can be arbitrary in shape. To account for these size and shape effects, one may use the FEAM to determine the displacement fields in each of the component problems such as in Fig. 3.3a, b, c wherein each problem may have a finite, arbitrary, shape. The integral equations for τ_{xz} and τ_{yz} in these finite arbitrary shapes may be formulated in much the same way as described earlier.
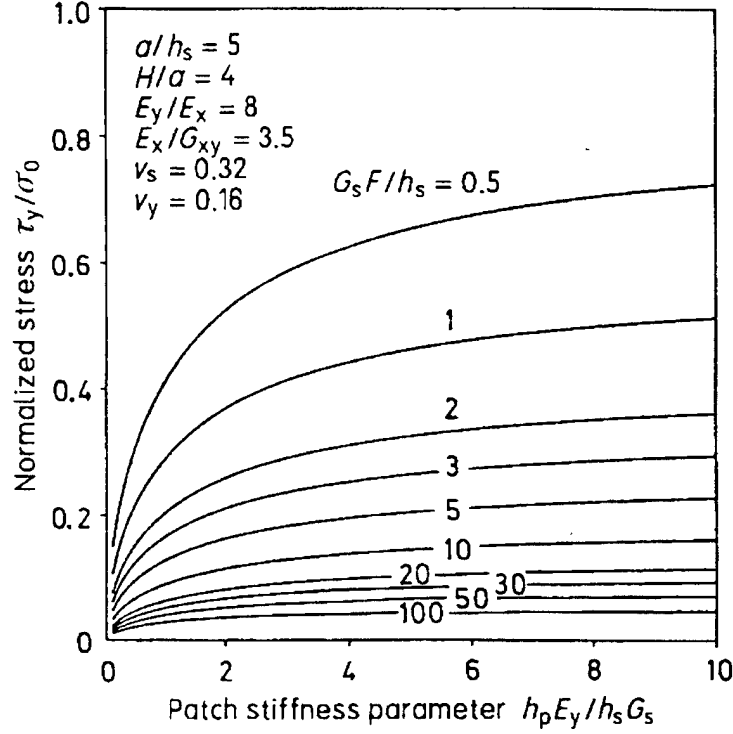
Figure 3.9: Variation of τ_{yz} at $x = 0$, $y = H$ as a function of the patch-stiffness and adhesive flexibility

3.1.2 Repair of cracks near loaded fastener holes in a lap joint (multiple-site damage)

Consider the model problem of repairing of symmetrical cracks emanating from a loaded fastener hole, as shown in Fig. 3.11.

A circular hole of radius R is located at the center of a rectangular plate of width $2W_s$, height $2H_s$ and thickness h_s. Two radial cracks of equal lengths $(a - R)$ each emanate from the hole, along the it axis. To repair these cracks, a rectangular orthotropic patch of width $2W_p$, height $2H_p$ and thickness h_p is assumed to be bonded onto the metal sheet. The thickness of the adhesive is h_a. The metal sheet is assumed to be subject to a far-field hoop stress σ_0 as well as the pin-loading $p(\theta)$ of the type:

$$p(\theta) = \frac{4W_s\sigma_0}{\pi R} |\sin\theta| \tag{3.43}$$

as Fig. 3.12a. Since the applied loading (σ_0 and $p(\theta)$) is not symmetric in the y direction, the crack may exhibit mode II behavior also. However, this mode II k-factor may be expected to be much smaller than the mode I component, and will be ignored hence forth.

The problem of Fig. 3.12a can be solved by a superposition of the two symmetric problems of Fig. 3.12b and c. If the crack-tip k-factor in Fig. 3.12b is K_{IB} and that in Fig. 3.12c is K_{IC}, respectively, then the k-factor of Fig. 3.12a may be written as:

$$K_{IA} = \frac{1}{2}(K_{IB} + K_{IC}). \tag{3.44}$$

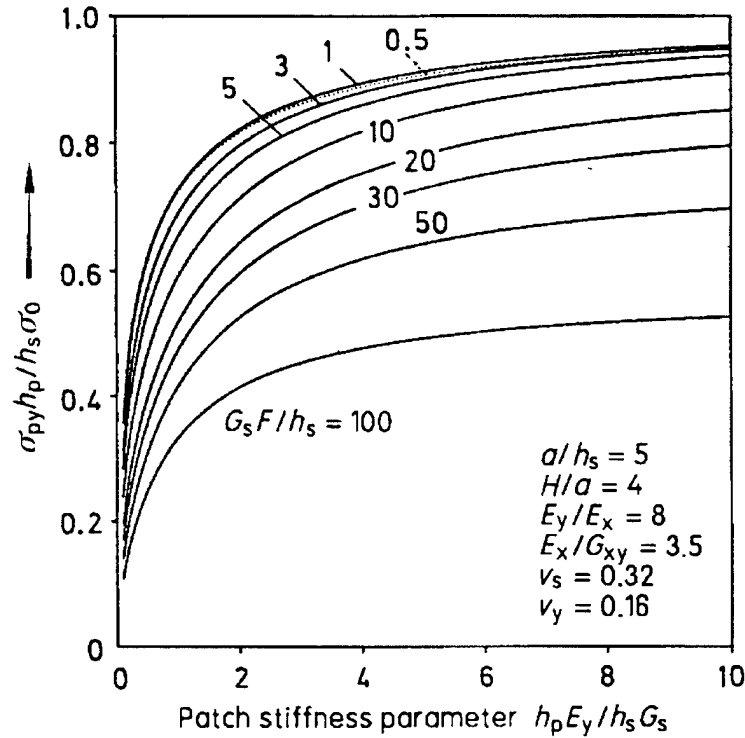Note that both the problems of Fig. 3.12b and c involve finite geometries.

Figure 3.10: Variation of σ_{yy}^p at $x = 0$, $y = H$ as a function of the patch-stiffness and adhesive flexibility

The problems in Fig. 3.12b and c, can, in turn, be solved by a linear superposition of the basic problems in Fig. 3.13: (A) the problem of a finite sized isotropic metal sheet with radial cracks emanating from an unloaded hole, the sheet being subject to far-field hoop stress σ_0; (B) the problem of a finite-sized isotropic metal sheet with radial cracks emanating from a hole, the hole surface being subject to symmetric load $p(\theta)$ (Fig. 3.13b); (C) the problem of a finite-sized isotropic metal sheet with cracks emanating from a hole, the plate being subjected to shear tractions τ_{xz} and τ_{yz} (from the adhesive layer) on its surface (Fig. 3.13c); and (D) the problem of a finite-sized orthotropic composite patch, subjected to shear tractions τ_{xz} and τ_{yz} (from the adhesive layer) on its surface (Fig. 3.13d).

In order to solve the above four basic problems, the FEAM is employed. In the case of the problem in Fig. 3.13a, the FEAM procedure is as follows:

1. First consider the analytical solution for the problem of a central crack in an infinite sheet, the crack-faces being subjected to arbitrary tractions. In the present problem of cracks emanating from a hole, as in Fig. 3.13a, in the FEAM procedure, residual tractions would arise on the crack-faces, $|x| \geq (R-a)$ (for a traction-free hole), and further, there will be steep stress gradient near $|x| = R$ because of the stress-concentration near the hole. Thus, in order to use the Gladwell and England (1977) solution, tractions on the fictitious crack-face $|x| < a$ will have to be interpolated with Chebyschev polynomials which is not desirable, since the residual tractions on the fictitious crack-faces $|x| < R$ are zero, while those on $|x| \geq (R_a)$ have a steep gradient. Due to this fact, an alternate analytical solution for a central crack in an infinite sheet, the crack faces being subject to equal and opposite point-loads at an arbitrary
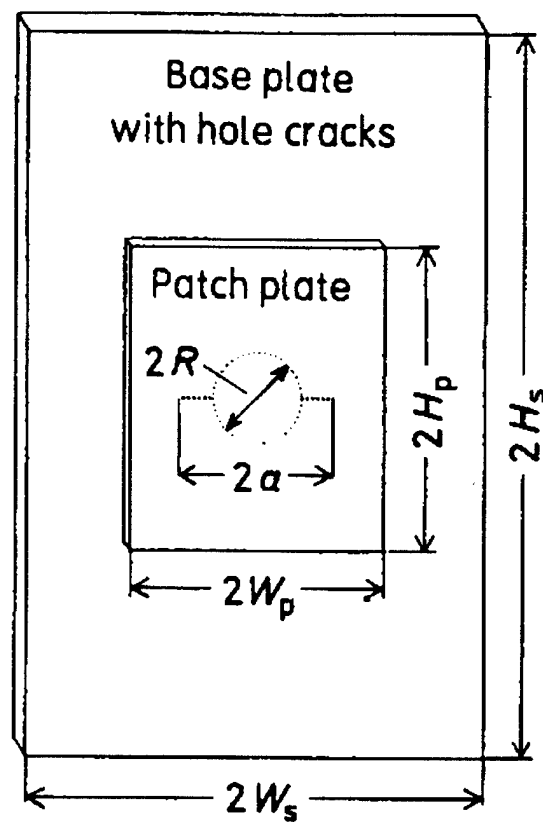
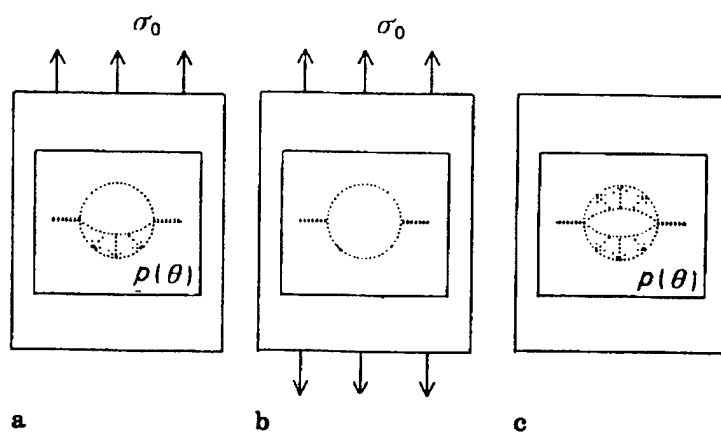Figure 3.11: Schematic of repaired cracks near a loaded fastener hole in a metal sheet

Figure 3.12: Linear superposition of problem B and C to solve a problem A: $K_{IA} = (K_{IB} + K_{IC})/2$
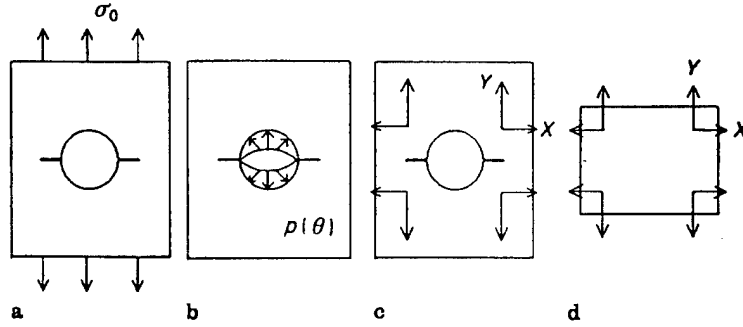
Figure 3.13: Basic problems to be solved in solving the problems of Fig. 3.12

location x, is considered.

Without loss of generality, consider the problem when a crack of length $2a$ exists in an infinite isotropic plate, and two point forces of magnitude Y are applied at points $x = \pm d$ on the upper crack surface, and two point forces $-Y$ are applied at $x = \pm d$ on the lower surface. Following Muskhelishvili (1953), the complex stress-functions for this problem are:

$$\Phi(z) = \Omega(z) = \frac{Y\sqrt{d^2 - a^2}}{2\pi i \sqrt{z^2 - a^2}} \left(\frac{1}{z+d} + \frac{1}{z-d} \right) \tag{3.45}$$

$$\varphi(z) = \omega(z) = \frac{-Y}{2\pi i} \left[\log \frac{2\sqrt{d^2 - a^2}\sqrt{z^2 - a^2} + 2dz - 2a^2}{z - d} + \log \frac{2\sqrt{d^2 - a^2}\sqrt{z^2 - a^2} - 2dz - 2a^2}{z + d} \right] \tag{3.46}$$

Here

$$\Phi(z) = \varphi'(z), \quad \Omega(z) = \omega'(z).$$

The stress intensity factor is given by:

$$K_I = \frac{Y}{\sqrt{\pi a}} \left(\frac{\sqrt{a+d}}{\sqrt{a-d}} - \frac{\sqrt{a-d}}{\sqrt{a+d}} \right). \tag{3.47}$$

The stresses and displacements are obtained from the following relations:

$$\sigma_{xx} + \sigma_{yy} = 2 \left[\Phi(z) - \overline{\Phi(z)} \right]. \tag{3.48}$$

$$\sigma_{yy} - i\tau_{xy} = \Phi(z) + (z - \bar{z})\overline{\Phi'(z)} + \Omega(\bar{z}) \tag{3.49}$$

and

$$2G(u + iv) = \kappa\varphi(z) - \omega(\bar{z}) - (z - \bar{z})\overline{\Phi(z)} \tag{3.50}$$

By using the above solutions as Green's functions, one can obtain the stress-intensity factors, and the stress and displacement fields, when arbitrary tractions are applied on the crack surface.

The main steps of the FEAM for solving the problem of Fig. 3.13a are:

2. Using the analytical solution for the problem of an infinite sheet with a hole (but no cracks) subjected to far-field stress σ_0 (see Muskhelishvili (1953)), obtain the residual tractions at the outer-boundaries of the finite sheet as well as at the locations of the crack, $|x| \geq (a - R)$.

3. To create a traction-free crack, erase the stresses, as found in step (2), on the crack-faces $|x| \geq (a - R)$, using the analytical solution for an infinite sheet with a crack, as in Eqs. 3.47-3.50. Determine the k-factors, and the displacement solutions using the Green's function solution, Eqs. 3.47 and 3.50.

4. Corresponding to the solution in step 3, determine the residual tractions at the surface of the hole as well as at the outer boundaries of the finite plate.

5. In order to satisfy the given traction $b \cdot c$ at the outer boundaries of the finite plate as well as at the hole surface, reverse the residual tractions at these surfaces, as calculated from steps (2) and (4). Calculate the equivalent nodal forces on these surfaces, at the chosen finite element nodes.

6. Using the usual finite element method, obtain the stresses at the location of the crack, and the displacement field everywhere, corresponding to the nodal loads in step (5).

7. Erase the crack-face stresses as computed from step (6), by repeating step (3).

8. Continue the iteration until the residual tractions in the repeated step (6) are vanishingly small.

9. By summing appropriate contributions, compute the total stress-intensity factor, and the total displacement field for the problem in Fig. 3.13a.

The procedures for the solutions of the problems in Fig. 3.13b and c are entirely analogous to that in solving the problem in Fig. 3.13a, as described above, except:

10. In solving the problem of Fig. 3.13b, the analytical solution in step (2) of the problem of Fig. 3.13a is replaced by an analytical solution for an infinite sheet with a hole (but no cracks), the hole surfaces being subject to symmetric pin-loading, $p(\theta)$.

11. In solving the problem of Fig. 3.13c, the analytical solution in step (2) of the problem of Fig. 3.13a is replaced by an analytical solution for an infinite sheet with a hole (but no cracks), the sheet being subjected to body forces τ_{xz} and τ_{yz} a rising from the adhesive layer. (This analytical solution is obtained using the complex variable information, as in Muskhelishvili (1953)).

In the case of the problem of Fig. 3.13d, the following steps are used:

(a) By using the analytical solution [Leknitskiic (1968)] of the problem of an infinite orthotropic sheet subjected to four sets of point loads applied symmetrically at $(\pm x_0; \pm y_0)$, we obtain the residual stresses at the outer boundaries of the patch, $x = \pm H_p$; and $y = \pm W_p$, as well as the displacement fields.

(b) In order to satisfy the traction-free boundary conditions at $x = \pm H_p$ and $y = \pm W_p$, reverse the residual tractions computed in step (i) above, and compute the equivalent nodal forces to be applied at the (coarse) finite-element mesh of the composite patch.

(c) Using the finite element method, obtain the displacement field corresponding to the loads in step (ii). Add the displacement fields of steps (i) and (iii).

Formulation of integral equations for the problem of repair of cracks near loaded fastener holes

By using the FEAM outlined in Sec. 3.1.2, we obtain the displacement fields in each of the four basic problems sketched in Fig. 3.13a-d, respectively. Let the displacement field of the problem in Fig. 3.13a be given by $u^{sA} = F_{1A}(x,y)$ and $v^{sA} = F_{2A}(x,y)$; and that for problem in Fig. 3.13b be given by $u^{sB} = F_{1B}(x,y)$ and $v^{sB} = F_{2B}(x,y)$. Let the displacement field for the problem in Fig. 3.13c be given by:

$$u^{sC}(x,y) = -\frac{1}{h_s} \int_D [H_{11}(x,y;x_0,y_0)\,\tau_{xz}(x_0,y_0) + H_{12}(x,y;x_0,y_0)\,\tau_{yz}(x_0,y_0)]\,dx_0dy_0 \tag{3.51}$$

and

$$v^{sC}(x,y) = -\frac{1}{h_s} \int_D [H_{21}(x,y;x_0,y_0)\,\tau_{xz}(x_0,y_0) +]\,dx_0dy_0 \tag{3.52}$$

where D is the domain of the finite patch (and of the adhesive layer). Likewise, the displacement field in the patch is given by

$$u^{P} = u^{pD}(x,y) = \frac{1}{h_p} \int_D [K_{11}(x,y;x_0,y_0)\,\tau_{xz}(x_0,y_0) + K_{12}(x,\ \ \ \ ,y_0)\,\tau_{yz}(x_0,y_0)]\,dx_0dy_0 \tag{3.53}$$

and

$$v^{P} = v^{pD}(x,y) = \frac{1}{h_p} \int_D [K_{21}(x,y;x_0,y_0)\,\tau_{xz}(x_0,y_0) + K_{22}(x,y;x_0,y_0)\,\tau_{yz}(x_0,y_0)]\,dx_0dy_0 \tag{3.54}$$

The total displacement in the metal sheet (see Fig. 3.13a-c) is given by:

$$u^{s} = \frac{1}{2}\left(u^{sA} + u^{sB}\right) + u^{sC} = \frac{1}{2}(f_{1A} + f_{1B}) + u^{sC} \tag{3.55}$$

and

$$v^{s} = \frac{1}{2}\left(v^{sA} + v^{sB}\right) + v^{sC} = \frac{1}{2}(f_{2A} + f_{2B}) + v^{sC} \tag{3.56}$$

The conditions of compatibility between the metal sheet and the orthotropic patch are given, again, by:

$$\tau_{xz} = \frac{u^{s} - u^{P}}{F} \quad \text{and} \quad \tau_{yz} = \frac{v^{s} - v^{P}}{F} \tag{3.57}$$
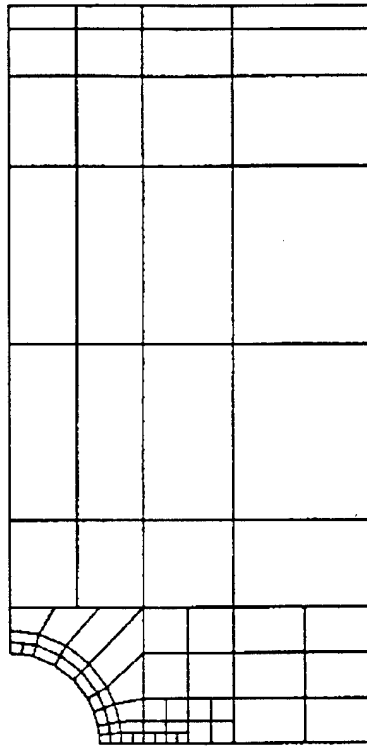
Figure 3.14: A typical finite element mesh of the adhesive layer

where F is the adhesive flexibility as defined in Eq. 3.9. By substituting Eqs. 3.51 to 3.56 in Eq. 3.57, one obtains the integral equations for τ_{xz} and τ_{yz}. Once these integral equations are solved for τ_{xz} and τ_{yz}, the free -body diagram of the stress-intensity factors near the crack-tips, as effected by the repair patch, can be computed.

By assuming constant values of τ_{xz} and τ_{yz} within each subdomain, the integral equations in Eqs. 3.56 and 3.57 are solved for. One example of the mesh used for solving the integral equation over D, for the case $W_p/R = 2$ and $H_p/W_p = 2.0$ is shown in Fig. 3.14.

In the problems of Fig. 3.12, the k-factor of the problems in Fig. 3.12a-c are identified as K_{IA}, K_{IB} and K_{IC} respectively, $\left(K_{IA} = \frac{1}{2} \left(K_{IB} + K_{IC} \right) \right)$. In the following, the results for the normalized k-factors, as functions of the material parameters $(G_s F/h_s)$, $(h_p E_y/h_s G_s)$ and the geometrical parameters a/R, R/h_s, W/R, and H/W, are discussed for the patched and unpatched cases.

Results and discussions

In order to examine the accuracy of the presently developed FEAM, first the problem of cracks emanating from a loaded fastener hole, without the presence of the repair patch, is solved first. The present results are compared with those of Cartwright and Parker (1972), for the case when $H/W = 2$, and $W/R = 4.0$. In the present FEAM, 65 eight-noded isoparametric elements were used, and the CPU time required to solve one crack case was about 55 seconds on a MicroVAX Station II. The present results are seen from Fig. 3.15 to
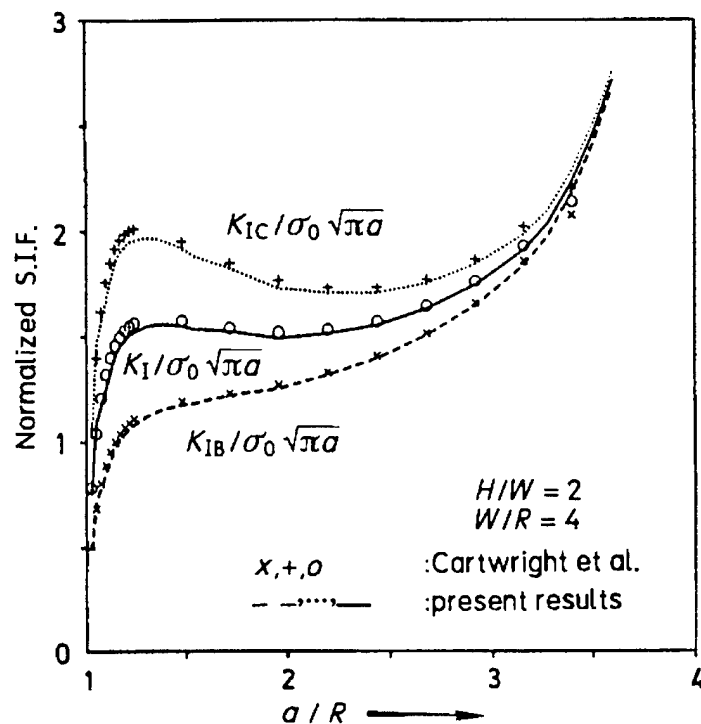
Figure 3.15: Variation of normalized k-factor as a function of the crack-length (unrepaired case)

agree excellently with those of Cartwright and Parker (1972).

Fig. 3.16a shows the effect of patching on the normalized stress-intensity factor, as the crack length increases, for given material and geometrical parameters of the patch as identified in the inset of Fig. 3.16a. Comparing Fig. 3.15 and 3.16a, the reduction in the normalized k-factor, as the crack grows, due to the presence of the composite patch, can be observed. For small cracks this reduction is not much, but as (a/R) increases, the effects of patching increases as well.

Fig. 3.16b shows the effect of patching on the actual stress-intensity factor, as the crack length increases, for given geometrical and material parameters as identified in the inset of Fig. 3.16b. Once again it is seen that even for a repaired crack near a loaded fastener hole, the actual k -factor becomes a constant as the crack-length increases under the patch. This appears to be a salient feature of all cases when the crack in a fuselage skin is repaired with a stiff composite patch. Fig. 3.17 shows the effect of the hole radius on the normalized k-factors for the repaired cracks.

Fig. 3.18 shows the effect of the adhesive layer flexibility and patch-stiffness on the normalized stress-intensity near the crack-tip, for the case of far-field hoop-stress loading α_0. Fig. 3.19 shows similar results for the case of the fastener loading on the hole, while Fig. 3.20 shows the combined effect of far-field loading as well as the fastener loading. As in the case of the central crack discussed in Sec. , the stiffer the adhesive layer and the stiffer the patch, the more reduction is achieved in the k-factor near the patched crack-tip. On the other hand, a stiff adhesive layer has a deleterious effect on the integrity of the patch itself, as the adhesive shear stresses also increase as the adhesive stiffness increases.
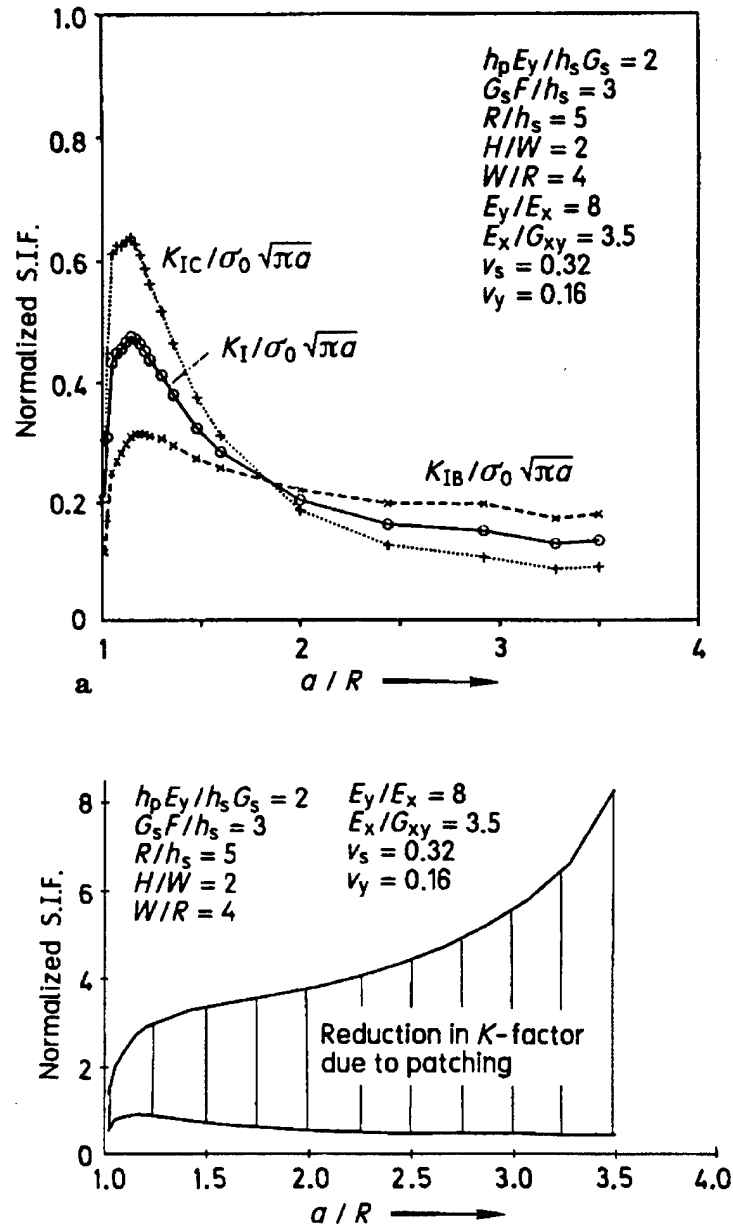
Figure 3.16: (a) Variation of nomalized k-factor as a function of the crack-length (repaired case); (b) reduction in k-factor (for $\sigma_o = 1$), due to repair, for cracks emanating from a loaded fastener hole
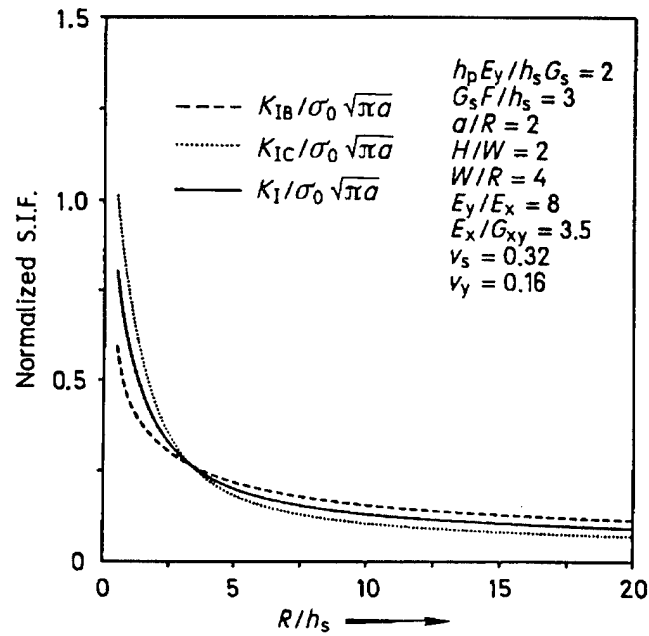
Figure 3.17: Variation of nomalized k-factor for a given crack length, as a function of the hole radius(repaired case)
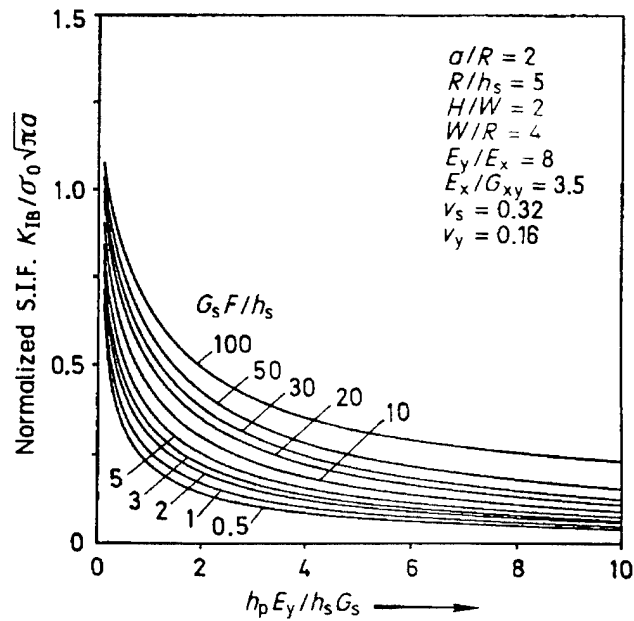
Figure 3.18: Variation of nomalized k-factor, K_{IB}, for a given crack length, as a function of the patch stiffness and adhesive flexibility
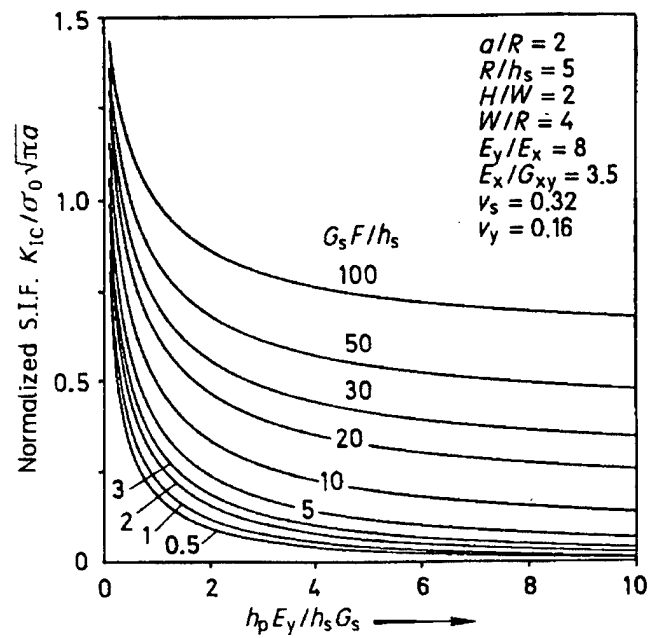
Figure 3.19: Variation of nomalized k-factor, K_{IC}, for a given crack length, as a function of the patch stiffness and adhesive flexibility
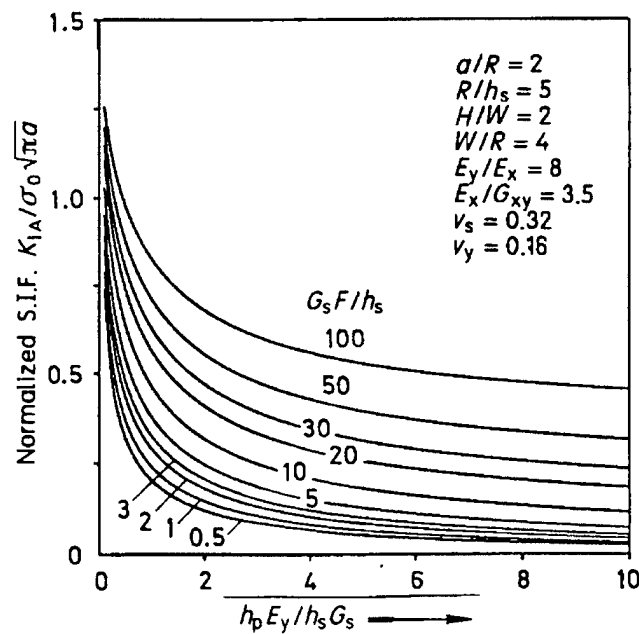
Figure 3.20: Variation of nomalized k-factor, K_{IA}, for a given crack length, as a function of the patch stiffness and adhesive flexibility
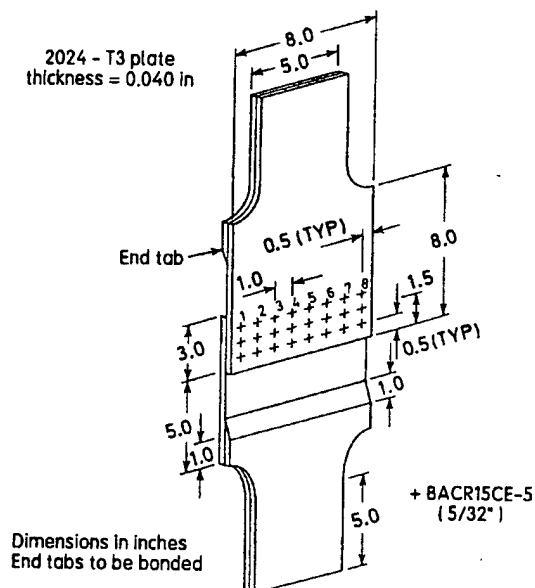
Figure 3.21: Uniaxial fuselage lap joint specimen

Multiple-site-damage in a fuselage lap-joint

A model of a typical lap joint, and a typical multiple site damage near a row of fastener holes, are illustrated in Fig. 3.21 and b, respectively. Taking into account the fastener flexibility, the fastener reaction forces on the upper (or lower) skin can be determined for the lap-splice joint configuration of Fig. 3.21, through the finite element method[Park, Ogiso, and Atluri (1992)]. Once these reaction forces, treated as concentrated forces, are determined, one may use the known elasticity solution, to approximate the stress field on the hole-surface in the skin, that is equivalent to these concentrated forces. Under the action of these fastener-interaction stress fields and the far-field hoop tension, the stress-intensity factors for multiple cracks near fastener holes can be determined using the FEAM described in this section. The corresponding reduction in k-factors due to patching can be obtained again, using the FEAM, as described in this section.

3.1.3 Three-dimensional analysis of surface-flaws with and without repairs

In the FEAM applied to three-dimensional problems of embedded and/or surface flaws (of elliptical or part-elliptical shapes) in structural components, the key ingredient is the analytical solution for an embedded elliptical flaw in an isotropic elastic solid, the crack-faces being subjected to arbitrary tractions [Atluri (1986); Nishioka and Atluri (1983); Atluri and Tong (1991)]. Here we describe some applications of the three-dimensional FEAM to the analysis of surface-flaws in aircraft structural components, with and without composite-patch repairs.

Corner flaw near a counter-sunk rivet hole

The problem of a counter-sunk rivet hole with a surface-flaw emanating from the corner is shown in Fig. 3.23. This is a typical situation in an aircraft-fuselage lap-joint. In the early stages of fatigue, this

2024 – T3 plate   Tolerance = 0.025 mm
$t = 0.040"$

"Crack angle = 0"

Upper plate

Crack length
1.225 mm

Hole $\varnothing$ = 3.85 mm

3.81   25.4   63.5

b   203.2
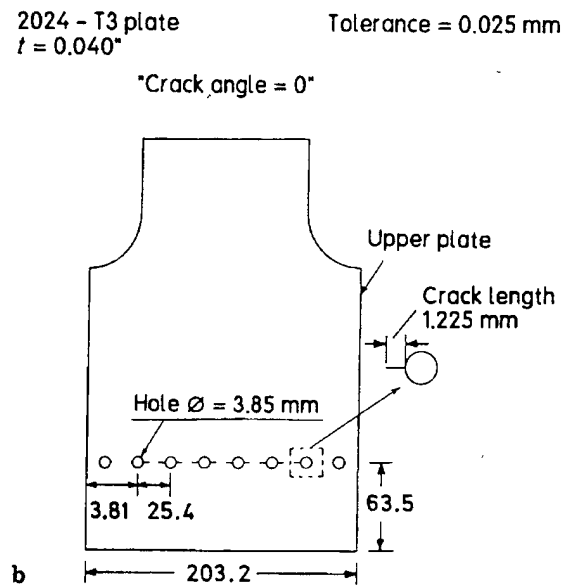
Figure 3.22: details of spark eroded crack starters

15 r

50°

Circular
surface
crack

2 r
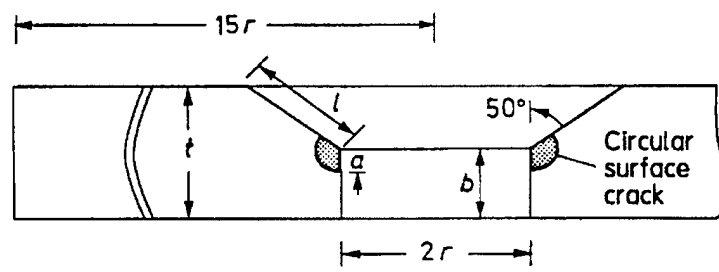
Configurations: a/l = 0.2, 0.5, 0.8
r/t = 2.0, 1.0, 0.5
b/t = 0 & b/t > 0.0

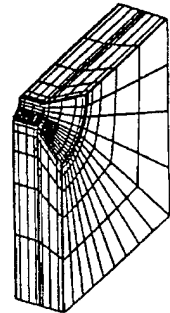Loading :   Remote tension
Remote bending

Figure 3.23: Schematic of a counter sunk rivet hole with a surface crack

Counter – sunk Rivet

Elements: 1,430   20–node elements
Nodes: 6,828
D.O.F.:   20,484

(Assumes symmetry of plate & cracks)

90 Elements only
(20 nodes)
202 Nodes
606 D.O.F.

Conventional FEM
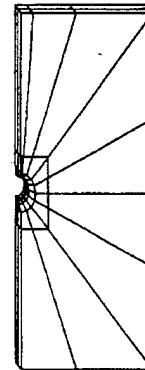
Present model
(Finite Element Alternating Method)

Figure 3.24: Typical finite element models

surface flaw grows into a through-the-thickness crack emanating from the fastener hole leading ultimately to the development of multiple-site-damage near a row of such fastener holes.

Fig. 3.24 shows a comparison of two different finite-element models: (i) Fig. 3.24a shows a finite element model of (1/4) of the plate when two surface cracks are assumed to emanate symmetrically from either side of the hole. In this finite element model, crack-tip elements are used in an explicit numerical modeling of the crack-tip singularity. Because of this, this model involves 1430 twenty-node finite elements, with a total of 20,484 degrees of freedom; (ii) Fig. 3.24b shows the finite element model in the present FEAM. In this model, only one surface crack is assumed to emanate from one side of the hole; and the crack-tip singularity is treated analytically through the solutions given in Vijayakumar and Atluri (1981) and Nishioka and Atluri (1983). Because of this, the finite element model involves only 90 twenty-node elements with a total of only 606 degrees of freedom. Thus, the savings in computational time, as well as in the data preparation time, in the present FEAM are truly significant.

In Fig. 3.25, a comparison of the results from a conventional FEM, and the present FEAM, is shown for the normalized k-factor at the tip of the minor axis of the quarter-elliptical flaw, as a function of the ratio of the depth of the hole (without counter-sink) to the depth of the plate. The FEAM with only 1575 d.o.f. gives as good a set of results as the conventional FEM with 20,484 d.o.f.

Three-dimensional problem of a plate with a surface crack: effect of patching

Consider the problem of a base plate with a surface crack, with a composite patch, as shown in Fig. 3.26. We assume that the sizes of the base plate and patch are infinite (this assumption is reasonable as long as the widths and lengths of the plate as well as the patch are about five times the length of the semi-major axis of the elliptical surface flaw, as in Fig. 3.26), but that the thicknesses of the base plate as well as the patch are finite. Let the thicknesses of the base plate and the patch be h_s and h_p respectively. The loading is assumed to be far-field tension, as in Fig. 3.26.
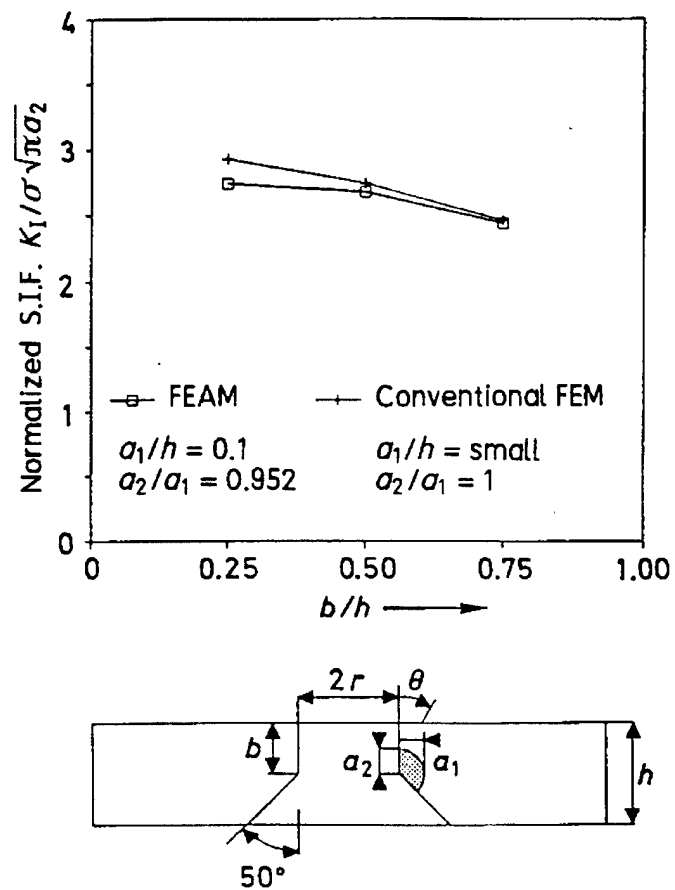
Figure 3.25: Variation of k-factor at minor axis of ellipse as a function of hole depth
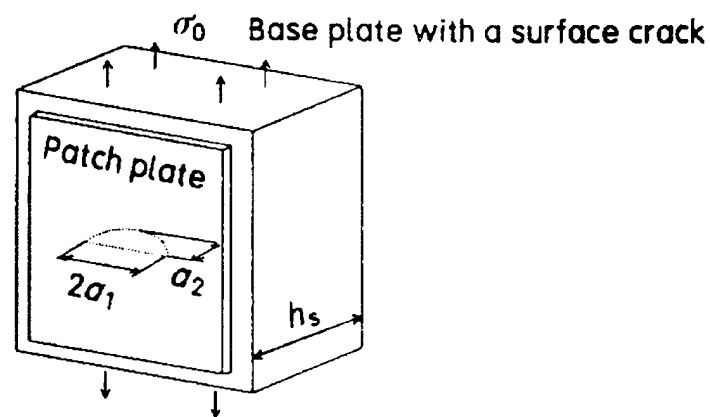
Figure 3.26: Schematic of a patched, surface-flawed thick plate
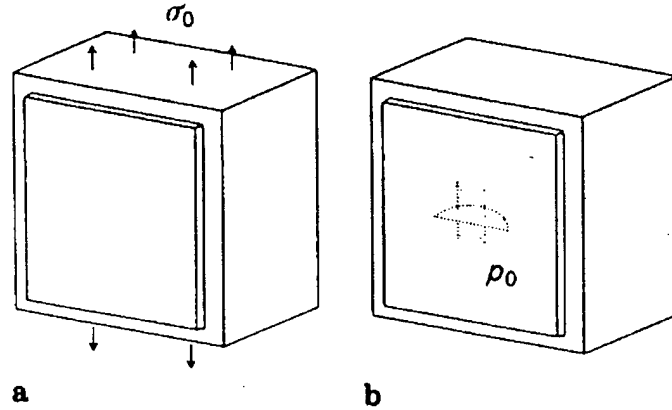
Figure 3.27: Linear superposition of (a) a patched plate without a crack subjected to far-field stress, and (b) patched plate with a crack subjected to crack-face pressure
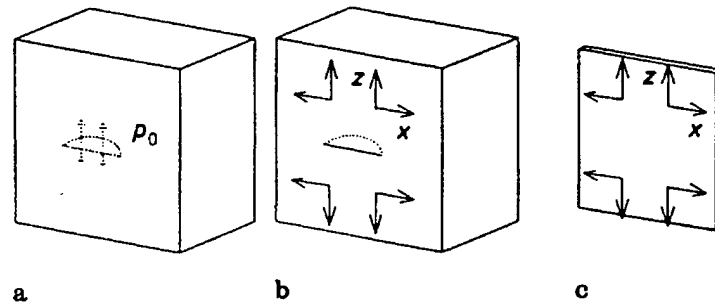
Figure 3.28: Linear superposition of basic problems

The problem in Fig. 3.26 can be solved by using the superposition principle as town in Fig. 3.27. In this case, the displacement fields of the basic problems as shown in Fig. 3.27 need to be solved for.

Fig. 3.28a is the case wherein uniform stress σ_0 is applied on the crack-surface. The displacement field for this problem is generated by using an analytical alternating technique, wherein the analytical solution for an infinite body containing an embedded elliptical flaw, subjected to arbitrary crack-face tractions, is employed. This analytical solution has been previously obtained by Nishioka and Atluri (1983).

Fig. 3.28b shows the problem wherein point loads X, Z are applied symmetrically at the points (x_0, z_0), $(x_0, -z_0)$, $(-x_0, z_0)$, $(-x_0, -z_0)$ on the plate with a semi-elliptical surface crack. Let the displacements at a point (x, z) on the front surface $(y = 0)$ be expressed as

$$u = H_{11}(x, z; x_0, z_0) X + H_{12}(x, z; x_0, z_0) Z$$
$$w = H_{21}(x, z; x_0, z_0) X + H_{22}(x, z; x_0, z_0) Z$$

The problem of Fig. 3.28c is one wherein point loads X, Z are applied symmetrically on an infinite
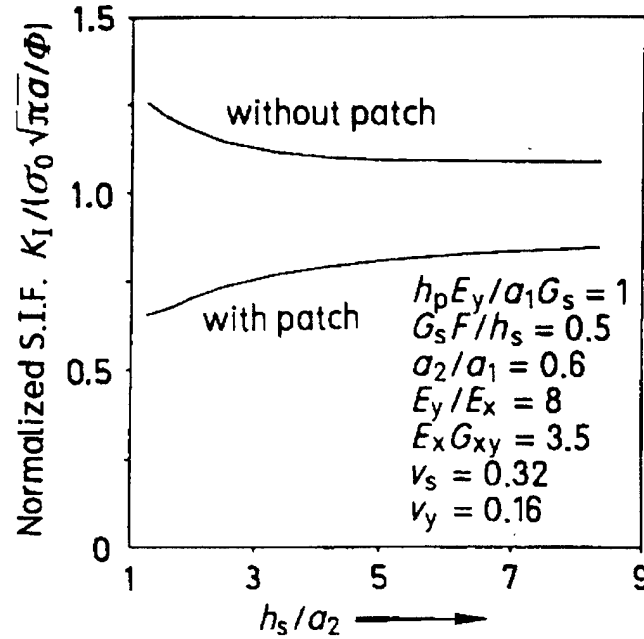
Figure 3.29: Reduction in k-factor due to patching as a function of crack-depth ratio

orthotropic plate. This solution has been reported on previously. Let the displacements at a point (x, z) for this problem be expressed as:

$$u^P = K_{11}(x,z;x_0,z_0)X + K_{12}(x,z;x_0,z_0)Z$$

$$w^P = K_{21}(x,z;x_0,z_0)X + K_{22}(x,z;x_0,z_0)Z$$

Let the displacements U5 and w5 denote the total displacements from problems 3.28A and B. The compatibility conditions between the base plate and the composite patch are expressed as

$$\tau_{xz} = \frac{u^s - u^P}{F}, \quad \tau_{yz} = \frac{w^s - w^P}{F}$$

where F is the adhesive flexibility, defined as earlier, as

$$F = \frac{h_a}{G_a} + \frac{3h_p}{8G_p}$$

By using these compatibility conditions, integral equations are derived for τ_{xz} and τ_{yz}. Once these are solved for, the k-factors are obtained in a manner described in earlier sections.

Fig. 3.29 shows the effect of the thickness of the base plate on the normalized stress-intensity factors for both the unrepaired and repaired cases. When the base plate thickness is small, about 50% reduction in k -factor is obtained. As the base plate becomes thicker, however, the effect of the patch is reduced (to about 40%), and the k-factor converges to a constant value. (Note that in the case of the surface-flaw, the k-factor that is considered is at the intersection of the crack-front with the front face of the base plate). From
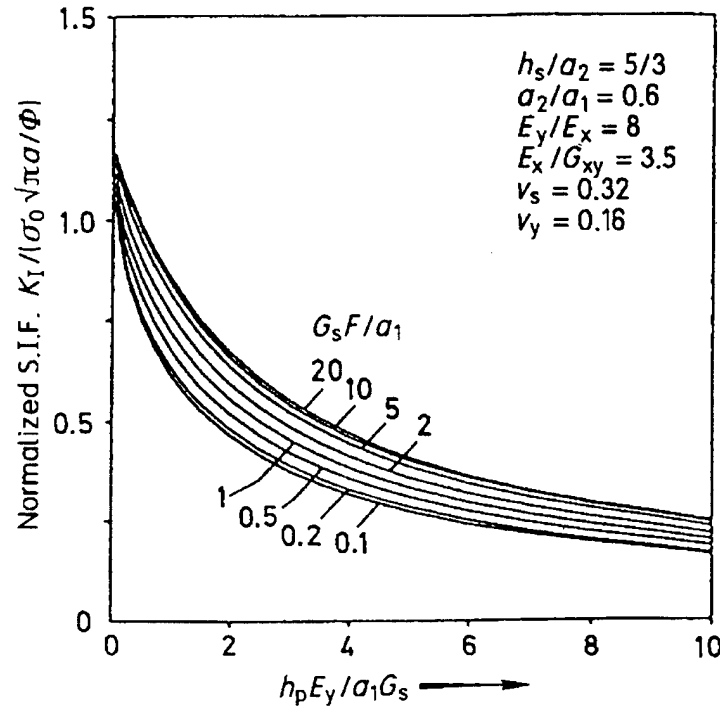
Figure 3.30: Effects of patch stiffness and adhesive flexibility on the k-factor of a surface flaw

Fig. 3.29 it is also noted that if one uses a very stiff patch, a better reduction in the k-factor is obtained. However, a stiff patch may increase the adhesive shear stresses.

Fig. 3.30 shows the effect of patch-stiffness parameters and adhesive flexibility parameters on the normalized k-factors.

Fig. 3.31 shows the effect of patch stiffness and adhesive flexibility on the adhesive shear stresses,τ_{yz}/σ_0 at $x = 0$, $y = 0$ and $z = 0$. Finally Fig. 3.32 shows the effect of the patch-stiffness and adhesive flexibility on the values of σ_{yy}^p.

Repair of a surface crack near a hole

The problem is shown schematically in Fig. 3.33. To repair the crack, a patch of width $2W_p$ and height $2H_p$ is applied, such that the center of the patch coincides with the center of the hole.

The basic component problems to be analyzed are shown in Fig. 3.34a-c. For problem 3.34a, the displacement fields on the front surface and the stress intensity factors can be obtained by using the 3D finite element alternating technique [Atluri (1986)].

As for problem 3.34b, when a point force (X, Z) is applied at the point (x_0, z_0) and a symmetrical point load $(X, -Z)$ is applied at $(x_0, -z_0)$, once again the 3D finite element alternating technique can be used.

In problem 3.34c, the displacement field in the patch is determined as before.

The finite element mesh used for problems 3.34a and b are shown in Fig. 3.35. The finite element mesh used for problem 3.34c is shown in Fig. 3.36.
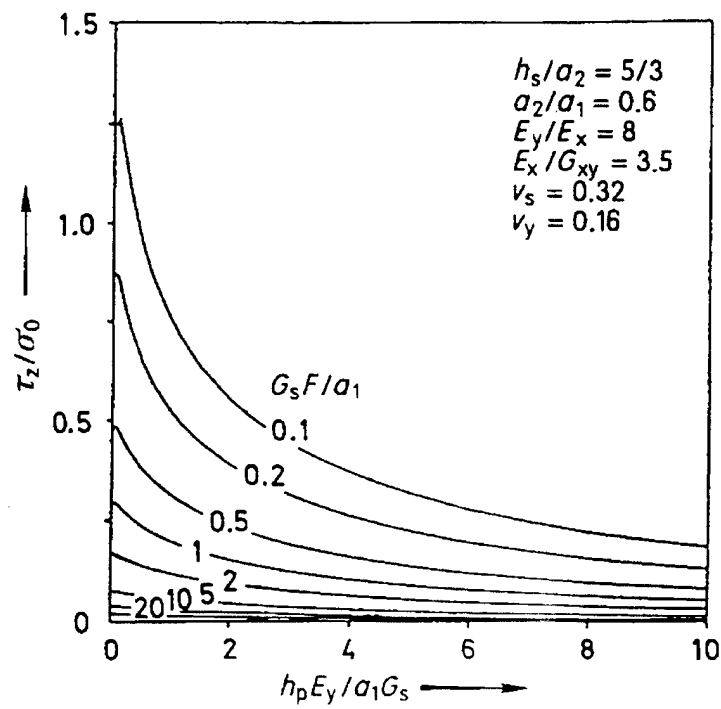
Figure 3.31: Effects of patch stiffness and adhesive flexibility on the shear stress in the adhesive at $x = y = z = 0$
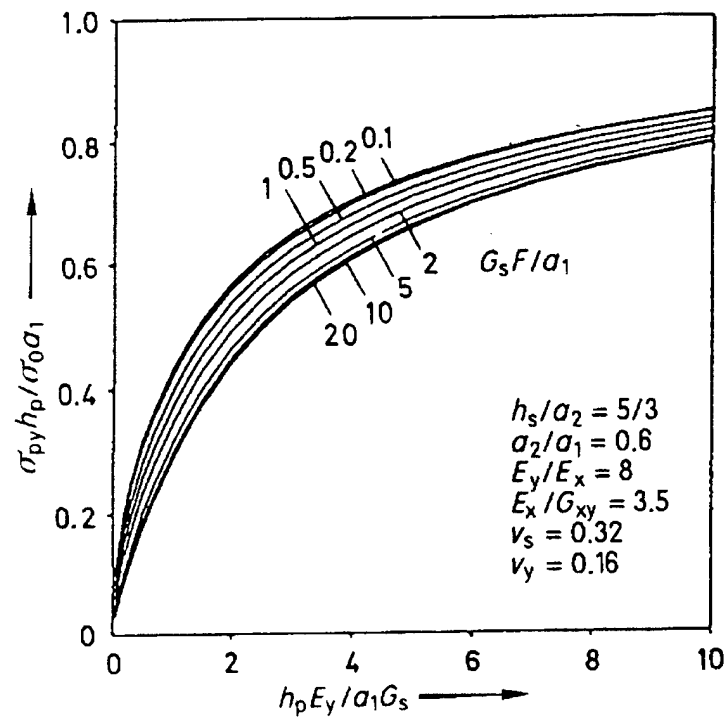
Figure 3.32: Effects of patch stiffness and adhesive flexibility on the tensile stress in the patch
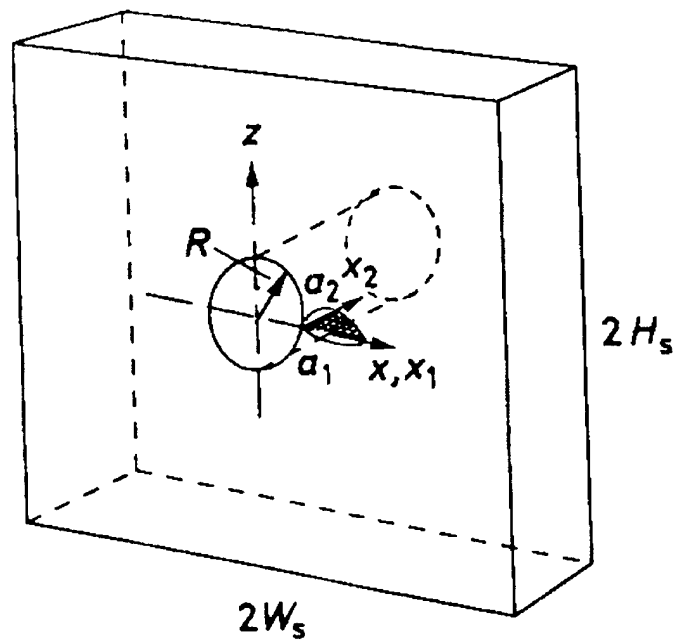
Figure 3.33: Schematic of a surface flaw near a fastener hole
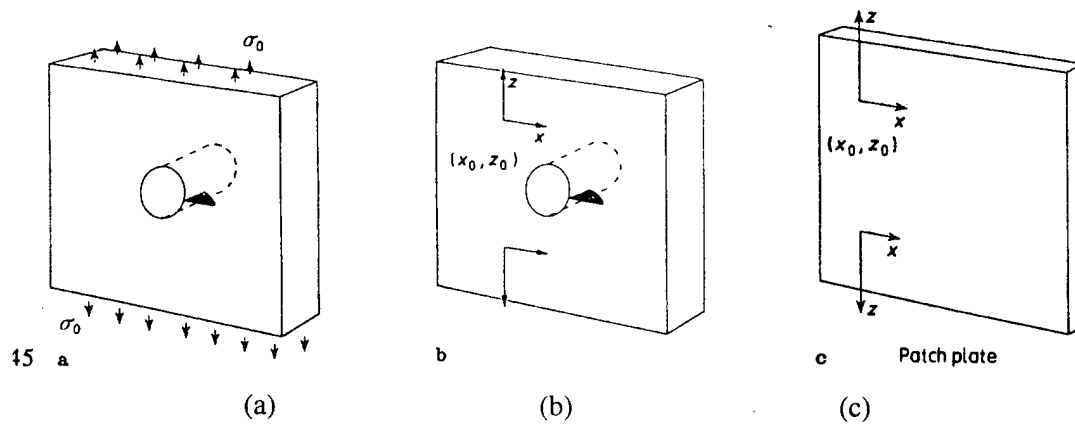
Figure 3.34: Linear superposition of basic problems in the analysis of patching of a surface flaw near a fastener hole
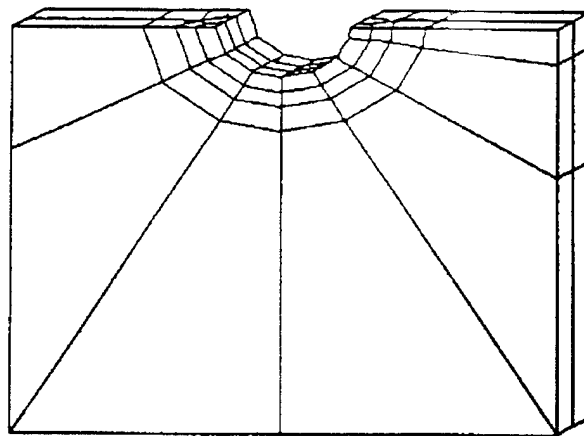
Figure 3.35: FEM mesh for base plate (56 ele., 401 nodes)
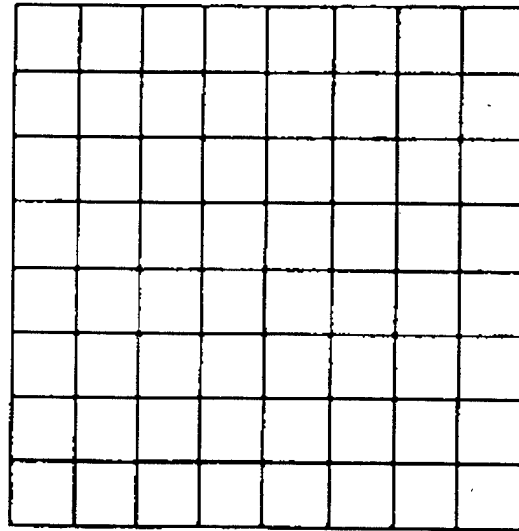
Figure 3.36: FEM mesh for patch plate, 64 2D 8 node isoparametric elements, 225 nodes
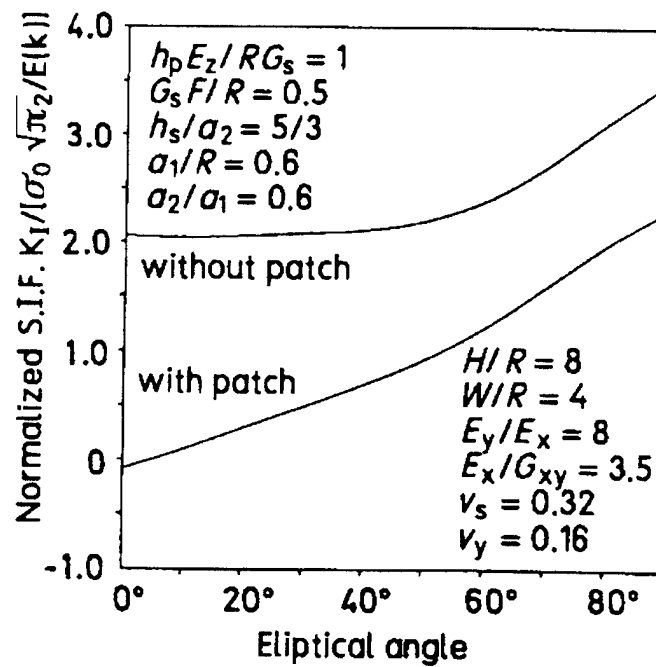
Figure 3.37: Variation of S.I.F near the border of a surface flaw near a fastener hole, with and without patching

The variations of the stress intensity factor along the crack front, with and without repair patch, are shown in Fig. 3.37. Once again, the significant reduction in the crack-growth retardation, achieved by the application of the patch, is evident.

Simplified computational procedures for the analysis of structural integrity problems in aging airplanes, with and without composite-patch repairs, have been developed, and their use is illustrated.

3.2 Patch repair and curved crack

3.3 Analysis Of Repaired Cracks in Pressurized Aircraft Fuselages

Repairs to pressurized fuselages have been done traditionally by using mechanical doublers. While bonding of metal structures and bonded repair techniques have existed for about 50 years now, bonded repairs have not gained as much acceptance as the mechanical doubler repairs. This is mainly due to the disappointing early experience with bonding and the lack of widespread understanding of bonded repairs among technicians. This provides the motivation for the development of effective analysis techniques that can be implemented on low end workstations. In this investigation, the mechanical doubler repairs have been compared with bonded repairs in the repair of cracks in the fuselage skin. To analyze the effect of global loading (viz. pressure loading in the fuselage shell), on the essentially local feature of repair, a hierarchical approach has been used. This allows the fuselage to be modeled with increasing detail over smaller regions. At the global level, the fuselage is modeled as a shell, with stiffeners modeled as beams, and with flexible fasteners. In the intermediate stage the degree of modeling is improved. A section of the fuselage from the global stage is now analyzed, with the stiffeners being modeled with shell elements. The kinematic boundary conditions applied to this smaller intermediate region are obtained from the global solution. The stress results from this intermediate zone are later applied to a still smaller zone that is analyzed in the local stage; and this local analysis is used to evaluate the stress intensity factors for repaired or unrepaired cracks. The local stage uses a 2D finite element alternating method (FEAM) to model the crack. At this stage, the bending effects caused by a bonded patch on one side of the skin are ignored. This assumption is considered sufficient as the substructure of the fuselage will restrict the effect of bending from being of any significance. The local analysis accounts for the non-linearity of the adhesive material by modeling it as an elastic perfectly plastic material. A large difference in the extensional stiffness of patch and the skin results in large strains being induced in the adhesive. Therefore, the necessity to model the adhesive as an elastic perfectly plastic material becomes more critical when the patch extensional stiffness is large when compared to the skin extensional stiffness. Using this approach the stress redistribution caused by mechanical doubler repair is compared with that caused by composite patch repairs. The residual strength and fatigue life of fuselages with composite patch repairs have been compared with those of the un-repaired case. The stress intensity factors have been evaluated by considering the adhesive as elastic material and as an elastic perfectly plastic material. Parametric studies of composite repairs are conducted using this methodology.

Most of the present day repairs to cracked aircraft fuselages are performed by using mechanical doublers. The cracked portion is cutout, a sheet is placed in the region thus created; and finally, another sheet is riveted to this cutout portion and the skin.

From the Second World War, successful applications of adhesive bonding have been made in aircraft structures. The Fokker F-27 aircraft is an example of successfully operating aircraft that has employed adhesive bonding for primary structure [Baker and Jones (1988)]. While such success stories exist , doubts about adhesive bonded repairs still exist. In this section we study such bonded repairs and compare them

with mechanical doubler repairs.

There are several methods for the analysis of patched cracks. They can be broadly divided as

1. Analytical

2. Finite Element Approach

The analytical approach of Rose (1981) is an elegant method based on Hart-Smith (1974) theory of bonds, elastic inclusion analogy, and on some simplifying assumptions. Fredell (1994), in his exhaustive thesis, has extended this analysis to include thermal effects. He has also carried out an evaluation of mechanical doubler repairs. Erdogan and Arin (1972) have used integral equations approach to study the patched cracks. The assumptions of Erdogan and Arin were subsequently used by Ko (1978) and Hong and Jeng (1985) in the analysis of sandwich plates with part-through crack.

Jones and co-workers [Jones and Callinan (1979)], Mitchell, Wooley, and Chivirut (1975); Chu and Ko (1989) used finite element method to study patched cracks. Park, Ogiso, and Atluri (1992) have used an integral approach combined with FEAM to estimate the stress intensity factors for patched panels. Tarn and Shek (1991) have combined boundary element method approach (for the plate) and finite element method (for the patch) to estimate the stress intensity factors. Other work in this area includes Atluri and Kathiresan (1978), Sethuraman and Mathi (1989), and Kan and Ratwani (1981).

In most of these approaches, only patches of infinite size, or very narrow strip type patches, or infinite sheet cases are considered. All of these cases are valid only for flat sheets. The loading for all these analyzes are hoop stresses evaluated from basic thin shell theory. While, in most cases this is a good approximation, this does not take into account the stress re-distributions due to the curvature and due to the presence of stiffeners.

The present work addresses the problem of the study of patched cracks in actual commercial airliner fuselages. A hierarchical modeling strategy is used to study the repairs to fuselages. The methodology is as follows. The whole of the fuselage is studied in the first stage. In the next stage, a portion of this is studied with an increase in complexity of the model. Finally a small portion around the crack and the repairs is studied to estimate the stress intensity factors. The procedure used to analyze the local zone is the finite element alternating method. This methodology to study repairs to fuselages. The stress re-distributions caused by mechanical doubler repairs is contrasted with those by patch repairs. The effect of various parameters such as the patch dimensions, patch material, patch thickness, adhesive material and adhesive thickness on patch efficiency is studied.

3.3.1   Methodology

The problem of cracks and their repairs is a localized phenomenon. The known loading conditions on the fuselage are essentially global – viz. the pressure loading. Therefore the analysis requirements are conflicting – a global loading and an essentially local phenomenon. This necessitates a hierarchical modeling strategy (Starnes and Britt 1991). Fig. 3.3.1. This allows an increasing level of complexity and fidelity in the modeling without a prohibitively high computational effort.

The global model is a linear elastic shell finite element analysis. In this analysis the stiffeners are modeled as beams. The fuselage is modeled with shell elements. The fasteners are modeled as shear springs. In the analysis of the cracked unrepaired fuselage, the crack is modeled in the global analysis only
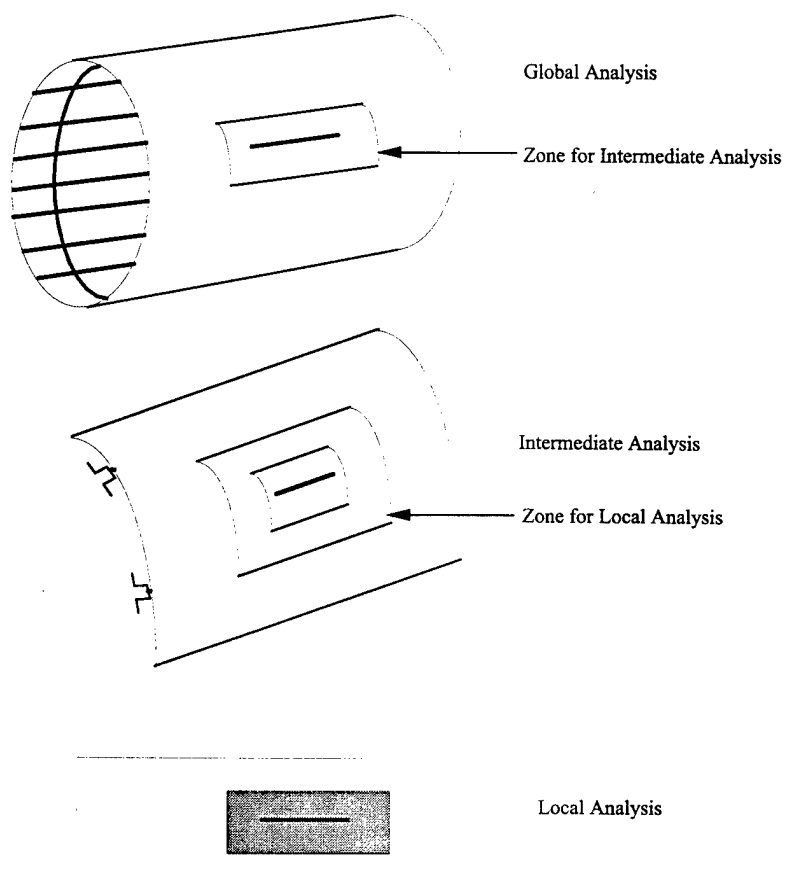
Figure 3.38: Schematic of the Hierarchical Modeling Strategy

crudely, i.e., via unconnected finite elements while ignoring the crack-tip singular fields. In the analysis of a composite patch-repaired fuselage, it is assumed that the bending caused by the patch dies down and at this global stage of analysis, it can be considered as an uncracked fuselage. Therefore, the repaired fuselage is considered as an intact fuselage in the global level of analysis. In both cases, symmetry conditions approximating a full fuselage are applied to the region analyzed. As the shell length considered is small when compared to the length of actual fuselages, the axial ends are restrained from motion in the axial direction.

A portion of the fuselage in the circumferential as well as longitudinal directions is now taken and analyzed in the intermediate model. In this model, the fidelity is increased by modeling the stiffeners with shell elements. The fasteners are modeled by short beams. The essential boundary conditions for this model are obtained from the global analysis. In both of the above models the loading is internal pressure.

A smaller portion of the fuselage that contains the crack and repair is then analyzed in the local analysis. As the region is small, the pressure loading and the curvature are disregarded. The loading on this region are the tractions obtained from the intermediate model. The local analysis proceeds in two stages. In the first stage, the crack is explicitly modeled with ordinary finite elements, (i.e , without paying attention to the singular fields) and the stresses exerted by the composite patch on the metallic sheet are deduced. The mesh for this analysis is not detailed as the aim at this stage is to obtain the stresses exerted by the patch and adhesive on the sheet and not to model the crack tip singularity. Once the patch stresses are deduced, the finite element alternating method is used to obtain the stress intensity factors.

Global Analysis

The stiffeners at this stage are modeled as beams. The beam element is obtained by collapsing the shell element described above. As the fastener flexibility is crucial (Swift (1974), (1984)), the fasteners are modeled by flexible shear springs. The stiffness for this fastener element is given as in Swift (1974, 1984) by

$$K = \frac{E_s D}{A + C\left(\frac{D}{t_1} + \frac{D}{t_2}\right)} \tag{3.58}$$

where E_s is the sheet Young's Modulus, D is the rivet diameter, t_1 and t_2 thicknesses of joined sheets, $A = 5.0$ for Al rivets and 1.66 for steel fasteners, and $C = 0.8$ for Al rivets and 0.86 for steel fasteners. The rivet holes are not explicitly modeled.

The crack is modeled with split nodes. There is no explicit modeling of the crack tip singularity.

Intermediate Analysis

The intermediate analysis is also a linear finite element analysis and is also based on the aforementioned principles. The element used at this stage is a four-noded six degree of freedom per node element (Rankin and Brogan(1991)). In the analysis of shells a two parameter specification of the the director field about the mid-surface is sufficient if the mid-surface is smooth. In the presence of shell intersections, this is not sufficient. A standard way of handling such intersections is the usage of shell elements with drilling degrees of freedom (See Simo (1993) and Fox and Simo (1992) for example). The element used is one such element. Therefore, the facets that arise as a result of modeling the stiffeners with shells elements can be handled. This element uses an incompatible displacement field with a cubic variation of the bending field and a linear/cubic variation of the in-plane field.

In this model, the stiffeners are also modeled with the same shell elements. The fasteners are modeled as short beams. As in the global model the rivet holes are not explicitly modeled. Again the cracks are modeled with split nodes and there is no explicit modeling of the stress singularity.

Local Analysis

The local analysis is a two stage analysis. They are

1. Evaluation of the stresses exerted by the adhesive and patch on the sheet, using a coarse mesh.

2. The stresses obtained from stage 1 are applied as body forces on the base sheet, and the finite element alternating method is used to find the stress intensity factor.

In step 1, a traditional finite element methodology is used to deduce the stresses exerted by the patch. As the crack tip is not meshed for the singularity, a coarse mesh is sufficient for this purpose. The sheet and the patch are modeled with eight noded 2D elements. The adhesive is modeled by elements as in Jones and co-workers [Jones and Callinan (1979)], Mitchell, Wooley, and Chivirut (1975). This element is obtained by assuming a constant shear stress in the adhesive. Under the present conditions the shear stress can be obtained from

$$\tau_{xz} = \frac{u_s - u_p}{\frac{t_a}{g_a} + \frac{3}{8}\left(\frac{t_s}{g_s} + \frac{t_p}{g_p}\right)} \tau_{yz} = \frac{v_s - v_p}{\frac{t_a}{g_a} + \frac{3}{8}\left(\frac{t_s}{g_s} + \frac{t_p}{g_p}\right)} \tag{3.59}$$

where u and v are the displacements in the x direction and y direction respectively, t, g are the thickness and shear modulus respectively. The subscripts a, s and p refer to the adhesive, sheet and the patch respectively.

Large strains are induced in the adhesive when the difference between the patch stiffness and sheet stiffness is large. Therefore, this results in the yielding of the adhesive. This reduces the patched efficiency, and a linear elastic analysis would grossly overestimate the efficiency and would be anti-conservative. Therefore, the adhesive is modeled as an elastic perfectly plastic material. As there is no unloading (crack growth is not considered), a deformation theory of plasticity is considered sufficient. An initial stress algorithm [Nayak and Zienkiewicz (1972)] has been implemented. In view of the model as in Jones and co-workers [Jones and Callinan (1979)], Mitchell, Wooley, and Chivirut (1975), the Von Mises yield criterion reduces to

$$\sqrt{\tau_{yz}^2 + \tau_{xz}^2} = \frac{\sigma_{yp}}{\sqrt{3}} = \tau_{yp} \tag{3.60}$$

The algorithm for this is as follows

1. A load step is taken and the displacements are found.

2. The stresses are computed at each Gauss Point and yielding is checked for.

3. The residual load is computed.

4. The displacements for this residual load are then computed.

5. Repeat steps 2, 3 and 4 for convergence. Convergence is reached when there is no yielding at any Gauss point.

6. Repeat the steps 1,2,3,4 and 5 for more load steps till the desired load is reached.

In finite element alternating method, the stresses in the uncracked body are first analyzed, by a traditional finite element method, for the given system of external loading. To model the crack, the tractions at the locations of the crack in an otherwise uncracked body must be erased.

Software

The above methodology has been implemented in a software based on several in-house and commercial finite element codes. The global model has been implemented in an in-house software called SOFRAC [Singh, Park, and Atluri (1994). The results from this analysis are taken and applied to the intermediate analysis. At this point it is relevant to point out the methodology adopted to interpolate the displacements between the models. While the fuselage shell has been modeled with shell elements in both the models, the stiffeners in the global model was modeled as beams; but are modeled as shells in the intermediate analysis. Therefore, a direct application of the displacements at the relevant locations becomes impossible. Instead, using the rotations and displacements in the beams that constitute the stiffeners in the global analysis, the displacements at the nodes of the shell elements that constitute the stiffeners in the intermediate model are obtained by extrapolation. It is noted at this point this could lead to a stress mismatch in the boundary of the intermediate model as the idealization is different.

The intermediate model, with the kinematic boundary conditions obtained as illustrated above, is now solved by using STAGS [Almroth, Brogan, and Stanley (1986)]. The pre-processor used to generate the input files for STAGS analysis is an in-house pre-processor that carries out the aforementioned extrapolations.

The solution from the above is now used as the applied boundary condition for the local analysis wherein only a very small portion of the skin(with the patch) are modeled. As indicated above, the local analysis is based on 2-D finite element alternating method. Therefore, only the in-plane stresses are used. The out-of-plane stresses are neglected. As the substructure of the structure would restrict any severe bending this is believed to be a good approximation. The local zone is implemented in an in-house software PAN-MD. The input files for this analysis are generated by an in-house post-processor for STAGS. The entire analysis from the global to local has been automated in a PERL script.

3.3.2 Analysis of Repaired Cracks

The fuselage as described by Tab. 3.3.2 is used for the various test cases studied. The stringers used are of hat cross section and the frames are of Zee cross section. The stiffener properties are given in Tab. 3.3.2. It is noted that the frame is attached to the sheet on the tearstraps. This is considered as an approximation to attaching the frame to the sheet with shear clips. In view of the unavailability of the exact stiffener dimensions this is considered sufficient. The crack is assumed to be a mid-bay crack. The rivets used are NAS1097DD6 rivets of 0.15625 in diameter.

The dimensions of the different models are given in Tab. 3.3. The finite element meshes used for various models are shown in Fig. 3.39, Fig. 3.40 and Fig. 3.41.

Patch Repairs

The above fuselage is repaired with a patch of dimensions 5 in X 3 in as shown in Fig. 3.42. The patch is 0.04 in thick and is made of Boron Epoxy. The adhesive is 0.004 in thick and has a shear modulus of 104.73

Table 3.1: Properties of The Fuselage Shell

Internal Pressure	9.0 psi
Radius	78 in
Thickness	0.036 in
Material	Al 2024T3
Young's Modulus	10,500 ksi
Poisson's Ratio	0.33
Yield Point	47.0 ksi

Table 3.2: Stiffener Properties

Rivet Specification	NAS1097DD6
Rivet Diameter	0.15625 in
Stringer Spacing	9.25 in
Stringer Area	0.0384 in^2
Stringer Moment of Inertia	0.162 in^4
Axis to skin distance	0.465 in
Frame Spacing	20.0 in
Frame Area	0.1248 in^2
Frame Moment of Inertia	0.3271 in^4
Axis to skin distance	1.148 in
Tear Strap Thickness	0.036 in
Tear Strap Width	2 in

Table 3.3: Dimension of different fuselage models

Global Region Length	100 in
Global Region Arc Length	46.25 in
Intermediate Region Length	40 in
Intermediate Region Arc Length	18.5 in
Local Region Length	10 in
Local Region Width (Arc Length)	8 in
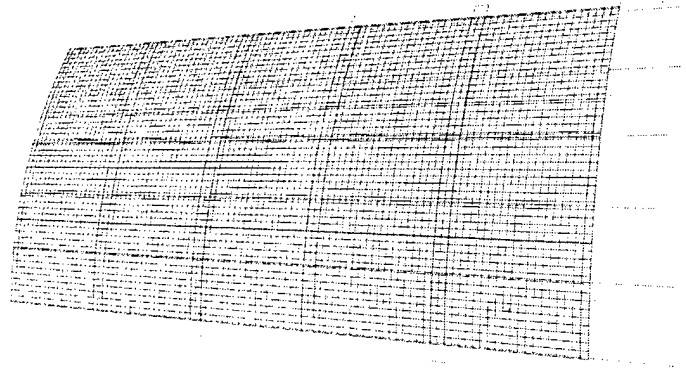
Figure 3.39: Mesh for Global Analysis
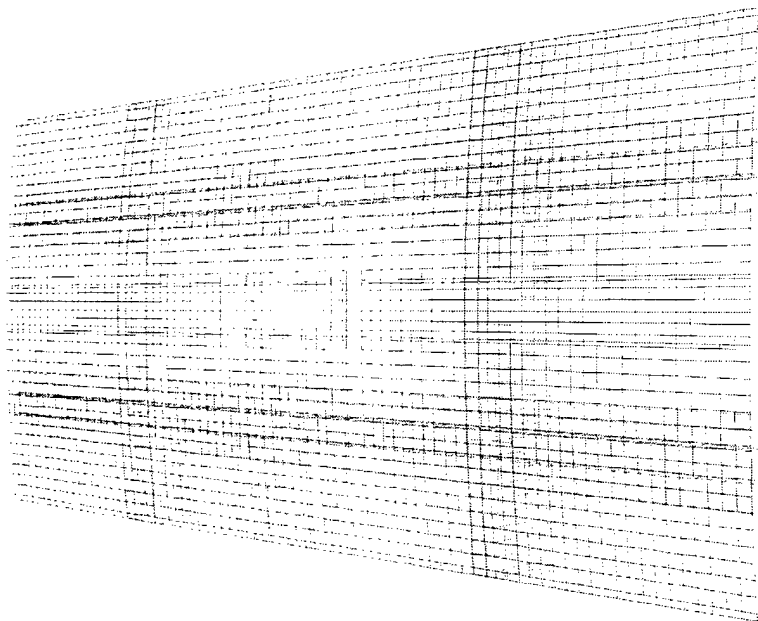
Figure 3.40: Mesh for Intermediate Analysis
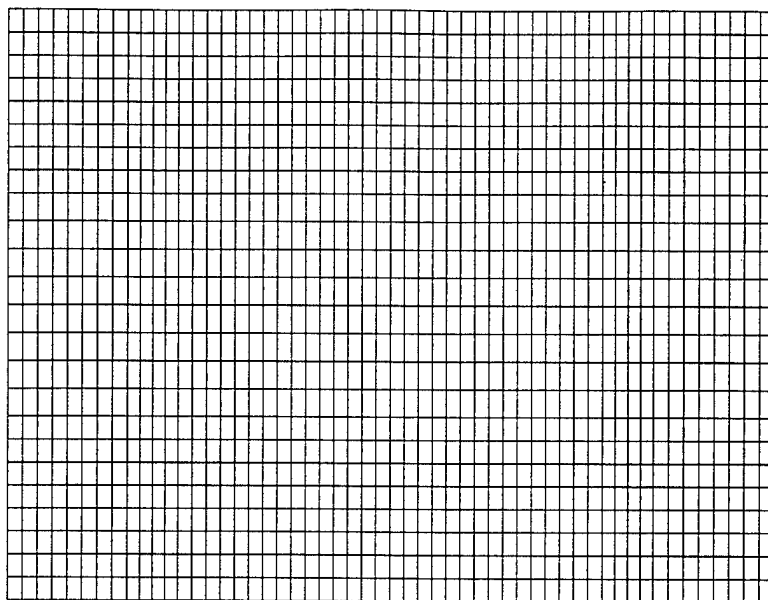
Figure 3.41: Mesh for Local Analysis

ksi with 5.250 ksi being the Yield Point in shear.

To analyze the effect of the patch, the crack length was varied from 1 in to 16 in. The variation of the stress intensity factor, K_I, with the crack length is shown in Fig. 3.43.(Unless otherwise noted all the stress intensity factors are in $ksi\sqrt{in}$ and the crack lengths are in in.) The efficiency of crack patching is plotted in Fig. 3.44. The efficiency is defined as

$$= \frac{SIF_{unpatched} - SIF_{patched}}{SIF_{unpatched}} \times 100$$

The asymptotic nature of the stress intensity factor, as in Fredell (1994) and Baker and Jones (1988) is clearly observed. Unlike the methodology of Rose (1981) and Fredell (1994), the present methodology can analyze cracks longer than the width of the patch. It is seen that while the stress intensity factors show a significant increase as the crack emerges from the patch, it still demonstrates an asymptotic behavior. In these two situations, viz. crack shorter than the width of the patch and longer than the width of the patch, the patch transfers load in significantly different ways. When the crack is shorter than the width of the patch, most of the load is transfered by the edges of the patch parallel to the crack. This is seen from the Fig. 3.46, where the effective stress in the adhesive has been plotted. As the crack grows longer than the width of the patch, the regions near the crack tips also start to transfer the load and the patch transfers the load as in bonded overlap joints. This is shown in the effective stress in the adhesive contour plot Fig. 3.47. This increase in the effective stress lead to a final yielding of the adhesive. Once the adhesive yields, a very significant reduction in the effectiveness in seen. (Fig. 3.44 and Fig. 3.45).

Patch Repairs and Mechanical Doubler Repairs

A mechanical doubler repair, Fig. 3.48, for the above mid-bay cracked fuselage is also analyzed. The axial (Fig. 3.49) and hoop stress (Fig. 3.50) resultants for the doubler repaired fuselage has been compared with
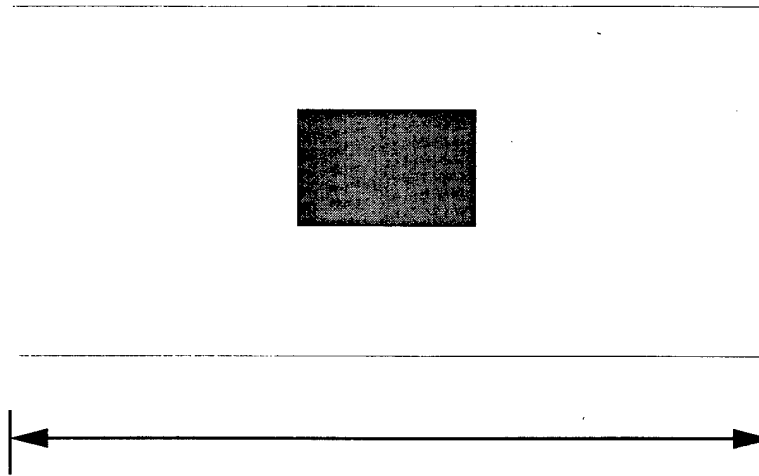
Figure 3.42: Geometry of the Local Zone showing the patch
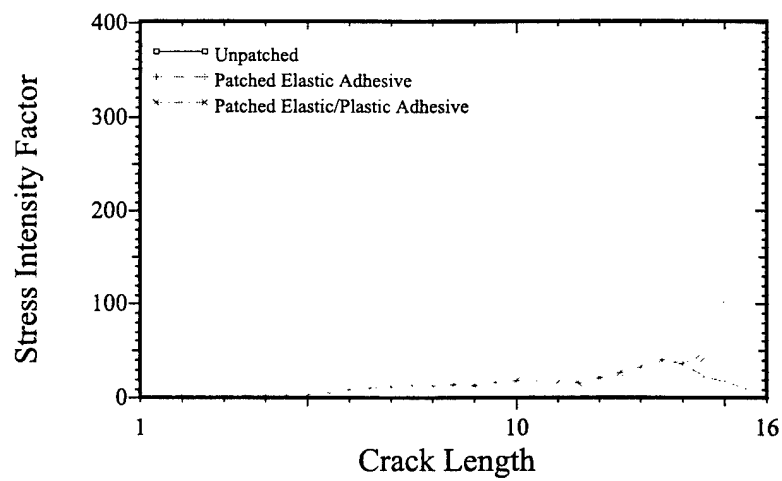
Figure 3.43: Stress Intensity factors Vs. Crack Length
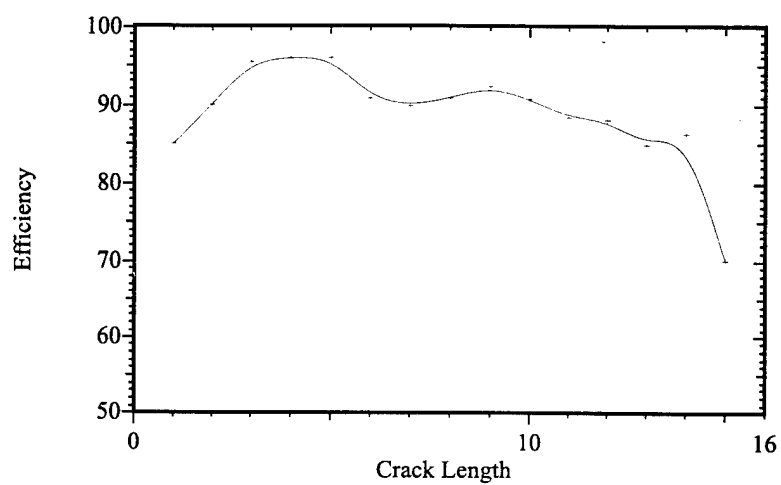
Figure 3.44: Efficiency of Crack Patching
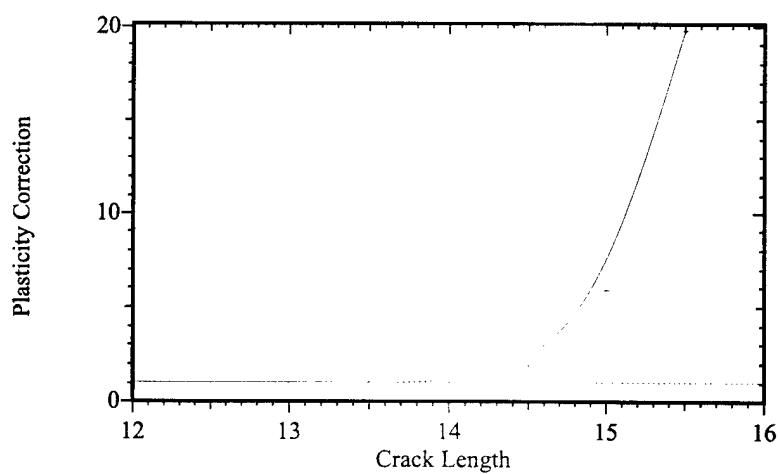
Figure 3.45: Effect of Plasticity
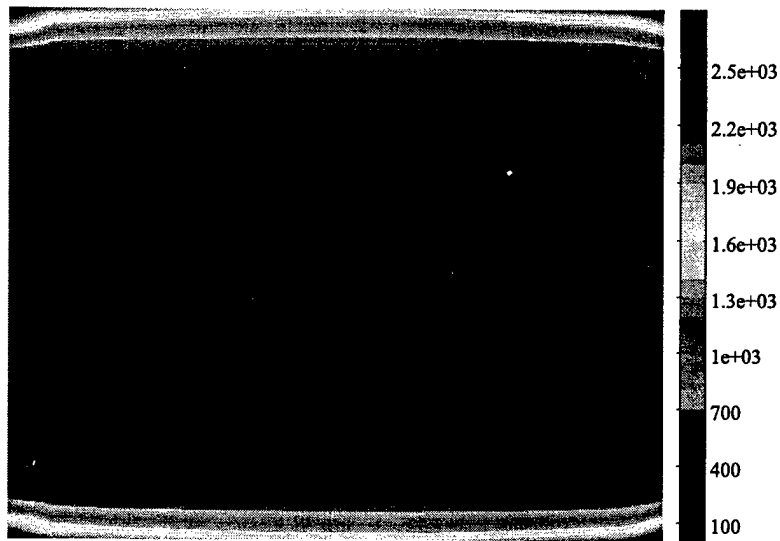
Figure 3.46: Effective Stress in the Adhesive for Crack Length 3 in
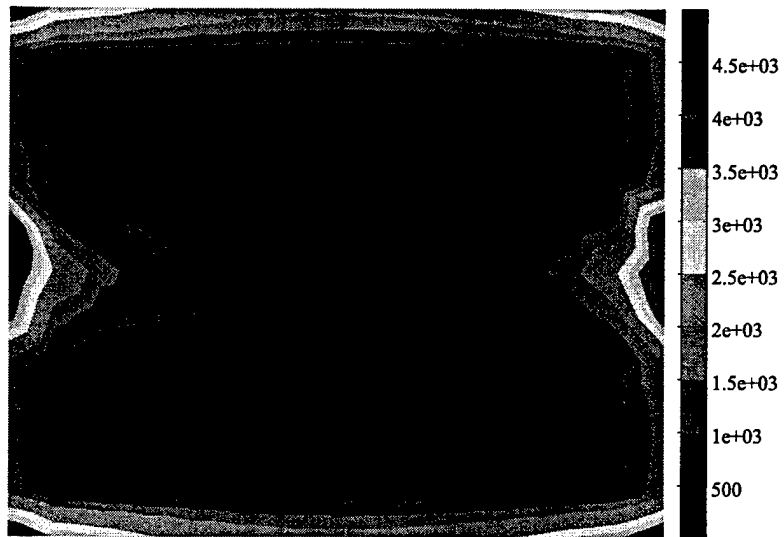
Figure 3.47: Effective Stress in the Adhesive for Crack Length 15 in
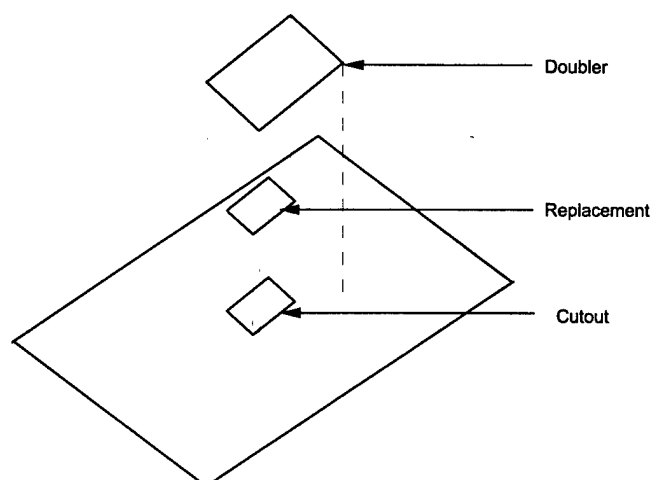
Figure 3.48: Geometry of the doubler repair
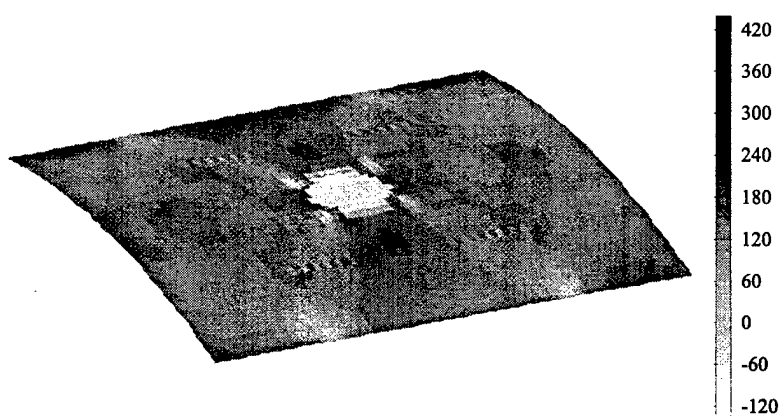
Figure 3.49: Axial Stress Resultant for Doubler Repair

that of the composite patch (Fig. 3.51 and Fig. 3.52) repaired fuselage and the intact fuselage (Fig. 3.53 and Fig. 3.54). As can be seen, a patch repair, despite the presence of the singularity involves a much lower value stress. In the doubler repair case, the cutout provides a site for stress concentration. Therefore, the maximum hoop stress in the doubler repair case increases from 19.1 ksi in the intact fuselage to 30 ksi. Whereas, in the fuselage repaired with a patch, the hoop stress went up marginally to 19.4 ksi. A similar pattern is also seen in the axial stresses where the stresses went up from 6.5 ksi to 11.7 ksi.

Effect of Patch Geometry

To study the effect of the patch overlap length of the patch (the length along the y direction), it was varied from 1.5in to 3.5 in. The results are in Fig. 3.55. The patch is 5 in wide and 0.04 in thick and is made of Boron/Epoxy composite. The adhesive is 0.004 in thick and has a shear modulus of 104.73 ksi.
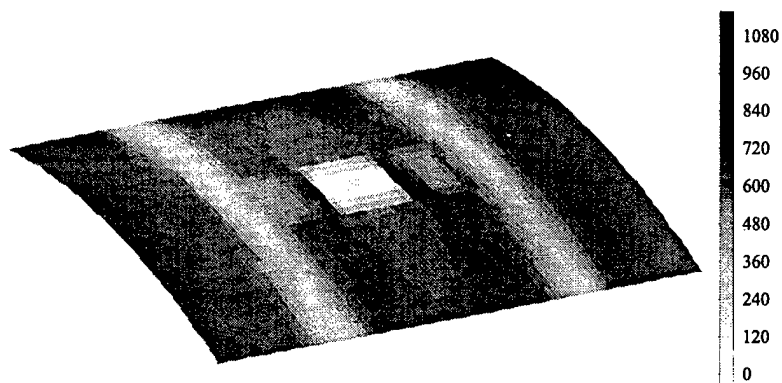
Figure 3.50: Hoop Stress Resultant for Doubler Repair
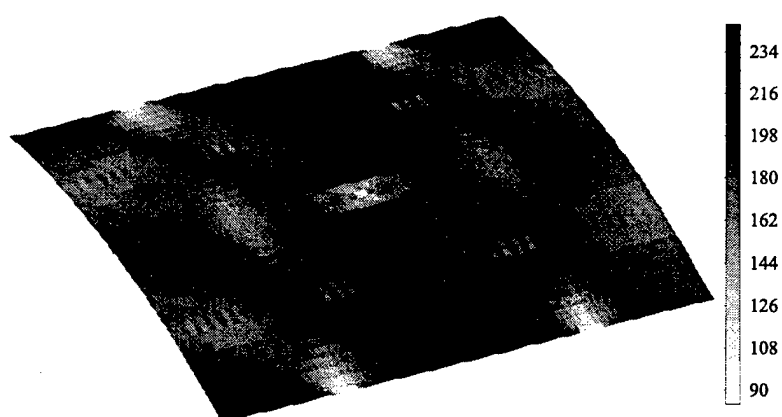
Figure 3.51: Axial Stress Resultant for Patch Repair
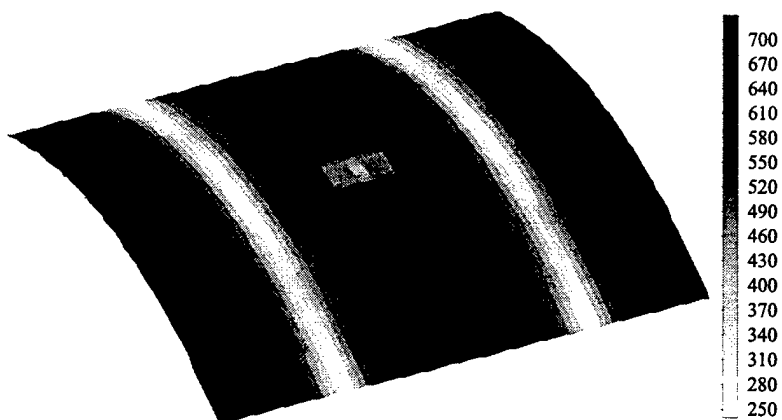
Figure 3.52: Hoop Stress Resultant for Patch Repair
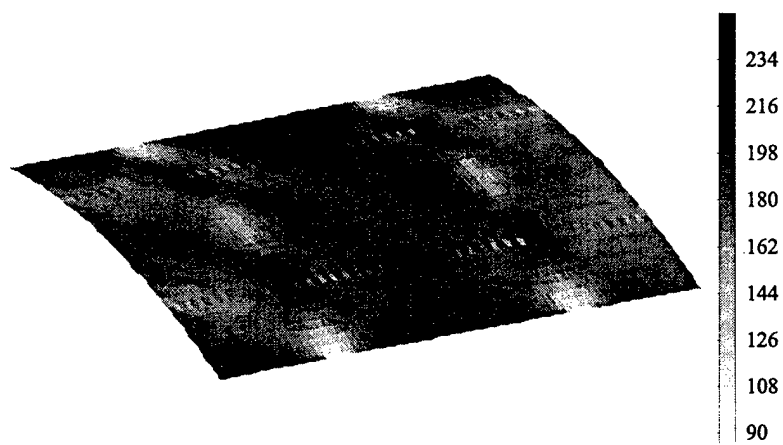
Figure 3.53: Axial Stress Resultant for Intact fuselage
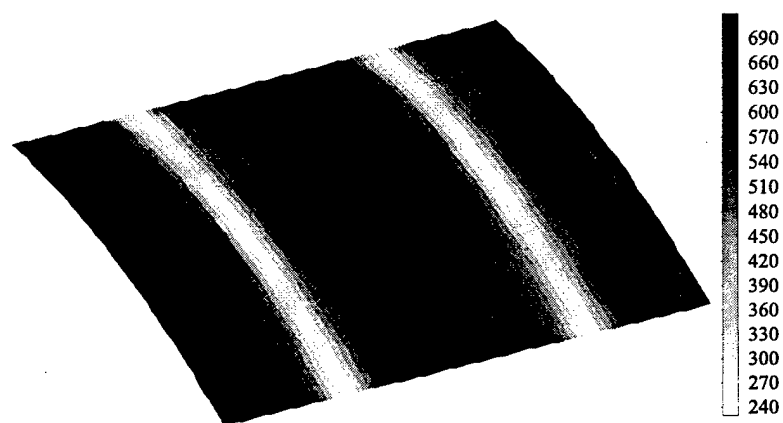
Figure 3.54: Hoop Stress Resultant for Intact Fuselage
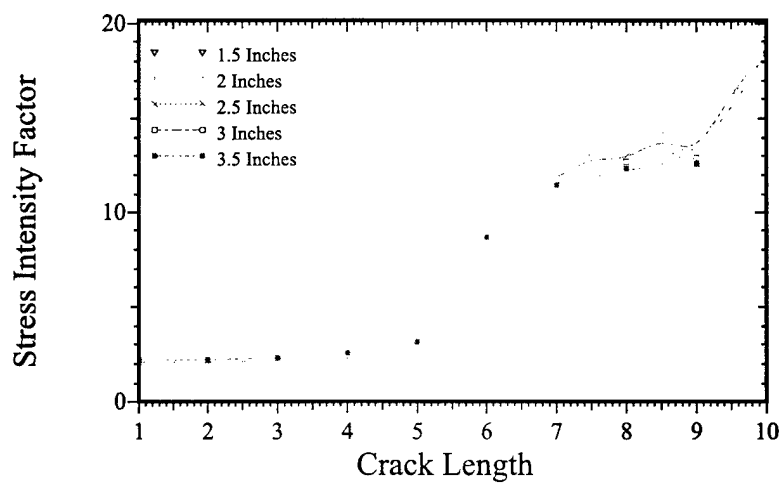
Figure 3.55: Effect of Patch Overlap Length on Stress Intensity Factor
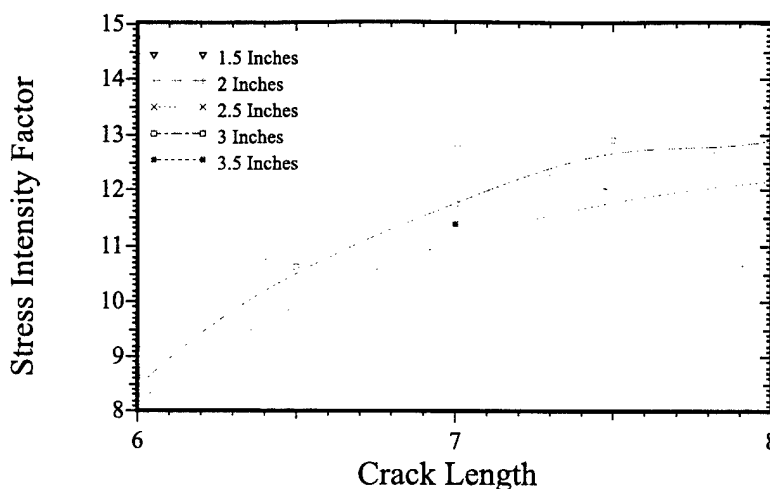
Figure 3.56: Effect of Patch Overlap Length on Stress Intensity Factor

When the crack is longer than the width of the patch, the patch serves to transfer the load across the crack and reduce the ligament stress near the crack tip. Therefore, a longer patch, having a longer overlap length and therefore larger area transfers this stress better and therefore perform better than the shorter patches (Fig. 3.55 and Fig. 3.56). Whereas, when the crack is shorter than the width of the patch, the longer patches perform poorly (Fig. 3.57). The composite system of the patch, adhesive and the sheet attracts parasitic load from other regions in the sheet, [Baker and Jones (1988). When the crack is shorter than the width of the patch, this parasitic load attaction, increases the load near the crack tip. Larger patches attract larger parasitic loads, therefore they perform poorly when compared to shorter ones. When the crack is longer, this parasitic load attraction does not increase the load near the crack tip, therefore a similar behavior in not seen in those cases.

The patch width is varied from 4 in to 8 in. The results are shown in Fig. 3.58. The patch is 3 in long, and 0.04 in thick and is made of Boron/Epoxy. The adhesive properties remain the same as above. As was illustrated earlier, the stress intensity factors shows two asymptotic values, one obtained when the crack is shorter than the width of the patch and the other when the crack is longer than the width of the patch. When the crack is shorter than the width of the patch, the asymptotic value reached does not vary much with the patch width. While wider patches cause the second asmptotic value to be reached at a longer crack length (the cracks emerge from the patch later with wider patches), the asymptotic value reached does not aprear to change. Therefore the narrower patches also seem to perform adequately. Wider patches, because of larger areas, have better damage tolerance.

The patch thickness was varied from 0.01 in thick to 0.04 in. The patch is 5 in wide and 3 in long and is made of Boron/Epoxy. As expected, thicker patches perform better (Fig. 3.59).

Effect of Patch Material

To evaluate different materials as possible candidates for patching materials several are investigated, following Fredell (1994). The properties of the materials are given in Tab. 3.3.2. In each of the cases the patch is 5 in wide and 3 in long and 0.04 in thick. The adhesive shear modulus is 104.7 ksi and the thickness
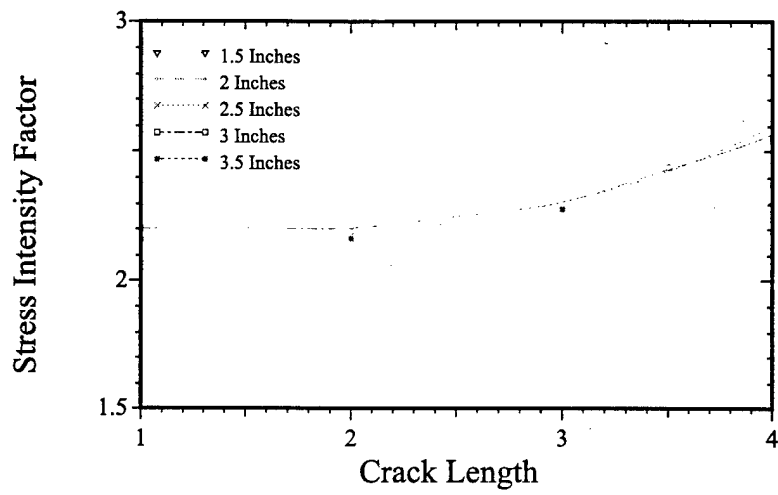
Figure 3.57: Effect of Patch Overlap Length on Stress Intensity Factor
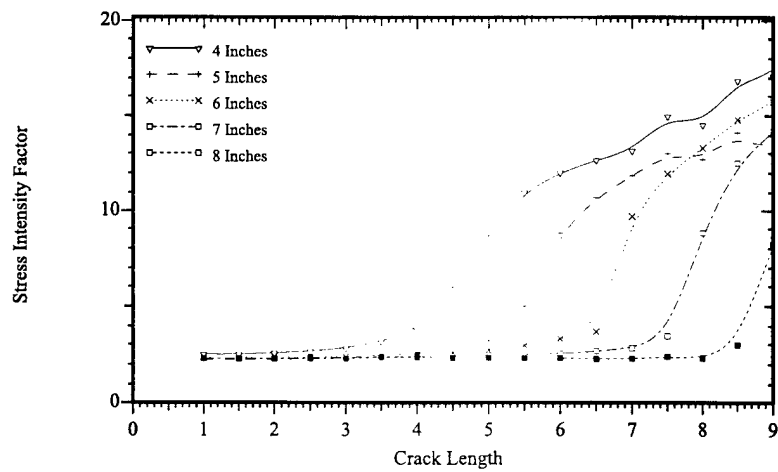
Figure 3.58: Effect of Patch Width on Stress Intensity Factor
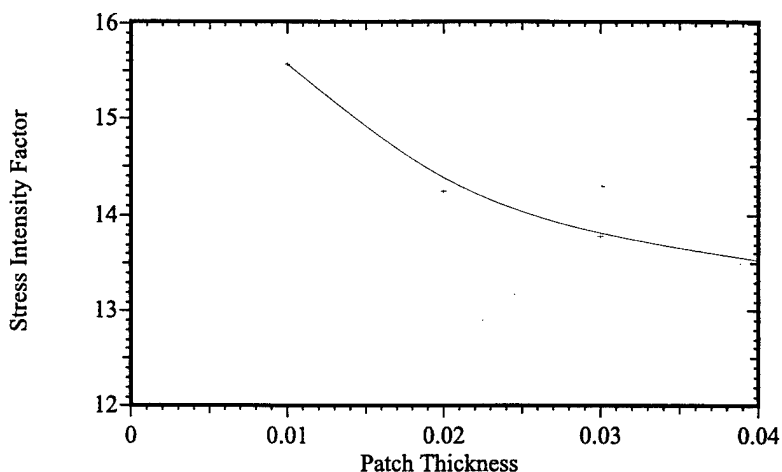
Figure 3.59: Effect of Patch Thickness on Stress Intensity Factor

Table 3.4: Properties of Various Patching Materials Considered

Material	E_1	E_2	ν_{12}	G_{12}
Boron/Epoxy	3.02×10^7 psi	3.69×10^6 psi	0.1677	1.05×10^6 psi
Carbon/Epoxy	1.97×10^7 psi	1.814×10^6 psi	0.30	1.015×10^6 psi
Al 2024-T3	1.05×10^7 psi	1.05×10^7 psi	0.32	3.977×10^6 psi
GLARE	9.565×10^6 psi	7.358×10^6 psi	0.33	2.685×10^6 psi

considered is 0.004 in. The Yield Stength of the adhesive is taken as 5254 psi. The results are depicted in Fig. 3.60.

The composite patches perform the best, followed by Al 2024-T3, and finally the metal laminate GLARE. When the crack is under the patch, the difference is marked . But once the crack becomes longer than the width of the patch, the difference is marginal. When the crack is shorter than the width of the patch, the induced strains cause larger stress to be transfered in stiffer patches. Therefore, the load near the crack tip is reduced and the stress intensity factor reduction is more pronounced for stiffer patches. On the other hand when the crack is longer than the width, the patch transfers the load as in a bonded lap joint and the load transferred is the ligament stress and has little relationship with the stiffness. This is confirmed by the fact that when the crack is extremely long, the stress intensity factor for patched cracks, with patch of various materials is almost the same.

Effect of Adhesive Properties

With the effect of the patch material and geometry determined the effect of the adhesive is now examined. With the boron-epoxy patch of 5 in X 3 in X 0.04 in, the adhesive thickness is varied from 0.001 to 0.005 for a crack of length 8 in. The results are shown in Fig. 3.61. Thin adhesive layers perform better than thick adhesive layers because, a thick adhesive makes the composite system of the sheet, adhesive layer and patch
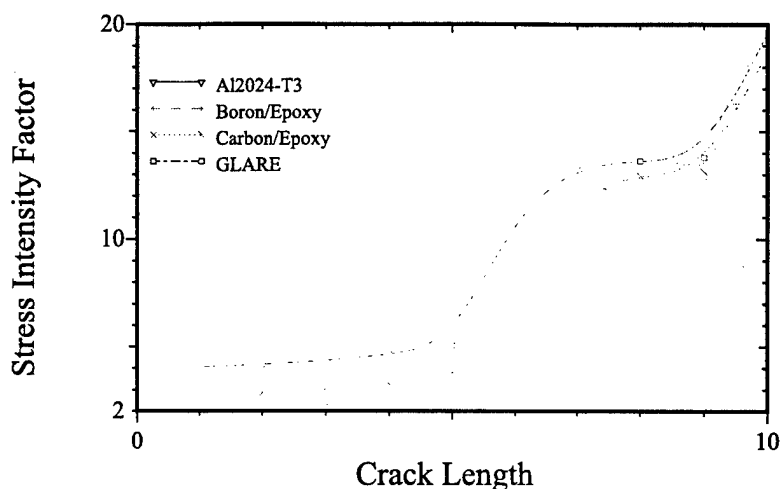
Figure 3.60: Comparison of Different Patching Materials

softer. Often, a thick adhesive layer is needed for good durability as a thick adhesive will experience lesser strains. As can be seen from Fig. 3.62 the detrimental effect of having a thick adhesive is not severe.

The shear modulus of the adhesive is varied for the same patch dimensions and for 0.004 in thick adhesive. The result is shown in Fig. 3.62. As can be seen, stiffer adhesives were found to perform better. While, the conditions considered were insufficient for adhesive yield, a stiffer adhesive would result in the yield point being reached earlier. Thus, the material would yield and reduce the patch effectiveness as illustrated earlier. This being the case, it is also noted that the advantage in using a stiffer adhesive (in terms of stress intensity reduction) is not significant.

3.3.3 Deficiencies of the methodology

Cracks on fasteners rivet rows can be studied using a different local analysis [as in Park, Ogiso, and Atluri (1992)]. As the methodology is based on a finite element alternating method, only straight cracks can be analyzed. In the present work, the pressure loading on the local zone is neglected. As this is a small region, it is good enough approximation. A better approach would be to use a different local zone that can take into account bending also.

In the intermediate model, the adhesive is discretized and modeled as beams. This results in lack of compatibility between the patch and the sheet. As the discretization at this level is not very dense for the adhesive, the error due to this lack of compatibility is thought to be small. A possible remedy for this is the usage of an element as the one used in the local model.

As the traction conditions are being transfered from intermediate to local, extra kinematic boundary conditions have to be applied. In the cases studied, the line of the crack is an axis of symmetry and therefore this line could be fixed. But such an approach might not be applicable in other cases. The effect of constraining other lines has not been studied. A possible remedy is to transfer kinematic conditions from intermediate to local and use a finite element alternating method as in Wang and Atluri (1995) which ca handle mixed boundary conditions on the boundary of the local zone. Also, only in-plane stresses are transfered, as a 2-D local analysis is used, the out-of-plane stresses are neglected. Again this can be remedied if a bending finite
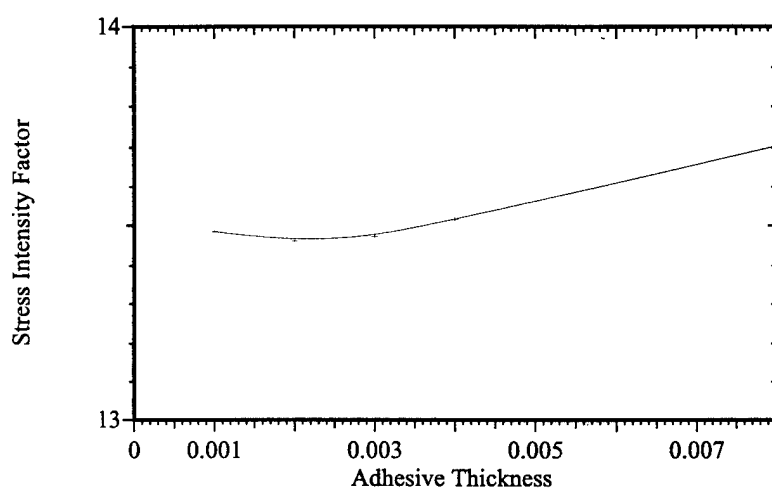
Figure 3.61: Effect of Adhesive Thickness on Patching Materials
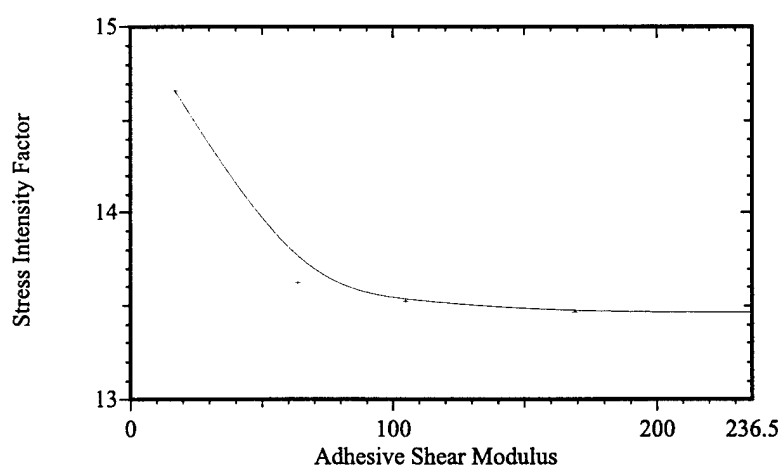
Figure 3.62: Effect of Adhesive Shear Modulus on Stress Intensity Factor

element alternating method is used. The transfer of kinematic conditions from the global to intermediate between different models (beams – shells) could lead to stress mismatch at the boundary of the models. The error accumulation in such a procedure is not known.

This analysis does not account for the thermal stresses induced during manufacture and operation. These stresses will reduce the patch efficiency. Fredell (1994) studied the influence of these stresses and has demonstrated that the efficiency reduction due to these is severe and that it cannot be ignored. The analysis done here has to be modified to take into account the thermal effects. This analysis does not take into account the peel (normal) stresses.

REFERENCES

Almroth, B. O.; Brogan, F. A.; Stanley, G. M. 1986: Structural analysis of general shells. *User's Instruction for STAGSC-1, Lockheed Missiles and Space Company, LMSC D633873, Palo Alto, CA*, 1986.

Atluri, S. N. 1986: Computational methods in the mechanics of fracture. *Amsterdam North Holland, also translated in Russian, Mir Puhlishers, Moscow*, 1986.

Atluri, S. N.; Kathiresan, K. 1978: Stress analysis of typical flaws in aerospace structural components using 3d hybrid displacement finite element method. *19th AIAA/ASME/SAE Structures, Structural Dynamics and Materials Conf., Bethesda, MD, 340-351*, 1978.

Atluri, S. N.; Tong, P. 1991: Computational schemes for integrity analyses of fuselage panels in aging airplanes. *Structural Integrity of Aging Airplanes, Springer Series in Computational Mechanics, Atluri. S.N. and Sampath, S.G. and Tong, P. eds, Springer-Verlag, Berlin.*, 1991.

Baker, A. A.; Jones, R. 1988: Bonded repair of aircraft structures. *Martinus Nijhoff Publishers, Dordrecht*, 1988.

Cartwright, D. J.; Parker, A. P. 1972: Opening mode stress intensity factors for cracks in pin-loads joints. *Int. J. Fracture 11, 65-71*, 1972.

Chu, R. C.; Ko, T. C. 1989: Isoparametric shear spring element applied to crack patching and instability. *Theoretical and Applied Fracture Mechanics, 11, 93-102.*, 1989.

Erdogan, F.; Arin, K. 1972: A sandwich plate with a part-through and a debondiog crack. *Fog. Frac. Mech. 4, 449-451*, 1972.

Fredell, R. S. 1994: Damage tolerant repair techniques for pressurized aircraft fuselages. *Ph. D. Dissertation, Faculty of Aerospace Engineering, Delft University of Technology.*, 1994.

Gladwell, G. M. L.; England, A. H. 1977: Orthogonal polynomial solutions to some mixed boundary-value prblems in elasticity theory. *Q. J. Mech. Appl. Math. 30, 175-185.*, 1977.

Hart-Smith, L. J. 1974: Analysis and design of advanced composite bonded joints. *NASA CR 2218.*, 1974.

Hong, C. S.; Jeng, K. Y. 1985: Stress intensity factors in anisotropic sandwich plate with a part-through crack under mixed mode deformation. *Eng. Frac. Mech. 21, 285-292*, 1985.

Jones, R.; Callinan, R. J. 1979: Finite element analysis of patched cracks. *J. Structural Mech. 7(2), 107-130.*, 1979.

Ko, W. L. 1978:   An orthotropic sandwich plate containing a part-through crack under mixed mode deformation. *Eng. Frac. Mech. 10, 15-23*, 1978.

Leknitskiic, S. G. 1968:   Anisotropic plates. *New York, Gordon and Breach*, 1968.

Mitchell, R. A., Wooley, R. M.; Chivirut, D. J. 1975:   Analysis of composite reinforced cutouts and cracks. *AIAAJ. 17,774-749*, 1975.

Muskhelishvili, N. I. 1953:   Some basic problems of the mathematical theory of elasticity. *Noordhoo, Groningen*, 1953.

Nagaswamy, V., Pipkins, D. D.; Atluri, S. N. 1995:   An feam based methodology for analyzing composite patch repairs of metallic structures. *ASME AD-vol 47, Structural Integrity in Aging Aircraft*, 1995.

Nayak, G. C.; Zienkiewicz, O. C. 1972:   Elasto-plastic stress analysis. a generalization for various constitutive relations including strain softening. *International Journal for Numerical Methods in Engineering, Vol.5, pp.113-135*, 1972.

Nishioka, T.; Atluri, S. N. 1983:   Analytical solution for embedded elliptical cracks, and finite element alternating method for elliptical surface cracks, subjected to arbitrary loadings. *Eng. Fract. Mech. 17, 247-268*, 1983.

Park, J. H.; Ogiso, T.; Atluri, S. N. 1992:   Analysis of cracks in aging aircraft structures, with and without composite-patch repairs. *Comput Mech v 10 n 3-4 1992 p 169-201*, 1992.

Roderick, G. L. 1980:   Green's functions for stresses, stress intensity factors and displacements in a cracked infinite isotropic sheet under symmetric loads. *Fog. Frac. Mcch. 17, 95-105*, 1980.

Rose, L. R. F. 1981:   An application of the inclusion analogy for bonded reinforcements. *Int. J. Solids Struct. 17, 127-171*, 1981.

Singh, R.; Park, J. H.; Atluri, S. N. 1994:   Growth of multiple cracks and their linkup in a fuselage lap joint. *AIAA J 32 11 Nov 1994 AIAA Washington DC USA p 2260-2268*, 1994.

Vijayakumar, K.; Atluri, S. N. 1981:   An embedded elliptical crack, in an infinite solid, subjected to arbitrary crack-face tractions. *J Appl Mech Trans ASME v 103 n 1 Mar 1981 p 88-96*, 1981.

Wang, L.; Atluri, S. N. 1995:   Implementation of the Schwartz-Neumann alternating method for collinear multiple cracks with mixed type of boundary conditions. *Comput Mech v 16 n 4 p 266-271*, 1995.

Progress Report
for
Mechanics of Widespread Fatigue Damage
&
Life Enhancement Methodologies
for
Aging Aerospace Structures

Grant # B-15-F43

Principal Investigator: Satya N. Atluri

Georgia Institute of Technology
Computational Modeling Center
Rm. 225 French Bldg.
Atlanta, GA 30332-0356

September 1995

Objectives
No change

Status of Effort
Progress towards achieving the research objectives of this project has been realized via the development of:
- a Finite Element Alternating Method (FEAM) based methodology for analyzing composite patch repairs of metallic structures, and
- an implementation of the Schwartz-Neumann Alternating Method for collinear multiple cracks with mixed type of boundary conditions.

These two developments are described in detail in the reports accompanying this progress report.

Accomplishments/New Findings
The development of a FEAM based methodology for analyzing composite patch repairs of metallic structures has resulted in an accurate and efficient means of designing repairs which will enhance the lives of aging U.S. Air Force aircraft. This methodology allows a designer to:
- compare mechanical doubler repairs with bonded composite patch repairs,
- calculate stress intensity factors for composite patch repaired cracks, and
- model the adhesive as an elastic-plastic material.

The above is accomplished without requiring detailed crack tip modeling, which makes the methodology developed unique in the field of computational fracture mechanics.

The implementation of the Schwartz-Neumann Alternating Method for collinear multiple cracks with mixed type of boundary conditions has resulted in an important advance in the application of the FEAM to widespread fatigue damage. Occurrences of widespread fatigue damage are currently posing a major risk to the continued airworthiness of several U.S. Air Force aircraft fleets (i.e. C-141). Prior to this research, local FEAM models of widespread fatigue damage could have only traction boundary conditions applied. As these local boundary conditions are determined via a global or intermediate analysis, which often makes use of displacement based finite elements, the ability to accommodate mixed type (i.e. displacement and traction) boundary conditions in the local FEAM model represents a substantial improvement.

Personnel Supported
Dr. S.N. Atluri, Professor
Dr. D.S. Pipkins, Research Engineer
Mr. L. Wang, Ph.D. student
Mr. R. Jansen, Ph.D. student
Mr. R. Cummings, Ph.D. student
Mr. V. Nagaswamy, M.Sc. student
Mr. B. Visser, M.Sc. student

Publications
V. Nagaswamy, D.S. Pipkins and S.N. Atluri, "A Finite Element Alternating Method (FEAM) Based Methodology for Analyzing Composite Patch Repairs of Metallic Structures", submitted to *Computational Mechanics*, September 1995.

L. Wang and S.N. Atluri, "An Implementation of the Schwartz-Neumann Alternating Method for Collinear Multiple Cracks with Mixed Type of Boundary Conditions", submitted to *Computational Mechanics*, March 1995.

Interactions/Transitions
- V. Nagaswamy, D.S. Pipkins, S.N. Atluri, "Repairs to Aging Aircraft", presented at ICES 95, Mauna Lani, HI, July 31-August 4, 1995.

- Collaboration is underway with Major R. Fredell of the U.S. Air Force Academy. The FEAM based composite patch repair methodology is being compared and contrasted with a software known as CALCUREP, being developed by Major Fredell.

New Discoveries, Inventions, or Patent Disclosures
None

Honors/Awards
- Dr. Atluri has been reappointed by the White House, to serve the U.S. engineering community as a Member of the Nomination Evaluation Committee for the National Medals of Technology, which are awarded annually to American corporations and extraordinarily distinguished engineers and scientists who made a significant difference to the quality of life for all Americans. These Medals are awarded each year, by the President of the United States in White House ceremonies.

- Dr. Atluri has also been asked to serve on the FAA's Research Advisory Committee. This committee advises the FAA administrator on a wide variety of issues concerning the FAA's various research initiatives.

- Dr. Atluri was made a Fellow of The United States Association of Computational Mechanics in June of 1995.

- Dr. Atluri received the Technical Achievement Award from the National Academy of Engineering in June of 1995.

- Dr. Atluri has been chosen to receive the 1995 A.C. Eringen Medal from the Society of Engineering Science.

Summary of Research

Alternating Method for Bending
of Plates

Brad Visser

December 15, 1994

Presented to:

Computational Modeling Center
Georgia Instititute of Technology
Atlanta, Georgia

2. FORTRAN code for the alternating method for bending of plates

The finite element part of the code is a modified portion of that appearing in *The Finite Element Method* by Zienkiewicz and Taylor [7]. Included with the code are several example problems that demonstrate the plane elasticity elements and the plate elements. The plate elements are the DKQ elements formulated in "Evaluation of a New Quadrilateral Thin Plate Bending Element," by Batoz and Tahar [1]. Explanation of the examples is included in Appendix D. The input mesh format is included in this same appendix.

NOTE: In the entire code, subroutines used from the 2D alternating method are in all capitals. Any changes made to these are in lower-case letters. Therefore, all changes made by this author are in lower-case letters, including the initial finite element routines.

What is the status of the code?

1. Using macro statements, plane elasticity and plate problems may be solved

2. The alternating method for 2D plane elasticity was implemented, but never was fully functional. The subroutines were taken from a 2D code from Venkat Nagaswamy.

3. The alternating method for the bending of thin plates is very close to being fully functional. The G-matrix which is multiplied by the coefficient matrix to get the nodal reactions seems to be in order. For the example, symmetric problem (2x2cracb.inp) the G-matrix appears to account for the symmetry and the boundary conditions at the end of the first iteration appear to be of the correct order and symmetrical. The problem seems to be resolving the mesh using these new boundary conditions. For some reason, the loads are very small, but the returned moments at the crack location are too large. The stress intensity factors then blow up instead of converging upon iteration. It appears, then, that the only problem is in the latter part of the iteration process where the mesh is resolved with the new boundary conditions.

4. Final output needs to be adjusted to line up correctly and to improve appearance.

NOTES:

1. The least squares method for determining the coefficients, used in the alternating method for bending, is correct.
2. The infinite integral solution functions (second half of Tmatrix subroutine - located in BNDMOM.FOR) have been verified using Mathematica. The solution of the entire infinite integral equations (first half of Tmatrix subroutine) is not verified because there is no exact solution, or way of approximating the exact solution, in some other analytic method.
3. Parts of the code that deal with anisotropic materials are commented. These were to implemented later when patching was part of the process.
4. An interesting concept is to implement the work of Murthy [3], which would adjust the stress intensity factors to account for crack closure. This is advantageous using the alternating method because the moments at the crack are known. It's been awhile since this paper was last read, but the concept was quite interesting at the time.

References

[1] Batoz, Jean-Louis and Mabrouk Ben Tahar. "Evaluation of a New Quadrilateral Thin Plate Bending Element."

[2] Chen, Wen-Hwa, with Kung-Chuan Yang, and Chenq-Shyoung Chang. "A finite element alternating approach fro the bending analysis of thin cracked plates." *International Journal of Fracture*, Volume 56, pages 93-110, 1992.

[3] Murthy, M.V., S. Viswanath, A.V. Krishna Murty, and K.P. Rao. "A Two-Dimensional Model for Crack Closure Effect in Plates Under Bending." *Engineering Fracture Mechanics*, Volume 29, No. 4, pp. 435-452, 1988.

[4] Park, J.H., T. Ogiso, and S.N. Atluri. "Analysis of cracks in aging aircraft structures, with and without composite-patch repairs." *Computational Mechanics*. Vol. 10, pp.169-201, 1992.

[5] Ian Sneddon. *Fourier Transforms*. McGraw-Hill Book Company, 1951.

[6] Ian Sneddon. *Mixed Boundary Value Problems in Potential Theory*. John Wiley & Sons, 1966.

[7] Zienkiewicz, O.C. and R.L. Taylor. *The Finite Element Method*. Fourth Edition. McGraw-Hill Book Company, 1989.

Appendix A

I. Verification of Part (1) of [2]

    A. The solution of the transverse displacement is shown to be of the form:

$$\hat{w}(x,\xi) = \left(c_1 + c_2 x\right)e^{-|\xi|x} \qquad (18)$$

    The constants c_1 and c_2 are solved for using the given boundary conditions. This verifies that the solution is:

$$\hat{w}(x,\xi) = \frac{-1}{(3+v)(1-v)D|\xi|^2}\,\hat{f}(\xi)\left[(1+v)-(1-v)|\xi|x\right]e^{-|\xi|x} \qquad (21)$$

    B. Given the above form of the displacement (21), the other seven functions are verified, which are Equations (22)-(29).

```
Clear[c1,c2,mx,vx]
w=(c1+c2 x) Exp[- Z x]
```

$$\frac{c1 + c2\,x}{E^{x\,Z}}$$

```
mx=-Dm(D[D[w,x],x]-nu Z^2 w)
```

$$-(Dm\ (\frac{-2\,c2\,Z}{E^{x\,Z}} + \frac{(c1 + c2\,x)\,Z^2}{E^{x\,Z}} - \frac{nu\,(c1 + c2\,x)\,Z^2}{E^{x\,Z}}))$$

```
Together[mx]
```

$$\frac{Dm\ (2\,c2\,Z - c1\,Z^2 + c1\,nu\,Z^2 - c2\,x\,Z^2 + c2\,nu\,x\,Z^2)}{E^{x\,Z}}$$

```
Solve[mx==fz,c1]
```

$$\{\{c1 \to -(\frac{-(E^{x\,Z}\,fz) + 2\,c2\,Dm\,Z - c2\,Dm\,x\,Z^2 + c2\,Dm\,nu\,x\,Z^2}{Dm\ (-Z^2 + nu\,Z^2)})\}\}$$

```
vx=-Dm(D[D[D[w,x],x],x]-Z^2 (2-nu) D[w,x])
```

$$-(Dm\ (\frac{3\,c2\,Z^2}{E^{x\,Z}} - \frac{(c1 + c2\,x)\,Z^3}{E^{x\,Z}} - (2 - nu)\,Z^2\ (\frac{c2}{E^{x\,Z}} - \frac{(c1 + c2\,x)\,Z}{E^{x\,Z}})))$$

```
Together[vx]
```

$$\frac{Dm\ (-(c2\,Z^2) - c2\,nu\,Z^2 - c1\,Z^3 + c1\,nu\,Z^3 - c2\,x\,Z^3 + c2\,nu\,x\,Z^3)}{E^{x\,Z}}$$

```
c1=-(-(Exp[x Z] fz)+2 c2 Dm Z-c2 Dm x Z^2+c2 Dm nu x Z^2)/(Dm(-Z^2+nu Z^2)
```

$$-(\frac{-(E^{x\,Z}\,fz) + 2\,c2\,Dm\,Z - c2\,Dm\,x\,Z^2 + c2\,Dm\,nu\,x\,Z^2}{Dm\ (-Z^2 + nu\,Z^2)})$$

```
Solve[vx==0,c2]
```

$$\{\{c2 \to \frac{E^{x\,Z}\,fz}{Dm\ (3 + nu)\,Z}\}\}$$

```
Clear[c1]
c2=fz/(Dm(3+nu)Z)
```

$$\frac{fz}{Dm\ (3 + nu)\,Z}$$

```
Solve[mx==fz,c1]
```

$$\{\{c1 \to -(\frac{2\,fz - 3\,E^{x\,Z}\,fz - E^{x\,Z}\,fz\,nu - fz\,x\,Z + fz\,nu\,x\,Z}{Dm\ (3 + nu)\ (-Z^2 + nu\,Z^2)})\}\}$$

w=-1/(2*P*(3+nu)(1-nu)Dm)*fz/Z^2*((1+nu)-(1-nu)Z x)Exp[-Z x- i Z y]

$$-\frac{(E^{-(x\ Z)\ -\ i\ y\ Z}\ fz\ (1\ +\ nu\ -\ (1\ -\ nu)\ x\ Z))}{2\ Dm\ (1\ -\ nu)\ (3\ +\ nu)\ P\ Z^2}$$

mx=Dm(-D[D[w,x],x]+nu Z^2 w)

$$Dm\ (\frac{E^{-(x\ Z)\ -\ i\ y\ Z}\ fz}{Dm\ (3\ +\ nu)\ P}\ +\ \frac{E^{-(x\ Z)\ -\ i\ y\ Z}\ fz\ (1\ +\ nu\ -\ (1\ -\ nu)\ x\ Z)}{2\ Dm\ (1\ -\ nu)\ (3\ +\ nu)\ P}\ -$$

$$\frac{E^{-(x\ Z)\ -\ i\ y\ Z}\ fz\ nu\ (1\ +\ nu\ -\ (1\ -\ nu)\ x\ Z)}{2\ Dm\ (1\ -\ nu)\ (3\ +\ nu)\ P})$$

Together[%]

$$\frac{E^{-(x\ Z)\ -\ i\ y\ Z}\ (3\ fz\ +\ fz\ nu\ -\ fz\ x\ Z\ +\ fz\ nu\ x\ Z)}{2\ (3\ +\ nu)\ P}$$

my=Dm(Z^2 w -nu D[D[w,x],x])

$$Dm\ (-\frac{(E^{-(x\ Z)\ -\ i\ y\ Z}\ fz\ (1\ +\ nu\ -\ (1\ -\ nu)\ x\ Z))}{2\ Dm\ (1\ -\ nu)\ (3\ +\ nu)\ P}\ -$$

$$nu\ (-\frac{E^{-(x\ Z)\ -\ i\ y\ Z}\ fz}{Dm\ (3\ +\ nu)\ P})\ -\ \frac{E^{-(x\ Z)\ -\ i\ y\ Z}\ fz\ (1\ +\ nu\ -\ (1\ -\ nu)\ x\ Z)}{2\ Dm\ (1\ -\ nu)\ (3\ +\ nu)\ P})$$

Together[%]

$$\frac{E^{-(x\ Z)\ -\ i\ y\ Z}\ (1\ -\ nu)\ (-fz\ +\ fz\ x\ Z)}{2\ (3\ +\ nu)\ P}$$

mxy=Dm(1-nu)(i Z) D[w,x]

$$Dm\ i\ (1\ -\ nu)\ Z\ (\frac{E^{-(x\ Z)\ -\ i\ y\ Z}\ fz}{2\ Dm\ (3\ +\ nu)\ P\ Z}\ +\ \frac{E^{-(x\ Z)\ -\ i\ y\ Z}\ fz\ (1\ +\ nu\ -\ (1\ -\ nu}{2\ Dm\ (1\ -\ nu)\ (3\ +\ nu)\ P\ Z}$$

Together[%]

$$\frac{E^{-(x\ Z)\ -\ i\ y\ Z}\ i\ (2\ fz\ -\ fz\ x\ Z\ +\ fz\ nu\ x\ Z)}{2\ (3\ +\ nu)\ P}$$

qx=-Dm(D[D[D[w,x],x],x]-Z^2 D[w,x])

$$-(Dm\ (\frac{3\ E^{-(x\ Z)\ -\ i\ y\ Z}\ fz\ Z}{2\ Dm\ (3\ +\ nu)\ P}\ +\ \frac{E^{-(x\ Z)\ -\ i\ y\ Z}\ fz\ Z\ (1\ +\ nu\ -\ (1\ -\ nu)\ x\ Z}{2\ Dm\ (1\ -\ nu)\ (3\ +\ nu)\ P}\ -$$

$$Z^2\ (\frac{E^{-(x\ Z)\ -\ i\ y\ Z}\ fz}{2\ Dm\ (3\ +\ nu)\ P\ Z}\ +\ \frac{E^{-(x\ Z)\ -\ i\ y\ Z}\ fz\ (1\ +\ nu\ -\ (1\ -\ nu)\ x\ Z)}{2\ Dm\ (1\ -\ nu)\ (3\ +\ nu)\ P\ Z}))$$

Together[%]

$$-(\frac{E^{-(x\ Z)\ -\ i\ y\ Z}\ fz\ Z}{(3\ +\ nu)\ P})$$

qy=Dm i (Z D[D[w,x],x]-Z^3 w)

$$Dm\ i\ \left(\frac{E^{-(x\ Z)\ -\ i\ y\ Z}\ fz\ Z\ (1\ +\ nu\ -\ (1\ -\ nu)\ x\ Z)}{2\ Dm\ (1\ -\ nu)\ (3\ +\ nu)\ P}\ +\right.$$

$$\left.Z\ \left(-\left(\frac{E^{-(x\ Z)\ -\ i\ y\ Z}\ fz}{Dm\ (3\ +\ nu)\ P}\right)\ -\ \frac{E^{-(x\ Z)\ -\ i\ y\ Z}\ fz\ (1\ +\ nu\ -\ (1\ -\ nu)\ x\ Z)}{2\ Dm\ (1\ -\ nu)\ (3\ +\ nu)\ P}\right)\right)$$

Together[%]

$$-\left(\frac{E^{-(x\ Z)\ -\ i\ y\ Z}\ fz\ i\ Z}{(3\ +\ nu)\ P}\right)$$

vx=-Dm(D[D[D[w,x],x],x]-Z^2 (2-nu) D[w,x])

$$-\left(Dm\ \left(\frac{3\ E^{-(x\ Z)\ -\ i\ y\ Z}\ fz\ Z}{2\ Dm\ (3\ +\ nu)\ P}\ +\ \frac{E^{-(x\ Z)\ -\ i\ y\ Z}\ fz\ Z\ (1\ +\ nu\ -\ (1\ -\ nu)\ x\ Z}{2\ Dm\ (1\ -\ nu)\ (3\ +\ nu)\ P}\right.\right.$$

$$(2\ -\ nu)\ Z^2\ \left(\frac{E^{-(x\ Z)\ -\ i\ y\ Z}\ fz}{2\ Dm\ (3\ +\ nu)\ P\ Z}\ +\ \frac{E^{-(x\ Z)\ -\ i\ y\ Z}\ fz\ (1\ +\ nu\ -\ (1\ -\ n}{2\ Dm\ (1\ -\ nu)\ (3\ +\ nu)\ P\ Z}\right.$$

Together[%]

$$E^{-(x\ Z)\ -\ i\ y\ Z}\ \frac{fz\ (-1\ +\ nu)\ x\ Z^2}{2\ (3\ +\ nu)\ P}$$

vy=-i Dm Z (Z^2 w - (2-nu) D[D[w,x],x])

$$-\left(Dm\ i\ Z\ \left(-\left(E^{-(x\ Z)\ -\ i\ y\ Z}\ \frac{fz\ (1\ +\ nu\ -\ (1\ -\ nu)\ x\ Z))}{2\ Dm\ (1\ -\ nu)\ (3\ +\ nu)\ P}\ -\right.\right.\right.$$

$$(2\ -\ nu)\ \left(-\left(\frac{E^{-(x\ Z)\ -\ i\ y\ Z}\ fz}{Dm\ (3\ +\ nu)\ P}\right)\ -\ \frac{E^{-(x\ Z)\ -\ i\ y\ Z}\ fz\ (1\ +\ nu\ -\ (1\ -\ n}{2\ Dm\ (1\ -\ nu)\ (3\ +\ nu)\ P}\right.$$

Together[%]

$$E^{-(x\ Z)\ -\ i\ y\ Z}\ \frac{i\ Z\ (-5\ fz\ +\ fz\ nu\ +\ fz\ x\ Z\ -\ fz\ nu\ x\ Z)}{2\ (3\ +\ nu)\ P}$$

$$G(\rho) = \phi(1)\int_0^\infty J_0(\xi\rho)\sin\xi\mathrm{d}\xi - \int_0^1 \phi'(t)\mathrm{d}t \int_0^\infty J_0(\xi\rho)\sin\xi t\,\mathrm{d}\xi.$$

If we make use of equation (2.1.14) we find that $G(\rho) = 0$ when $\rho > 1$ so that the equation (3.2.2) is automatically satisfied by a function $A(\xi)$ of the form (3.5.1). Also we note that

$$G(\rho) = \frac{\phi(1)}{\sqrt{(1-\rho^2)}} - \int_\rho^1 \frac{\phi'(t)\mathrm{d}t}{\sqrt{(t^2-\rho^2)}}, \quad 0 \leqq \rho < 1. \qquad (3.5.4)$$

To find the appropriate form of the function $\phi(t)$ we substitute from equation (3.5.1) into the integral defining the function

$$F(\rho) = \int_0^\infty \xi^{-1}A(\xi)J_0(\xi\rho)\mathrm{d}\xi \qquad \cdot \qquad (3.5.5)$$

to find that

$$F(\rho) = \begin{cases} \displaystyle\int_0^\rho \frac{\phi(t)\mathrm{d}t}{\sqrt{(\rho^2-t^2)}}, & 0 \leqq \rho < 1 \qquad (3.5.6) \\[3mm] \displaystyle\int_0^1 \frac{\phi(t)\mathrm{d}t}{\sqrt{(\rho^2-t^2)}}, & \rho > 1. \qquad (3.5.7) \end{cases}$$

Since equation (3.2.1) is equivalent to the equation $F(\rho) = f(\rho)$, $0 \leqq \rho < 1$ we see from equation (3.5.6) that $\phi(t)$ is the solution of the integral equation

$$\int_0^\rho \frac{\phi(t)\mathrm{d}t}{\sqrt{(\rho^2-t^2)}} = f(\rho), \qquad 0 \leqq \rho < 1 \qquad (3.5.8)$$

from which it follows by the result expressed by the equations (2.3.7) that if $f(\rho)$ is continuously differentiable in $[0,1]$

$$\phi(t) = \frac{2}{\pi}\frac{\mathrm{d}}{\mathrm{d}t}\int_0^t \frac{\rho f(\rho)\mathrm{d}\rho}{\sqrt{(t^2-\rho^2)}}. \qquad (3.5.9)$$

Substituting from equation (3.5.9) and integrating by parts, we find that

$$A(\xi) = \frac{2\xi}{\pi}\left\{ \cos\xi\int_0^1 \frac{uf(u)\mathrm{d}u}{\sqrt{(1-u^2)}} + \xi\int_0^1 \sin\xi t\,\mathrm{d}t \int_0^t \frac{uf(u)\mathrm{d}u}{\sqrt{(t^2-u^2)}} \right\}$$

which can easily be transformed to give the solution

$$A(\xi) = \frac{2\xi}{\pi}\left\{ \cos\xi\int_0^1 \frac{uf(u)\mathrm{d}u}{\sqrt{(1-u^2)}} + \xi\int_0^1 \frac{u\mathrm{d}u}{\sqrt{(1-u^2)}} \int_0^1 vf(uv)\sin\xi v\,\mathrm{d}v \right\}. \quad (3.5.10)$$

It is easily verified that when $f(\rho) = 1$, $0 \leqq \rho < 1$, this formula leads to the expression (3.1.6) for $A(\xi)$.

In some applications the quantity

$$Q = 2\pi \int_0^1 \rho G(\rho) \mathrm{d}\rho \qquad (3.5.11)$$

has a physical significance. If we substitute from equation (3.5.4) into equation (3.5.11) we have

$$Q = 2\pi\phi(1) \int_0^1 \frac{\rho\mathrm{d}\rho}{\sqrt{(1-\rho^2)}} - 2\pi \int_0^1 \rho\mathrm{d}\rho \int_\rho^1 \frac{\phi'(t)\mathrm{d}t}{\sqrt{(t^2-\rho^2)}}.$$

The first of these two integrals can be evaluated immediately; to evaluate the second we interchange the order of the integrations, carry out the ρ-integration and then perform the t-integration by using the rule for integration by parts. In this way we find that

$$Q = 2\pi \int_0^1 \frac{\rho f(\rho)\mathrm{d}\rho}{\sqrt{(1-\rho^2)}}. \qquad (3.5.12)$$

For example, if $f(\rho)$ is the polynomial

$$f(\rho) = \sum_{r=0}^n a_r \rho^r \qquad (3.5.13)$$

then it is easily calculated that

$$Q = \pi^{3/2} \sum_{r=0}^n a_r \frac{\Gamma(\tfrac{1}{2}r + \tfrac{1}{2})}{\Gamma(\tfrac{1}{2}r + 1)}. \qquad (3.5.14)$$

We saw in §1.5 how it is possible to reduce the second basic problem to the first one in a simple way, but because it occurs so often in applications in physics and mechanics we shall show how to derive (by an elementary method) the solution of the pair of dual integral equations

$$\int_0^\infty \xi\psi(\xi)J_0(\xi\rho)\mathrm{d}\xi = f(\rho), \quad 0 \leq \rho < 1 \qquad (3.5.15)$$

$$\int_0^\infty \psi(\xi)J_0(\xi\rho)\mathrm{d}\xi = 0, \qquad \rho > 1. \qquad (3.5.16)$$

In this case we make the representation

$$\psi(\xi) = \int_0^1 \chi(t)\sin\xi t\,\mathrm{d}t, \qquad \chi(0) = 0. \qquad (3.5.17)$$

It is obvious from equations (2.1.14) that the form (3.5.17) satisfies the equation (3.5.15) automatically. If we integrate by parts we find that

$$\int_0^\infty \xi\psi(\xi)J_0(\xi\rho)\mathrm{d}\xi = \int_0^\infty J_0(\xi\rho)\mathrm{d}\xi\left\{-\chi(1)\cos\xi + \int_0^1 \chi'(t)\cos\xi t\,\mathrm{d}t\right\}$$

$$= \int_0^1 \chi'(t)\mathrm{d}t \int_0^\infty J_0(\rho\xi)\cos\xi t\,\mathrm{d}\xi - \chi(1)\int_0^\infty J_0(\rho\xi)\cos\xi\,\mathrm{d}\xi.$$

Making use of the result expressed by equations (2.1.13) we see that the integral equation determining $\chi(t)$ is

$$\int_0^\rho \frac{\chi'(t)\mathrm{d}t}{\sqrt{(\rho^2 - t^2)}} = f(\rho), \quad 0 \leqq \rho < 1.$$

This is exactly the same as the equation (3.5.8) for $\phi(t)$ and so has solution

$$\chi'(t) = \frac{2}{\pi}\frac{\mathrm{d}}{\mathrm{d}t}\int_0^t \frac{\rho f(\rho)\mathrm{d}\rho}{\sqrt{(t^2 - \rho^2)}}.$$

If we now integrate with respect to t and use the fact that $\chi(0) = 0$, we have

$$\chi(t) = \frac{2}{\pi}\int_0^t \frac{\rho f(\rho)\mathrm{d}\rho}{\sqrt{(t^2 - \rho^2)}}. \tag{3.5.18}$$

Inserting this expression into equation (3.5.17) we see that the dual integral equations (3.5.15) and (3.5.16) have the solution

$$\psi(\xi) = \frac{2}{\pi}\int_0^1 \sin\xi t\,\mathrm{d}t \int_0^t \frac{\rho f(\rho)\mathrm{d}\rho}{\sqrt{(t^2 - \rho^2)}}. \tag{3.5.19}$$

In particular, if the free term in equation (3.5.15) is $f(\rho) = 1, 0 \leqq \rho < 1$,

$$\psi(\xi) = \frac{2}{\pi\xi}\left\{\frac{\sin\xi}{\xi} - \cos\xi\right\}. \tag{3.5.20}$$

3.6. Methods based on the Integral Representation of Harmonic Functions

We saw in the last section that a solution of the first basic problem is obtained if we substitute the form (3.5.1) into the harmonic function (3.1.2) provided that $\phi(t)$ is given by equation (3.5.9). If we make this substitution then by the analysis of the last section

$$V(\rho, z) = \int_0^\infty e^{-\xi z}J_0(\xi\rho)\mathrm{d}\xi\int_0^1 \phi(t)\cos\xi t\,\mathrm{d}t \tag{3.6.1}$$

is a harmonic function in the half-space $z \geqq 0$ with the property that

$$\left[\frac{\partial V}{\partial z}\right]_{z=0} = 0. \tag{3.6.2}$$

Sneddon "Mixed Boundary Value Problems in Potential Theory"

Section 3.5

Elementary Solution of the Dual Integral Equations of Beltrami's Method.

$$\int_0^\infty \xi^{-1} A(\xi)\, J_0(\xi\rho)\, d\xi = 1 \qquad 0 \leq \rho < 1$$

$$\int_0^\infty A(\xi)\, J_0(\xi\rho)\, d\xi = 0 \qquad \rho > 1$$

If we let $\quad A(\xi) = \xi \int_0^1 \phi(t) \cos \xi t\, dt$

$$A(t) = \phi(t) \sin \xi t \Big|_0^1 - \int_0^1 \phi'(t) \sin \xi t\, dt$$

$$= \phi(1) \sin \xi - \int_0^1 \phi'(t) \sin \xi t\, dt$$

$$u = \phi(t) \qquad\qquad dv = \xi \cos \xi t$$

$$du = \frac{d\phi(t)}{dt} dt \qquad v = \sin \xi t$$

Define $\quad G(\rho) = \int_0^\infty A(\xi)\, J_0(\xi\rho)\, d\xi$

$$G(\rho) = \phi(1) \int_0^\infty J_0(\xi\rho) \sin \xi\, d\xi - \int_0^1 \phi'(t)\, dt \int_0^\infty J_0(\xi\rho) \sin \xi t\, d\xi$$

Given $\quad \displaystyle\int_0^\infty J_0(\xi\rho) \sin a\xi\, d\xi = \begin{cases} (a^2 - \rho^2)^{-\frac{1}{2}} & 0 \leq \rho < a \\ 0 & \rho > a \end{cases}$

$$\int_0^\infty J_0(\xi\rho) \sin \xi\, d\xi = \begin{cases} (1 - \rho^2)^{-\frac{1}{2}} & 0 \leq \rho < 1 \\ 0 & \rho > 1 \end{cases}$$

$$\int_0^\infty J_0(\xi \rho) \, s \cdots (\xi \, d\xi \quad = \quad (t^2 \cdot \rho^2)^{-1/2} \qquad 0 \le \rho < t$$

$$0 \qquad \begin{array}{l} \rho > t \\ \downarrow \\ t < \rho \end{array}$$

$$G(\rho) = \frac{\phi(1)}{\sqrt{(1-\rho^2)}} \quad - \quad \int_\rho^1 \frac{\phi'(t)}{\sqrt{t^2 \cdot \rho^2}} \, dt \qquad 0 \le \rho < 1$$

Demonstrates that $G(\rho) = 0$ when $\rho > 1$ — 2nd equation

$$F(\rho) = \int_0^\infty \xi^{-1} A(\xi) J_0(\xi \rho) \, d\xi$$

$$A(\xi) = \xi \int_0^1 \phi(t) \cos \xi t \, dt$$

$$F(\rho) = \int_0^1 \phi(t) \, dt \int_0^\infty J_0(\xi \rho) \cos \xi t \, d\xi$$

$$\int_0^\infty J_0(\xi \rho) \cos \xi t \, d\xi = \begin{array}{ll} 0 & 0 \le \rho < t \\[2mm] \dfrac{1}{\sqrt{\rho^2 \cdot t^2}} & \rho > t \end{array}$$

$$F(\rho) = \begin{cases} \displaystyle\int_0^\rho \frac{\phi(t) \, dt}{\sqrt{\rho^2 \cdot t^2}} & 0 \le \rho < 1 \\[4mm] \displaystyle\int_0^1 \frac{\phi(t) \, dt}{\sqrt{\rho^2 \cdot t^2}} & \rho > 1 \end{cases}$$

$$F(\rho) = f(\rho) \qquad \text{for} \qquad 0 \le \rho < 1$$

Therefore:

$$f(\rho) = \int_0^1 \frac{\phi(t)}{\sqrt{\rho^2 - t^2}}\, dt \qquad . \qquad 0 \le \rho < 1$$

The solution for an integral equation of this type is:

$$\phi(t) = \frac{2}{\pi} \sin\frac{\pi}{2} \quad \frac{d}{dt} \int_0^t \frac{\rho f(\rho)}{\sqrt{t^2 - \rho^2}}\, d\rho$$

$$A(\zeta) = \left\{ \int_0^1 \frac{2}{\pi} \frac{d}{dt} \int_0^t \frac{\rho f(\rho)}{\sqrt{t^2 - \rho^2}}\, d\rho \right\} \cos \zeta t\, dt$$

$$u = \zeta\left(\frac{2}{\pi}\right)\cos\zeta t \qquad\qquad dv = \frac{d}{dt} \int_0^t \frac{\rho f(\rho)}{\sqrt{t^2 - \rho^2}}\, d\rho$$

$$du = -\zeta^2\left(\frac{2}{\pi}\right)\sin\zeta t \qquad\qquad v = \int_0^t \frac{\rho f(\rho)}{\sqrt{t^2 - \rho^2}}\, d\rho$$

$$A(\zeta) = \left[\frac{2\zeta}{\pi} \cos \zeta t \int_0^t \frac{\rho f(\rho)\, d\rho}{\sqrt{t^2 - \rho^2}} \right]_0^1 - \frac{2}{\pi}\zeta^2 \int_0^1 \sin \zeta t \int_0^t \frac{\rho f(\rho)\, d\rho}{\sqrt{t^2 - \rho^2}}$$

$$A(\zeta) = \frac{2\zeta}{\pi} \cos \zeta \int_0^1 \frac{u f(u)\, du}{\sqrt{t^2 - u^2}} - \frac{2}{\pi}\zeta^2 \int_0^1 \sin \zeta t\, dt \int_0^t \frac{u f(u)\, du}{\sqrt{t^2 - u^2}}$$

$$\chi(x) = \int_0^\infty A(u)J_0(xu)du, \tag{4.4.10}$$

then we find that dual integral equations of the kind

$$\phi_1(x) = F(x), \quad \chi_2(x) = G(x) \tag{4.4.11}$$

arise in the discussion of axisymmetric problems concerning the distribution of stress in the vicinity of penny-shaped cracks in infinite elastic bodies.

If we substitute the values $\alpha = -\frac{1}{2}$, $\nu = 0$ into equation (4.2.21) we find that

$$A(u) = \frac{2}{\pi} \int_0^1 \sin ut\, dt \int_0^t \frac{\tau F(\tau)d\tau}{\sqrt{(t^2 - \tau^2)}} - \frac{2}{\pi} \sin u \int_1^\infty \frac{\tau G(\tau)d\tau}{\sqrt{(\tau^2 - 1)}}$$

$$+ \frac{2u}{\pi} \int_0^1 \cos ut\, dt \int_t^\infty \frac{\tau G(\tau)d\tau}{\sqrt{(\tau^2 - t^2)}}. \tag{4.4.12}$$

Similarly from equations (4.3.13) and (4.3.14) we derive the expressions

$$\phi_2(x) = \frac{2}{\pi} \frac{d}{dx} \int_1^x \frac{uG^*(u)du}{\sqrt{(x^2 - u^2)}} - \frac{2x\sqrt{(x^2 - 1)}}{\pi} \int_0^1 \frac{t\sqrt{(1 - t^2)}F(t)dt}{x^2 - t^2}, \tag{4.4.13}$$

$$\chi_1(x) = \frac{2}{\pi} \int_x^1 \frac{F^*(u)du}{\sqrt{(u^2 - x^2)}} + \frac{2}{\pi\sqrt{(1 - x^2)}} \int_1^\infty \frac{tG(t)dt}{(t^2 - x^2)\sqrt{(t^2 - 1)}}, \tag{4.4.14}$$

where $F^*(u)$, $G^*(u)$ are given by the equations

$$F^*(u) = \int_0^u \frac{sF(s)ds}{\sqrt{(u^2 - s^2)}}, \quad G^*(u) = -\frac{d}{du} \int_u^\infty \frac{sG(s)ds}{\sqrt{(s^2 - u^2)}}. \tag{4.4.15}$$

In this case it is readily shown that

$$2\pi \int_0^1 x\chi_1(x)dx = 4 \int_0^1 x\sqrt{(1 - x^2)}F(x)dx + 4 \int_1^\infty \frac{X(t)G(t)dt}{t\sqrt{(t^2 - 1)}} \tag{4.4.16}$$

where

$$X(t) = {}_2F_1(1,1; \tfrac{3}{2}; t^{-2}), \quad t > 1. \tag{4.4.17}$$

4.5. Dual Integral Equations with Trigonometrical Kernels

If we write

$$\phi(x) = \int_0^\infty u^{-1}A(u)\cos xu\, du \tag{4.5.1}$$

$$\chi(x) = \int_0^\infty A(u)\cos xu\, du \tag{4.5.2}$$

then the dual integral equations

$$\int_0^\infty u^{-1} A(u) \cos xu \, du = F(x), \quad x \in I_1, \qquad (4.5.3)$$

$$\int_0^\infty A(u) \cos xu \, du = 0, \qquad x \in I_2, \qquad (4.5.4)$$

which arise in the analysis of mixed boundary value problems in the plane (and which are the two-dimensional analogue of the first pair of dual equations considered in the last section), can be written in components as

$$\phi_1(x) = F(x), \qquad \chi_2(x) = 0. \qquad (4.5.5)$$

These equations are of Titchmarsh type with $\alpha = \frac{1}{2}$, $\beta = 0$, $\nu = -\frac{1}{2}$. This is a particular case which is not covered by the Titchmarsh-Busbridge solution (4.22.2) so that special methods have to be derived for the solution. Recently Srivastava (1963) has considered the equations (4.5.) with $\chi(x)$ defined by equation (4.5.2) but with $\phi(x)$ defined by the equation

$$\phi(x) = \int_0^\infty u^{2k-1} A(u) \cos xu \, du$$

but the cases $k = 0, 1$ are the only ones which are of physical interest and we shall therefore consider these cases by the method of Sneddon (1962c).

As a special case of the Weber-Schafheitlin discontinuous integral (2.1.20) we find that

$$\int_0^\infty J_1(u) \cos xu \, du = 1, \quad x \in I_1; \quad \int_0^\infty u^{-1} J_1(u) \cos xu \, du = 0, \quad x \in I_2$$

and that, if q is a positive integer,

$$\int_0^\infty u^{-1} J_{2q}(u) \cos xu \, du = (2q)^{-1} \mathfrak{F}_q(0, \tfrac{1}{2}, x^2), \quad x \in I_1$$

$$\int_0^\infty J_{2q}(u) \cos xu \, du = 0, \qquad x \in I_2$$

where $\mathfrak{F}_q$ denotes the Jacobi polynomial defined by equation (2.1.21). Hence we see that

$$A(u) = a_0 u J_1(u) + 2 \sum_{q=1}^\infty q a_q J_{2q}(u) \qquad (4.5.6)$$

will be a solution of the pair of equations (4.5.5) provided that the constants a_q are so chosen that

$$F(x) = a_0 + \sum_{q=1}^{\infty} a_q \mathfrak{F}_q(0, \tfrac{1}{2}, x^2), \quad x \in I_1.\tag{4.5.7}$$

From equations (2.6.4) and (2.6.5) we see that the orthogonality relation for the polynomials $\mathfrak{F}_q$ can be written in the form

$$\int_0^1 u^{-\frac{1}{2}}(1-u)^{-\frac{1}{2}}\mathfrak{F}_q(0, \tfrac{1}{2}, u)\mathfrak{F}_s(0, \tfrac{1}{2}, u)du = \begin{cases} \tfrac{1}{2}\pi\delta_{qs}, & \text{if } q \neq 0, \\ \pi\delta_{qs}, & \text{if } q = 0, \end{cases}$$

where δ_{qs} denotes the Kronecker delta. Using this relation and the formula

$$\mathfrak{F}_q(0, \tfrac{1}{2}, u) = {}_2F_1(-q, q; \tfrac{1}{2}; u) = \frac{\Gamma(\tfrac{1}{2})}{\Gamma(q+\tfrac{1}{2})} u^{\frac{1}{2}}(1-u)^{\frac{1}{2}}D_u^q[u^{q-\frac{1}{2}}(1-u)^{q-\frac{1}{2}}]$$

$(D_u = d/du)$ we find that

$$a_0 = \frac{1}{\pi} \int_0^1 u^{-\frac{1}{2}}(1-u)^{-\frac{1}{2}}F(u^{\frac{1}{2}})du$$

and that if $q \geqq 1$

$$a_q = \frac{2}{\Gamma(\tfrac{1}{2})\Gamma(q+\tfrac{1}{2})} \int_0^1 F(u^{\frac{1}{2}})D_u^q[u^{q-\frac{1}{2}}(1-u)^{q-\frac{1}{2}}]du$$

$$= \frac{2(-1)^q}{\Gamma(\tfrac{1}{2})\Gamma(q+\tfrac{1}{2})} \int_0^1 u^{q-\frac{1}{2}}(1-u)^{q-\frac{1}{2}}D_u^q F(u^{\frac{1}{2}})du,$$

so that

$$a_0 = \frac{2}{\pi} \int_0^1 \frac{F(x)dx}{\sqrt{(1-x^2)}},\tag{4.5.8}$$

$$a_q = \frac{(-1)^q 2^{2-q}}{\Gamma(\tfrac{1}{2})\Gamma(q+\tfrac{1}{2})} \int_0^1 x^{2q}(1-x^2)^{q-\frac{1}{2}}(x^{-1}D_x)^q F(x)dx, \quad q \geqq 1.\tag{4.5.9}$$

Since the integral

$$\int_0^\infty uJ_1(u)\cos u\, du$$

is divergent and the integral

$$\int_0^\infty J_{2q}(u)\cos u\, du \quad (q \geqq 1)$$

is convergent we see from equation (4.5.6) that if we impose the additional requirement* on our solution $A(u)$ that $\chi(x)$ must remain finite as $x \to 1-$,

---

* In contact problems in two-dimensional elasticity this condition is usually imposed by physical considerations.

then the function $F(x)$ must be such that $a_0 = 0$, and we see from equation (4.5.8) that this is equivalent to the condition

$$\int_0^1 \frac{F(x)dx}{\sqrt{(1-x^2)}} = 0. \tag{4.5.10}$$

If $x > 1$

$$\int_0^\infty u^{-1} J_{2q}(u) \cos xu \, du = \frac{(-r)^q}{2q}$$

where

$$r = [x + \sqrt{(x^2-1)}]^{-2} \tag{4.5.11}$$

so that we obtain the formula

$$\phi_2(x) = \sum_{q=1}^\infty (-r)^q a_q \tag{4.5.12}$$

where the a_q are given by equation (4.5.9) and r by equation (4.5.11). Similarly, by making use of the result

$$\int_0^\infty J_{2q}(u) \cos xu \, du = (1-x^2)^{-\frac{1}{2}} \mathfrak{F}_q(0,\tfrac{1}{2},x^2), \quad x \in I_1$$

we find that

$$\chi_1(x) = \frac{2}{\sqrt{(1-x^2)}} \sum_{q=1}^\infty q p_q \mathfrak{F}_q(0,\tfrac{1}{2},x^2).$$

Chong (1953) considered the case in which $F(x)$ is a polynomial

$$F(x) = \sum_{n=0}^m c_n x^n. \tag{4.5.14}$$

If we substitute this expression into equation (4.5.10) we find that the condition which must be satisfied if $\chi(x)$ is to remain finite as $x \to 1 -$ is

$$\sum_{n=0}^m \frac{\Gamma(\tfrac{1}{2}n + \tfrac{1}{2})}{\Gamma(\tfrac{1}{2}n + 1)} c_n = 0. \tag{4.5.15}$$

This is the criterion derived otherwise by Chong.

If $F(x)$ is a polynomial containing only even powers of x, the results are much simpler. Suppose, for example, that

$$F(x) = \sum_{n=0}^m c_{2n} x^{2n} \tag{4.5.16}$$

then it is easily shown that

$$D_u^q F(u^{\frac{1}{2}}) = \begin{cases} \sum_{n=0}^{m-q} \dfrac{(q+n)!}{n!} c_{2q+2n} u^n, & (q \leqq n), \\ \\ 0, & (q > n) \end{cases}$$

and hence from equation (4.5.9) that $a_q = 0$ if $q > n$ and that

$$a_q = \frac{2(-1)^q}{\sqrt{\pi}} \sum_{n=0}^{m-q} \frac{(q+n)! \Gamma(q+n+\frac{1}{2})}{n! \Gamma(2q+n+1)} c_{2q+2n} \quad (q \leqq n). \tag{4.5.17}$$

It should also be noted that if $\chi_2(x) = 0$ and $\phi_1(x)$ is a polynomial of degree m in x^2 then

$$\chi_1(x) = \frac{\Pi_m(x^2)}{\sqrt{(1-x^2)}} \tag{4.5.18}$$

where $\Pi_m(x^2)$ denotes a polynomial of degree m in x^2, and $\phi_2(x)$ is a polynomial of degree $2m$ in $q = [x + \sqrt{(x^2-1)}]^{-2}$.

If $F(x) = \cos n\pi x$ then it is easily shown that

$$D_u^q F(u^{\frac{1}{2}}) = \Gamma(\tfrac{1}{2}) \sum_{s=0}^{\infty} \frac{(-\frac{1}{4}\pi^2 n^2)^{s+q} u^s}{s! \Gamma(s+q+\frac{1}{2})}$$

and it follows from equation (4.5.9) that

$$a_q = 2(\tfrac{1}{2}\pi n)^{2q} \sum_{s=0}^{\infty} \frac{(-\frac{1}{4}\pi^2 n^2)^s}{s!(s+2q)!} = 2J_{2q}(n\pi).$$

Also

$$a_0 = \frac{2}{\pi} \int_0^1 \frac{\cos n\pi v \, dv}{\sqrt{(1-v^2)}} = J_0(n\pi)$$

so that the solution corresponding to $F(x) = \cos n\pi x$ is

$$A(u) = uJ_1(u)J_0(n\pi) + 4\sum_{q=1}^{\infty} qJ_{2q}(n\pi)J_{2q}(u).$$

Hence if

$$F(x) = \sum_{n=0}^{\infty} b_n \cos n\pi x, \qquad x \in I_1 \tag{4.5.19}$$

the solution of the dual integral equations (4.5.5) is

$$A(u) = uJ_1(u) \sum_{n=0}^{\infty} b_n J_0(n\pi) + 4\sum_{n=0}^{\infty}\sum_{q=1}^{\infty} qb_n J_{2q}(n\pi) J_{2q}(u). \tag{4.5.20}$$

If $\chi(x)$ is to remain finite as $x \to 1-$, the coefficients b_n must satisfy the linear relation

$$a_0 + \sum_{n=1}^{\infty} a_n J_0(n\pi) = 0. \tag{4.5.21}$$

The solution (4.5.20) was first derived by Fredricks (1958).

In a similar way it can be shown that if $F(0) = 0$, the solution of the dual integral equations

$$\left. \begin{array}{l} \displaystyle\int_0^{\infty} u^{-1} A(u) \sin xu \, du = F(x), \qquad x \in I_1 \\[3mm] \displaystyle\int_0^{\infty} A(u) \sin xu \, du = 0, \qquad x \in I_2 \end{array} \right\} \tag{4.5.22}$$

can be expressed in the form

$$A(u) = \sum_{q=0}^{\infty} (2q+1) a_q J_{2q+1}(u), \tag{4.5.23}$$

where

$$a_q = \frac{2(-1)^q}{\Gamma(\tfrac{1}{2})\Gamma(q+\tfrac{1}{2})} \int_0^1 u^{q+\frac{1}{2}}(1-u)^{q-\frac{1}{2}} D_u^q [u^{-\frac{1}{2}} F(u^{\frac{1}{2}})] du \tag{4.5.24}$$

(cf. Sneddon, 1963c, §5). From this it can readily be deduced that

$$F(x) = \sum_{n=1}^{\infty} b_n \sin n\pi x, \quad x \in I_1 \tag{4.5.25}$$

then the solution of the pair of equations (4.5.22) is

$$A(u) = \sum_{n=1}^{\infty} \sum_{q=0}^{\infty} (2q+1) b_n J_{2q+1}(n\pi) J_{2q+1}(u) \tag{4.5.26}$$

in agreement with Fredricks' result (Fredricks, 1958).

If we write

$$\phi(x) = \int_0^{\infty} u A(u) \cos xu \, du \tag{4.5.27}$$

and define $\chi(x)$ by equation (4.5.2) then the equations (4.5.5) are of the type we encounter in discussing crack problems in the two-dimensional theory of elasticity. An elementary solution of these equations can be found by a method similar to that used in §3.5. If we represent $A(u)$ in terms of a function $g(t)$ by the formula

$$A(u) = \int_0^1 g(t) J_0(tu) dt \tag{4.5.28}$$

then substituting in equation (4.5.2) and interchanging the order of the integrations we find that

$$\chi(x) = \int_0^1 g(t)dt \int_0^\infty J_0(tu) \cos xu \, du$$

and using the result (2.1.13) we see that, in this case,

$$\chi_1(x) = \int_x^1 \frac{g(t)dt}{\sqrt{(t^2 - x^2)}}, \quad \chi_2(x) = 0. \quad (4.5.29)$$

Similarly if we write

$$\phi(x) = \frac{d}{dx} \int_0^\infty A(u) \sin xu \, du,$$

substitute the form (4.5.28) for $A(u)$, interchange the order of the integrations and make use of equation (2.1.14) we find that

$$\phi_1(x) = \frac{d}{dx} \int_0^x \frac{g(t)dt}{\sqrt{(x^2 - t^2)}}, \quad \phi_2(x) = \frac{d}{dx} \int_0^1 \frac{g(t)dt}{\sqrt{(x^2 - t^2)}}. \quad (4.5.30)$$

It follows immediately that (4.5.28) will give a solution of the dual integral equations (4.5.5) provided $g(t)$ is a solution of the integral equation

$$\frac{d}{dx} \int_0^x \frac{g(t)dt}{\sqrt{(x^2 - t^2)}} = F(x), \quad x \in I_1.$$

It is easily shown by means of equations (2.3.7) that

$$g(t) = \frac{2t}{\pi} \int_0^t \frac{F(w)dw}{\sqrt{(t^2 - w^2)}}. \quad (4.5.31)$$

The solution of the dual integral equations is given by equations (4.5.28) and (4.5.31) and the auxiliary functions $\chi_1(x)$, $\phi_2(x)$ by equations (4.5.29), (4.5.30) and (4.5.31). It should also be noted that the first equation of the pair (4.5.29) leads to the result

$$\int_0^1 \chi_1(x)dx = \frac{1}{2}\pi \int_0^1 g(t)dt$$

and that substitution of the form (4.5.31) for $g(t)$ into this equation gives the formula

$$\int_0^1 \chi_1(x)dx = \int_0^1 \sqrt{(1 - w^2)} F(w)dw.$$

A solution of this type has been derived by Tranter (1963a) for the pair of equations (4.5.3) and (4.5.4). If we integrate equation (4.5.4) with respect to x we obtain the equation

$$\int_0^\infty u^{-1} A(u) \sin xu \, du = C, \quad x \in I_2,$$

where C is a constant. Now it is well-known that

$$\lim_{x \to \infty} \int_0^\infty u^{-1} A(u) \sin xu \, du = \tfrac{1}{2}\pi A(+0)$$

and if the integral $\phi(x)$ defined by equation (4.5.1) is to exist we must have $A(+0) = 0$ so that $C = 0$ and equation (4.5.4) is equivalent to

$$\int_0^\infty u^{-1} A(u) \sin xu \, du = 0. \tag{4.5.32}$$

If now we multiply equation (4.5.3) by $(\rho^2 - x^2)^{-\frac{1}{2}}$ and integrate with respect to x from 0 to ρ we find, on making use of the relation

$$\int_0^\rho \frac{\cos ux \, dx}{\sqrt{(\rho^2 - x^2)}} = \frac{1}{2} \pi J_0(\rho u)$$

obtained by applying Hankel's inversion theorem to equations (2.1.13), that

$$\frac{1}{2} \pi \int_0^\infty u^{-1} A(u) J_0(\rho u) du = \int_0^\rho \frac{F(x) dx}{\sqrt{(\rho^2 - x^2)}}, \quad 0 \leqq \rho < 1.$$

Similarly, if we multiply equation (4.5.32) by $(x^2 - \rho^2)^{-\frac{1}{2}}$ and integrate with respect to x from ρ to ∞, we find that

$$\frac{1}{2} \pi \int_0^\infty u^{-1} A(u) J_0(\rho u) du = 0, \quad \rho > 1.$$

Applying the Hankel inversion to the last two equations we find that the function $A(u)$ is given by the equation

$$A(u) = \frac{2u^2}{\pi} \int_0^1 \rho J_0(\rho u) d\rho \int_0^\rho \frac{F(x) dx}{\sqrt{(\rho^2 - x^2)}}. \tag{4.5.33}$$

Similarly to solve the pair of equations (4.5.22) we differentiate the first equation with respect to x to obtain the equivalent relation

$$\int_0^\infty A(u) \cos xu \, du = F'(x), \quad x \in I_1.$$

Proceeding in the same way as in the previous case we can then show that

$$\frac{1}{2}\pi \int_0^\alpha A(u)J_0(\rho u)\mathrm{d}u = H(1-\rho)\int_0^\rho \frac{F'(x)\mathrm{d}x}{\sqrt{(\rho^2-x^2)}}$$

from which it follows by an application of Hankel's inversion theorem that

$$A(u) = \frac{2u}{\pi}\int_0^1 \rho J_0(\rho u)\mathrm{d}\rho \int_0^\rho \frac{F'(x)\mathrm{d}x}{\sqrt{(\rho^2-x^2)}}. \tag{4.5.34}$$

4.6. Dual Integral Equations with Hankel Kernel and Arbitrary Weight Function

In this section we shall consider the solution of dual integral equations of the type

$$\phi_1(x) = F(x), \quad \chi_2(x) = G(x) \tag{4.6.1}$$

where the functions $F(x)$ and $G(x)$ are prescribed in the intervals I_1 and I_2 respectively and the functions $\phi(x)$ and $\chi(x)$ are defined in terms of the known function $k(u)$ and the unknown function $A(u)$ by means of the equations

$$\phi(x) = \int_0^\infty u^{-2\alpha}[1 + k(u)]A(u)J_\nu(xu)\mathrm{d}u, \quad \chi(x) = \int_0^\infty A(u)J_\nu(xu)\mathrm{d}u. \tag{4.6.2}$$

If we write $A(u) = u\psi(u)$ and define two functions $f(x)$ and $g(x)$ by the equations

$$f(x) = S_{\frac{1}{2}\nu-\alpha,2\alpha}\{[1 + k(u)]\psi(u); x\}, \quad g(x) = S_{\frac{1}{2}\nu,0}\psi(x) \tag{4.6.3}$$

then the equations (4.6.1) are easily shown to be equivalent to the pair

$$f_1(x) = 2^{2\alpha}x^{-2\alpha}F(x), \quad g_2(x) = G(x). \tag{4.6.4}$$

4.6.1. Reduction to a Fredholm Equation

We can reduce the problem of solving the dual integral equations (4.6.4) to that of solving a Fredholm integral equation of the second kind by using a method similar to that employed in §4.2.4 above. Putting $\beta = 0$ in equation (4.2.45) we make the representation

$$\psi(u) = S_{\frac{1}{2}\nu,-\alpha}h(u) \tag{4.6.5}$$

of the unknown function $\psi(u)$ in terms of a new unknown function $h(u)$. Substituting from equation (4.6.5) into equations (4.6.3) we find that

$$f(x) = S_{\frac{1}{2}\nu-\alpha,2\alpha}S_{\frac{1}{2}\nu,-\alpha}h(x) + S_{\frac{1}{2}\nu-\alpha,2\alpha}\{k(x)S_{\frac{1}{2}\nu,-\alpha}h(x)\}$$

and that

$$g(x) = S_{\frac{1}{2}\nu,0}S_{\frac{1}{2}\nu,-\alpha}h(x).$$

Section 4.5   Dual Integral Equations with
                     Trigonometric Kernels

p.103

(1)
$$\int_0^\infty u\, A(u)\cos xu\, du = \phi(x)$$

(2)
$$\int_0^\infty A(u)\cos xu\, du = \chi(x)$$

$\downarrow$

$$\int_0^\infty u\, A(u)\cos xu\, du = F(x) \qquad x \in I_1$$

$$\int_0^\infty A(u)\cos xu\, du = 0 \qquad x \in I_2$$

$$A(u) = \int_0^1 g(t)\, J_0(tu)\, dt$$

Substitute into (2)

$$\chi(x) = \int_0^1 g(t)\, dt \underbrace{\int_0^\infty J_0(tu)\cos xu\, du}$$

$$\int_0^\infty J_0(tu)\cos xu\, du = \begin{cases} 0 & 0 \le t < x \\[2mm] \dfrac{1}{\sqrt{t^2 - u^2}} & t > x \end{cases}$$

$$\chi_1 = \int_x^1 \frac{g(t)\, dt}{\sqrt{t^2 - x^2}} \qquad\qquad \chi_2 = 0$$

Satisfies boundary conditions 2

Rewriting equation 1),

$$\phi(t) = \frac{d}{dx}\int_0^\infty A(u)\sin xu\, du$$

$$\phi(x) = \frac{d}{\pi x} \quad g(t) \, dt \quad \int_0^a J_0(tu) \, s_i \, x u \, du$$

$$\int_0^\alpha J_0(tu) \, s_i \, x u \, dx \quad = \quad \sqrt{\frac{1}{x^2 - t^2}} \qquad \qquad 0 \le t < x$$

$$\qquad \qquad \qquad \qquad \qquad \qquad \qquad 0 \qquad \qquad t > x$$

$$\phi_1(t) = \frac{d}{dx} \int_0^x \frac{f^{(x)} \, dt}{x^2 - t^2}$$

$$\phi_2(x) = \frac{d}{dx} \int_0^1 \frac{g(t) \, dt}{\sqrt{x^2 - t^2}}$$

$$F(x) = \frac{d}{dx} \int_0^x \frac{g(t) \, dt}{\sqrt{x^2 - t^2}} \qquad \qquad x \in I_1$$

$$\int F(x) \, dx = \int_0^x \frac{g(t) \, dt}{\sqrt{x^2 - t^2}}$$

$$g(t) = \frac{2}{\pi} \frac{d}{dt} \int_0^t \frac{u \, F(u) \, du}{\sqrt{t^2 - u^2}}$$

$$g(t) = \frac{2t}{\pi} \int_0^t \frac{F(w) \, dw}{\sqrt{t^2 - w^2}}$$

$$A(u) = \int_0^1 \frac{2t}{\pi} \int_0^t \frac{F(w) \, dw}{\sqrt{t^2 - w^2}} \quad J_0(tu) \, dt$$

Appendix C

I. When Equations (47) and (49) are substituted into the even and odd parts of Equations (30)-(37) and (38)-(45), respectively, the resulting equations are of the form shown in these handwritten notes. You will realize that both parts of each function are not fully written out because the minor differences in the equations may be accounted for by observation.

II. The infinite integrals are solved analytically by a method similar to Sneddon, pp. 496-497 [5]. The derivations and symbols are slightly different than those used in [2].

The following is equivalent to Equation (75), (142), and (143) in [5]:

$$C_n^m(a,x,y) = \int_0^\infty \xi^{n-2} \cos(\xi y) J_m(a\xi) e^{-\xi x} d\xi \tag{75}$$

$$S_n^m(a,x,y) = \int_0^\infty \xi^{n-2} \sin(\xi y) J_m(a\xi) e^{-\xi x} d\xi \tag{142}$$

$$C_n^m(a,x,y) - i S_n^m(a,x,y) = Z_n^m(a, x + iy) \tag{143}$$

NOTE: The Mathematica output is utilized in the handwritten portion. The notation is the same.

$$w'_{odd} = \frac{-1}{\pi(3+\nu)(1-\nu)D} \int_0^\infty \frac{1}{\xi_i} \left[\frac{1}{2} a^2 \pi^{-1/2} \sum_{n=1,3,5}^{N} \frac{\Gamma(\frac{n}{2}+1)}{\Gamma(\frac{n}{2}+\frac{5}{2})} C_n \, J_{-1}(a\xi) \right.$$

$$\left. + a\xi \int_0^1 y^{n+2} J_{-2}(a\xi y) \, dy \right] \left[(1+\nu) - (1-\nu)\xi x \right] e^{-\xi x} \sin(\xi y) \, d\xi$$

$$w_{odd} = \frac{-a^2}{2\pi^{1/2}(3+\nu)(1-\nu)D} \int_0^\infty \frac{1}{\xi} \left\{ \sum_{n=1,3,5,\ldots}^{N} \frac{\Gamma(\frac{n}{2}+1)}{\Gamma(\frac{n}{2}+\frac{5}{2})} C_n \left[J_{-1}(a\xi) \right] (1+\nu)-(1-\nu)\xi x \right. \cdot$$

$$e^{-\xi x} \sin(\xi y)\, d\xi$$

$$- \frac{a^2}{2\pi^{1/2}(3+\nu)(1-\nu)D} \int_0^\infty \left\{ \sum_{n=1,3,5,\ldots}^{N} C_n \int_0^1 y_i^{n+2} J_2(a\xi y_i)\, dy_i \right\}$$

$$\left[(1+\nu) - (1-\nu)\xi x \right] e^{-\xi x} \sin(\xi y) \, d\xi$$

$$w_{odd} = K_1 \left\{ \sum_{n=1,3,5,\ldots}^{N} \frac{\Gamma(\frac{n}{2}+1)}{\Gamma(\frac{n}{2}+\frac{5}{2})} C_n \left[\int_0^\infty \frac{(1+\nu)}{\xi} J_1(a\xi) e^{-\xi x}\sin(\xi y)\, d\xi \right. \right.$$

$$\left. \left. - \int_0^\infty (1-\nu) x \, J_1(a\xi) e^{-\xi x}\sin(\xi y)\, d\xi \right] \right\} +$$

$$K_2 \left\{ \sum_{n=1,3,5,\ldots}^{N} \frac{\Gamma(\frac{n}{2}+1)}{\Gamma(\frac{n}{2}+\frac{5}{2})} C_n \left[\int_0^1 y_i^{n+2}\, dy_i \int_0^\infty (1+\nu) J_2(a\xi y_i) e^{-\xi x}\sin(\xi y)\, d\xi \right. \right.$$

$$\left. \left. - \int_0^1 y_i^{n+2}\, dy_i \int_0^\infty (1-\nu)x \, J_2(a\xi y_i) e^{-\xi x}\sin(\xi y)\, d\xi \right] \right\}$$

$$w_{odd} = K_1 (1+\nu) S_1^1 - K_1 (1-\nu) x \, S_2^1 +$$

$$K_2 \int_0^1 (1+\nu) y_i^{n+2} S_2^2 \, dy_i - K_2 \int_0^1 (1-\nu) x \, y_i^{n+2} S_3^2 \, dy_i$$

2

$$W_{even} = \frac{-1}{\sim(3+\nu)(1-\nu)D}\int_0^\infty \frac{1}{\zeta^2}\left[\frac{1}{2}a^2 \sim \frac{1}{2}\right\}\sum_{n=0,2,}^{N}\frac{\Gamma(\frac{n}{2}+\frac{1}{2})}{\Gamma(\frac{n}{2}+2)}C_n\left[J_0(a\zeta)\right.$$

$$+ a\zeta\int_0^1 y^{n+2}J_1(a\zeta y)dy\Big][(1+\nu)-(1-\nu)\zeta x]e^{-\zeta x}\cos(\zeta \gamma)d\zeta$$

$$W_{even} = \frac{-a^2}{2\pi^{1/2}(3+\nu)(1-\nu)D}\int_0^\infty \frac{1}{\zeta}\sum_{n=0,2}^{N}\frac{\Gamma(\frac{n}{2}+\frac{1}{2})}{\Gamma(\frac{n}{2}+2)}C_n J_0(a\zeta)[(1+\nu)-(1-\nu)\zeta$$
$$\cos(\zeta\gamma)d\zeta$$

$$\frac{-a^3}{2\pi^{1/2}(3+\nu)(1-\nu)D}\int_0^\infty\sum_{n=0,2}^{N}\frac{\Gamma(\frac{n}{2}+\frac{1}{2})}{\Gamma(\frac{n}{2}+2)}C_n\int_0^1 y_i^{n+2}J_1(a\zeta y_i)dy_i$$

$$\left[(1+\nu)-(1-\nu)\zeta x\right]e^{-\zeta x}\cos(\zeta\gamma)d\zeta$$

$$W_{even} = K_1\left\{\sum_{n=0,2,..}^{N}\frac{\Gamma(\frac{n}{2}+\frac{1}{2})}{\Gamma(\frac{n}{2}+2)}C_n\left[\int_0^\infty(1+\nu)\frac{1}{\zeta}J_0(a\zeta)e^{-\zeta x}\cos(\zeta\gamma)d\zeta\right.\right.$$

$$-\int_0^\infty(1-\nu)x\ J_0(a\zeta)e^{-\zeta x}\cos(\zeta\gamma)d\zeta\Big]\Big\} +$$

$$K_2\left\{\sum_{n=0,2}^{N}\frac{\Gamma(\frac{n}{2}+\frac{1}{2})}{\Gamma(\frac{n}{2}+2)}C_n\left[\int_0^1 y_i^{n+2}\int_0^\infty(1+\nu)J_1(a\zeta y_i)e^{-\zeta x}\cos\zeta\gamma\,d\zeta\,dy_i\right.\right.$$

$$-\int_0^1 y_i^{n+2}\int_0^\infty(1-\nu)x\ \zeta J_1(a\zeta y_i)e^{-\zeta x}\cos(\zeta\gamma)d\zeta\,dy_i\Big]\Big\}$$

$$W_{even} = K_1'(1+\nu)C_1^0 - K_1'(1-\nu)x\ C_2^0$$

$$+ K_2'\int_0^1 y_i^{n+2}(1+\nu)C_2^1\,dy_i - K_2'\int_0^1 y_i^{n+2}(1-\nu)x\ C_3^1\,dy_i$$

$$m_{x_{even}} = \frac{1}{\pi(3+\nu)} \int_0^\infty \left[\frac{1}{2} a^2 \sim^{1/2} \left\{ \sum_{n=2,\dots}^{N} \frac{\Gamma(\frac{n}{2}+\frac{1}{2})}{\Gamma(\frac{n}{2}+2)} c_n J_0(a\xi) \right. \right.$$

$$a_i^3 \int_0^1 y_i^{n+2} J_1(a\xi y_i) dy_i \left[(3+\nu) - (1+\nu)\xi x \right] e^{-\xi x} \cos(\xi y) d\xi$$

$$m_{x_{even}} = \frac{a^2}{2\pi^{1/2}(3+\nu)} \int_0^\infty \left\{ \sum_{n=2}^{N} \frac{\Gamma(\frac{n}{2}+\frac{1}{2})}{\Gamma(\frac{n}{2}+2)} c_n J_0(a\xi) \left[(3+\nu) - (1+\nu)\xi x \right] e^{-\xi x} \cos(\xi y) d\xi \right.$$

$$+ \frac{a^3}{2\pi^{1/2}(3+\nu)} \int_0^\infty \sum_{n=2}^{N} \frac{\Gamma(\frac{n}{2}+\frac{1}{2})}{\Gamma(\frac{n}{2}+2)} c_n \int_0^1 y_i^{n+2} J_1(a\xi y_i) dy_i$$

$$\xi^2 \left[(3+\nu) - (1+\nu)\xi x \right] e^{-\xi x} \cos(\xi y) d\xi$$

$$m_{x_{even}} = K_1 \left\{ \sum_{n=0,2,\dots}^{N} \frac{\Gamma(\frac{n}{2}+\frac{1}{2})}{\Gamma(\frac{n}{2}+2)} c_n \left[\int_0^\infty (3+\nu) \xi J_0(a\xi) e^{-\xi x} \cos(\xi y) d\xi \right. \right.$$

$$- \int_0^\infty (1+\nu) x \xi^2 J_0(a\xi) e^{-\xi x} \cos(\xi y) d\xi \right] \right\}$$

$$+ K_2 \left\{ \sum_{n=0,2,\dots}^{N} \frac{\Gamma(\frac{n}{2}+\frac{1}{2})}{\Gamma(\frac{n}{2}+2)} c_n \left[\int_0^1 y_i^{n+2} \int_0^\infty (3+\nu) \xi^2 J_1(a\xi y_i) e^{-\xi x} \cos(\xi y) d\xi dy_i \right. \right.$$

$$- \int_0^1 y_i^{n+2} \int_0^\infty (1+\nu) x \xi^2 J_1(a\xi y_i) e^{-\xi x} \cos(\xi y) d\xi dy_i \right] \right\}$$

$$m_{x_{even}} = K_1' (3+\nu) C_3^0 - K_1' (1+\nu) x C_4^0$$

$$+ K_2' \int_0^1 y_i^{n+2} (3+\nu) C_4' dy_i - K_2' \int_0^1 y_i^{n+2} (1+\nu) x C_5' dy_i$$

$$m_{x_{odd}} = \frac{1}{x(3+\nu)} \int_0^\infty \left[\frac{1}{2} a^2 \pi^{1/2} \int \sum_{n=0,2...}^{N} \frac{\Gamma(\frac{n}{2}+1)}{\Gamma(\frac{n}{2}+\frac{5}{2})} c_n \ldots \right] +$$

$$a \xi \int_0^1 y^{n+2} J_2(a^i y_i) dy_i \right] \ldots (1+\nu) \ldots e^{-\xi x} \sin(\xi \gamma) d\xi$$

$$m_{x_{odd}} = \frac{a^2}{2\pi^{1/2}(3+\nu)} \int_0^\infty \left\{ \sum_{n=0,2...}^{N} \frac{\Gamma(\frac{n}{2}+1)}{\Gamma(\frac{n}{2}+\frac{5}{2})} c_n J_1(a\xi) \left[(3+\nu) - (1+\nu)\xi x \right] \right.$$
$$\left. e^{-\xi x} \sin(\xi \gamma) d\xi \right.$$

$$+ \frac{a^2}{2\pi^{1/2}(3+\nu)} \int_0^\infty \left\{ \sum_{n=0,2...}^{N} \frac{\Gamma(\frac{n}{2}+1)}{\Gamma(\frac{n}{2}+\frac{5}{2})} c_n \int_0^1 y_i^{n+2} J_2(a\xi y_i) dy_i \right.$$

$$\xi^2 \left[(3+\nu) - (1+\nu)\xi x \right] e^{-\xi x} \sin(\xi \gamma) d\xi$$

$$m_{x_{odd}} = K_1 \left\{ \sum_{n=0,2...}^{N} \frac{\Gamma(\frac{n}{2}+1)}{\Gamma(\frac{n}{2}+\frac{5}{2})} c_n \left[\int_0^\infty (3+\nu)\xi J_1(a\xi) e^{-\xi x} \sin(\xi \gamma) d\xi \right. \right.$$

$$\left. \left. - \int_0^\infty (1+\nu) x \xi^2 J_1(a\xi) e^{-\xi x} \sin(\xi \gamma) d\xi \right] \right\}$$

$$+ K_2 \left\{ \sum_{n=0,2...}^{N} \frac{\Gamma(\frac{n}{2}+1)}{\Gamma(\frac{n}{2}+\frac{5}{2})} c_n \left[\int_0^1 y_i^{n+2} \int_0^\infty (3+\nu)\xi^2 J_2(a\xi y_i) e^{-\xi x} \sin(\xi \gamma) d\xi dy_i \right. \right.$$

$$\left. \left. - \int_0^1 y_i^{n+2} \int_0^\infty (1+\nu) x \xi^3 J_2(a\xi y_i) e^{-\xi x} \sin(\xi \gamma) d\xi dy_i \right] \right\}$$

$$m_{x_{odd}} = K_1' (3+\nu) S_3' - K_1' (1+\nu) x S_4' +$$

$$K_2' \int_0^1 y_i^{n+2} (3+\nu) C_4^2 dy_i - K_2' \int_0^1 y_i^{n+2}(1+\nu) x$$

$$C_5^2 dy_i$$

$$m_{y_{oven}} = \frac{(1-\nu)}{\nu(3+\nu)} \left[\frac{1}{2} \int \cdots \frac{1}{2} \sum_{n=0,2,\ldots}^{N} \frac{\Gamma(\frac{n}{2}+\frac{1}{2})}{\Gamma(\frac{n}{2}+2)} C_n \cdots \cos(\xi y) - \right.$$

$$\left. a_i^3 \int_0^1 y^{n-2} J_1(a\xi y_i) dy_i \right] \left[-1 + \xi x \right] \xi^2 e^{-\xi x} \cos(\xi y) d\xi \}$$

$$m_{y_{even}} = \frac{a^2(1-\nu)}{2\eta^{1/2}(3+\nu)} \int_0^\infty \xi \sum_{n=0,2,\ldots}^{N} \frac{\Gamma(\frac{n}{2}+\frac{1}{2})}{\Gamma(\frac{n}{2}+2)} C_n J_0(a\xi)\left[-1+\xi x\right] e^{-\xi x} \cos(\xi y) d\xi$$

$$+ \frac{(1-\nu) a^3}{2\eta^{1/2}(3+\nu)} \int_0^\infty \sum_{n=0,2,\ldots}^{N} \frac{\Gamma(\frac{n}{2}+\frac{1}{2})}{\Gamma(\frac{n}{2}+2)} C_n \int_0^1 y_i^{n-2} J_1(a\xi y_i) dy_i$$

$$\xi^2\left[-1+\xi x\right] e^{-\xi x} \cos(\xi y) d\xi$$

$$m_{y_{even}} = K_1 \left\{ \sum_{n=0,2}^{N} \frac{\Gamma(\frac{n}{2}+\frac{1}{2})}{\Gamma(\frac{n}{2}+2)} C_n \left[-\int_0^\infty \xi J_0(a\xi) e^{-\xi x} \cos(\xi y) d\xi \right. \right.$$

$$\left. + \int_0^\infty x \xi^2 J_0(a\xi) e^{-\xi x} \cos(\xi y) d\xi \right] \right\}$$

$$+ K_2 \left\{ \sum_{n=0,2,\ldots}^{N} \frac{\Gamma(\frac{n}{2}+\frac{1}{2})}{\Gamma(\frac{n}{2}+2)} C_n \left[-\int_0^1 y_i^{n+2} \int_0^\infty \xi^2 J_1(a\xi y_i) e^{-\xi x} \cos(\xi y) d\xi dy_i \right. \right.$$

$$\left. + \int_0^1 y_i^{n+2} \int_0^\infty x \xi^3 J_1(a\xi y_i) e^{-\xi x} \cos(\xi y) d\xi dy_i \right] \right\}$$

$$m_{y_{even}} = -K_1' C_3^0 + K_1' x C_4^0$$

$$- K_2' \int_0^1 y_i^{n+2} C_4' dy_i + K_2' \int_0^1 y_i^{n+2} C_5' dy_i$$

$$m_{xy\,even} = \frac{-1}{\pi^{1/2}(3+\nu)} \int_0^\infty \frac{1}{\zeta} a^2 e^{-\zeta x} \sum_{n=2}^{N} \frac{\Gamma(\frac{n}{2}+\frac{1}{2})}{\Gamma(\frac{n}{2}+2)} c_n \cdots$$

$$a_j^2 \int_0^\infty y^{n+2} J_1(a\zeta y)\,dy \Big]\Big[-2 + (1-\nu)\zeta x \Big] e^{-\zeta x} \sin(\zeta y)\,d\zeta$$

$$m_{xy\,even} = \frac{-a^2}{2\pi^{1/2}(3+\nu)}\int_0^\infty \Big\{ \sum_{n=2}^{N} \frac{\Gamma(\frac{n}{2}+\frac{1}{2})}{\Gamma(\frac{n}{2}+2)} c_n \, J_0(a\zeta)\Big[-2 + (1-\nu)\zeta x\Big] e^{-\zeta x}\sin(\zeta y)\zeta$$

$$- \frac{a^3}{2\pi^{1/2}(3+\nu)}\int_0^\infty \sum_{n=2}^{N} \frac{\Gamma(\frac{n}{2}+\frac{1}{2})}{\Gamma(\frac{n}{2}+2)} c_n \int_0^1 y_i^{n+2} J_1(a\zeta y_i)\,dy_i$$

$$\zeta^2\Big[-2 + (1-\nu)\zeta x\Big] e^{-\zeta x}\sin(\zeta y)\,d\zeta$$

$$m_{xy\,even} = K_1 \Big\{ \sum_{n=2}^{N} \frac{\Gamma(\frac{n}{2}+\frac{1}{2})}{\Gamma(\frac{n}{2}+2)} c_n \Big[\int_0^\infty -2\,\zeta\, J_0(a\zeta)\, e^{-\zeta x}\sin(\zeta y)\,d\zeta$$

$$+ \int_0^\infty (1-\nu)x\,\zeta^2\, J_0(a\zeta)\, e^{-\zeta x}\sin(\zeta y)\,d\zeta \Big]\Big\}$$

$$+ K_2\Big\{ \sum_{n=2}^{N} \frac{\Gamma(\frac{n}{2}+\frac{1}{2})}{\Gamma(\frac{n}{2}+2)} c_n \Big[\int_0^1 y_i^{n+2}\int_0^\infty -2\zeta^2 J_1(a\zeta y_i)\, e^{-\zeta x}\sin(\zeta y)\,d\zeta\,dy_i$$

$$+ \int_0^1 y_i^{n+2}\int_0^\infty (1-\nu)x\,\zeta^2 J_1(a\zeta y_i)\, e^{-\zeta x}\sin(\zeta y)\,d\zeta\,dy_i \Big]\Big\}$$

$$m_{xy\,even} = -2 K_1'\, S_3^0 \;+\; K_1'(1-\nu)x\, S_4^0$$

$$-2K_2'\int_0^1 y_i^{n+2} S_4'\,dy_i \;+\; K_2'\int_0^1 (1-\nu)x\, y_i^{n+2} S_5'\,dy_i$$

$$g_{x\,even} = \frac{-2}{\pi i(n)}\int_0^\infty \tfrac{1}{2}a^2 \, n \, \xi^2 \left\{ \frac{\Gamma(\frac{\xi}{2}+\frac{1}{2})}{\Gamma(\frac{n}{2}+2)} \left\{ J_0(a\xi) + a\xi\int_0^1 y^{n+2} J_1(a\xi y)\,dy \right\} \right\} \left[\xi e^{-\xi x}\cos(\xi y) \right] d\xi$$

$$g_{x\,even} = K \int_0^\infty \xi^2 J_0(a\xi)\, e^{-\xi x}\cos(\xi y)\, d\xi$$
$$+ Ka \int_0^1 y^{n+2}\, dy \int_0^\infty \xi^3 J_1(a\xi y)\, e^{-\xi x}\cos(\xi y)\, dy$$

$$g_{x\,even} = \frac{K\, C_4^0}{y_m^3} + Ka \int_0^1 \frac{y^{n+2}}{y_m^4} C_5^1\, dy$$

$$g_{x\,odd} = \frac{K\, S_4^1}{y_m^3} + Ka \int_0^1 \frac{y^{n+2}}{y_m^4} S_5^2\, dy$$

$$g_{y\,even} = \frac{-2}{\pi i(n)}\int_0^\infty \tfrac{1}{2}a^2 \, n \, \xi^2 \left\{ \frac{\Gamma(\frac{\xi}{2}+\frac{1}{2})}{\Gamma(\frac{n}{2}+2)} \left\{ J_0(a\xi) + a\xi\int_0^1 y^{n+2} J_1(a\xi y)\,dy \right\} \right\} \left[\xi e^{-\xi x}\sin(\xi y) \right] d\xi$$

$$g_{y\,even} = K \int_0^\infty \xi^2 J_0(a\xi)\, e^{-\xi x}\sin(\xi y)\, d\xi$$
$$+ Ka \int_0^1 y^{n+2}\, dy \int_0^\infty \xi^3 J_1(a\xi y)\, e^{-\xi x}\sin(\xi y)\, dy$$

$$g_{y\,even} = \frac{K\, S_4^0}{y_m^3} + Ka \int_0^1 \frac{y^{n+2}}{y_m^4} S_5^1\, dy$$

$$g_{y\,odd} = \frac{K\, C_4^1}{y_m^3} + Ka \int_0^1 \frac{y^{n+2}}{y_m^2} C_5^2\, dy$$

$$N_{x_{even}} = \frac{-1-\gamma)\pi}{\pi(3+\gamma)} \int_0^{1/2 a^2 \pi} \cdots = \frac{\Gamma(\frac{n}{2}+1)}{\Gamma(\frac{n}{2}+2)} \left(J_0(a\xi) + \cdots y^{n-2} \cdots y \right) \cdots$$

$$\cdots \xi^2 e^{-\xi x \cos(\xi y)} \Big] d\xi$$

$$N_{x_{even}} = K \int_0^\infty \xi^3 J_0(a\xi) e^{-\xi x \cos(\xi y)} d\xi$$

$$+ K \int_0^1 a y^{n-2} dy \int_0^\infty \xi^4 J_1(a\xi y) e^{-\xi x \cos(\xi y)} d\xi$$

$$N_{x_{even}} = \frac{K}{y_m^4} C_5^0 + Ka \int_0^1 \frac{y^{n-2}}{y_m^5} C_6^1 dy$$

$$N_{x_{odd}} = \frac{K_2}{y_m^4} S_5^1 + K_2 a \int_0^1 \frac{y^{n-2}}{y_m^5} S_6^2 dy$$

$$v_{y_{cat}} = \frac{-1}{\Gamma(3+\nu)} \int_0^\infty \frac{1}{2} a^2 \zeta^{-1} \left\{ \left[\frac{\Gamma(\frac{5}{2}+\frac{\nu}{2})}{\Gamma(\frac{\nu}{2}+2)} \cdots \right] + a_{10} \cdots \right.$$

$$\left. \left\{ -5 -\nu) - (1-\nu)\{x\right] e^{-\zeta x} \sin(\zeta y) \right\} d\zeta$$

$$v_{y_{extn}} = K \int_0^\infty (5-\nu) \zeta^2 J_0(x\zeta) e^{-\zeta x} \sin(\zeta y) d\zeta$$

$$- K \int_0^\infty (1-\nu) x \zeta^3 J_0(a\zeta) e^{-\zeta x} \sin(\zeta y) d\zeta$$

$$+ K \int_0^1 (5-\nu) a y^{n+2} dy \int_0^\infty \zeta^3 J_1(a\zeta y) e^{-\zeta x} \sin(\zeta y) d\zeta$$

$$- K \int_0^1 (1-\nu) a x y^{n+2} dy \int_0^\infty \zeta^4 J_1(a\zeta y) e^{-\zeta x} \sin(\zeta y) d\zeta$$

$$v_{y_{even}} = (5-\nu)\frac{K}{Y_m^3} S_4^0 - \frac{K}{Y_m^4}(1-\nu)x \; S_5^0$$

$$+ (5-\nu) a K \int_0^1 \frac{y^{n+2}}{Y_m^4} S_5^1 dy$$

$$- (1-\nu) a x K \int_0^1 \frac{y^{n+2}}{Y_5^4} S_6^1 dy$$

$$v_{y_{odd}} = \frac{(5-\nu)K_2}{Y_m^3} C_4^1 - \frac{K_2(1-\nu)x}{Y_m^4} C_5^1$$

$$+ (5-\nu) a K_2 \int_0^1 \frac{y^{n+2}}{Y_m^4} C_5^2 dy$$

$$- (1-\nu) a x K_2 \int_0^1 \frac{y^{n+2}}{Y_m^5} C_6^2 dy$$

Z=1/(a^2+w^2)^(1/2)

$$\frac{1}{\text{Sqrt}[a^2 + w^2]}$$

 Integrate[Z,w]

$$\text{Log}[w + \text{Sqrt}[a^2 + w^2]]$$

 Z01=w + Sqrt[a^2+w^2]

$$w + \text{Sqrt}[a^2 + w^2]$$

 w=x+I y

$$x + I\, y$$

 Z01

$$x + \text{Sqrt}[a^2 + (x + I\, y)^2] + I\, y$$

 ComplexExpand[Expand[Z01]]

$$x + (4\, x^2\, y^2 + (a^2 + x^2 - y^2)^2)^{1/4}$$

$$\text{Cos}\left[\frac{\text{Arg}[a^2 + x^2 + 2\, I\, x\, y - y^2]}{2}\right] +$$

$$I\, (y + (4\, x^2\, y^2 + (a^2 + x^2 - y^2)^2)^{1/4}$$

$$\text{Sin}\left[\frac{\text{Arg}[a^2 + x^2 + 2\, I\, x\, y - y^2]}{2}\right])$$

 ro=((r Cos[O]+R^(1/2)Cos[Fe/2])^2+(r Sin[O]+R^(1/2)Sin[Fe/2])^2)^(1/2)

$$\text{Sqrt}\left[\left(\text{Sqrt}[R]\,\text{Cos}\left[\frac{Fe}{2}\right] + r\,\text{Cos}[O]\right)^2 +\right.$$

$$\left.\left(\text{Sqrt}[R]\,\text{Sin}\left[\frac{Fe}{2}\right] + r\,\text{Sin}[O]\right)^2\right]$$

 Simplify[ro]

$$\text{Sqrt}\left[r^2 + R + 2\, r\,\text{Sqrt}[R]\,\text{Cos}\left[\frac{Fe}{2} - O\right]\right]$$

 Zo2=(a^2+(x+I y)^2)^(-1/2)

$$\frac{1}{\text{Sqrt}[a^2 + (x + I\, y)^2]}$$

`ComplexExpand[Expand[Zo2]]`

$$\frac{\cos\left[\dfrac{\text{Arg}[a^2 + x^2 + 2\,I\,x\,y - y^2]}{2}\right]}{(4\,x^2\,y^2 + (a^2 + x^2 - y^2)^2)^{1/4}} - $$

$$\frac{I\,\sin\left[\dfrac{\text{Arg}[a^2 + x^2 + 2\,I\,x\,y - y^2]}{2}\right]}{(4\,x^2\,y^2 + (a^2 + x^2 - y^2)^2)^{1/4}}$$

`Z03=(x+I y)/(a^2+(x+I y)^2)^(3/2)`

$$\frac{x + I\,y}{(a^2 + (x + I\,y)^2)^{3/2}}$$

`ComplexExpand[Expand[Z03]]`

$$\frac{x\,\cos\left[\dfrac{3\,\text{Arg}[a^2 + x^2 + 2\,I\,x\,y - y^2]}{2}\right]}{(4\,x^2\,y^2 + (a^2 + x^2 - y^2)^2)^{3/4}} + $$

$$\frac{y\,\sin\left[\dfrac{3\,\text{Arg}[a^2 + x^2 + 2\,I\,x\,y - y^2]}{2}\right]}{(4\,x^2\,y^2 + (a^2 + x^2 - y^2)^2)^{3/4}} + $$

$$I\left(\frac{y\,\cos\left[\dfrac{3\,\text{Arg}[a^2 + x^2 + 2\,I\,x\,y - y^2]}{2}\right]}{(4\,x^2\,y^2 + (a^2 + x^2 - y^2)^2)^{3/4}} - \right.$$

$$\left.\frac{x\,\sin\left[\dfrac{3\,\text{Arg}[a^2 + x^2 + 2\,I\,x\,y - y^2]}{2}\right]}{(4\,x^2\,y^2 + (a^2 + x^2 - y^2)^2)^{3/4}}\right)$$

`Z04=-1/(a^2+(x+I y)^2)^(3/2)+3(x+I y)^2/(a^2+(x+I y)^2)^(5/2)`

$$-(a^2 + (x + I\,y)^2)^{-(3/2)} + \frac{3\,(x + I\,y)^2}{(a^2 + (x + I\,y)^2)^{5/2}}$$

`ComplexExpand[Together[ExpandAll[Z04]]]`

$$\frac{(-a^2 + 2x^2 - 2y^2) \, \text{Cos}\left[\frac{5 \, \text{Arg}[a^2 + x^2 + 2\,I\,x\,y - y^2]}{2}\right]}{(4x^2y^2 + (a^2 + x^2 - y^2)^2)^{5/4}} +$$

$$\frac{4xy \, \text{Sin}\left[\frac{5 \, \text{Arg}[a^2 + x^2 + 2\,I\,x\,y - y^2]}{2}\right]}{(4x^2y^2 + (a^2 + x^2 - y^2)^2)^{5/4}} +$$

$$I \left(\frac{4xy \, \text{Cos}\left[\frac{5 \, \text{Arg}[a^2 + x^2 + 2\,I\,x\,y - y^2]}{2}\right]}{(4x^2y^2 + (a^2 + x^2 - y^2)^2)^{5/4}} - \right.$$

$$\left.\frac{(-a^2 + 2x^2 - 2y^2) \, \text{Sin}\left[\frac{5 \, \text{Arg}[a^2 + x^2 + 2\,I\,x\,y - y^2]}{2}\right]}{(4x^2y^2 + (a^2 + x^2 - y^2)^2)^{5/4}}\right)$$

`Z05=-3/2 G (x+I y)/(a^2+(x+I y)^2)^(5/2)+5/2 G (x+I y)^3/(a^2+(x+I y)^2)^`

$$\frac{-3 \, G \, (x + I \, y)}{2 \, (a^2 + (x + I \, y)^2)^{5/2}} + \frac{5 \, G \, (x + I \, y)^3}{2 \, (a^2 + (x + I \, y)^2)^{7/2}}$$

`Together[Z05]`

$$(-3a^2 G x + 2 G x^3 - 3 I a^2 G y + 6 I G x^2 y - 6 G x y^2 -$$

$$2 I G y^3) \, / \, (2 \, (a^2 + x^2 + 2 I x y - y^2)^{7/2})$$

```
ComplexExpand[Together[Z05]]
```

$$((-3 a^2 G x + 2 G x^3 - 6 G x y^2)$$

$$\mathrm{Cos}\left[\frac{7\, \mathrm{Arg}[a^2 + x^2 + 2\, I\, x\, y - y^2]}{2}\right]) /$$

$$(2\, (4\, x^2\, y^2 + (a^2 + x^2 - y^2)^2)^{7/4}) +$$

$$((-3 a^2 G y + 6 G x^2 y - 2 G y^3)$$

$$\mathrm{Sin}\left[\frac{7\, \mathrm{Arg}[a^2 + x^2 + 2\, I\, x\, y - y^2]}{2}\right]) /$$

$$(2\, (4\, x^2\, y^2 + (a^2 + x^2 - y^2)^2)^{7/4}) +$$

$$I\, (((-3 a^2 G y + 6 G x^2 y - 2 G y^3)$$

$$\mathrm{Cos}\left[\frac{7\, \mathrm{Arg}[a^2 + x^2 + 2\, I\, x\, y - y^2]}{2}\right]) /$$

$$(2\, (4\, x^2\, y^2 + (a^2 + x^2 - y^2)^2)^{7/4}) -$$

$$((-3 a^2 G x + 2 G x^3 - 6 G x y^2)$$

$$\mathrm{Sin}\left[\frac{7\, \mathrm{Arg}[a^2 + x^2 + 2\, I\, x\, y - y^2]}{2}\right]) /$$

$$(2\, (4\, x^2\, y^2 + (a^2 + x^2 - y^2)^2)^{7/4}))$$

```
Z06=(p^2+a^2)^(-5/2)*G5*LegendreP[4,p/(p^2+a^2)^(1/2)]
```

$$\frac{G5\, (3 a^4 - 24 a^2 p^2 + 8 p^4)}{8\, (a^2 + p^2)^{9/2}}$$

```
p=x+I y
```

$$x + I\, y$$

```
ComplexExpand[Z06]
```

$$\left(G5\ \left(3\ a^4 - 24\ a^2\ (x^2 - y^2) + 8\ (x^4 - 6\ x^2\ y^2 + y^4)\right)\right.$$

$$\left.\cos\left[\frac{9\ \text{Arg}[a^2 + (x + I\ y)^2]}{2}\right]\right) \Big/$$

$$\left(8\ \text{Abs}[a^2 + (x + I\ y)^2]^{9/2}\right) +$$

$$\left(G5\ (-48\ a^2\ x\ y + 8\ (4\ x^3\ y - 4\ x\ y^3))\right.$$

$$\left.\sin\left[\frac{9\ \text{Arg}[a^2 + (x + I\ y)^2]}{2}\right]\right) \Big/$$

$$\left(8\ \text{Abs}[a^2 + (x + I\ y)^2]^{9/2}\right) +$$

$$I\ \left(\left(G5\ (-48\ a^2\ x\ y + 8\ (4\ x^3\ y - 4\ x\ y^3))\right.\right.$$

$$\left.\cos\left[\frac{9\ \text{Arg}[a^2 + (x + I\ y)^2]}{2}\right]\right) \Big/$$

$$\left(8\ \text{Abs}[a^2 + (x + I\ y)^2]^{9/2}\right) -$$

$$\left(G5\ \left(3\ a^4 - 24\ a^2\ (x^2 - y^2) + 8\ (x^4 - 6\ x^2\ y^2 + y^4)\right)\right.$$

$$\left.\sin\left[\frac{9\ \text{Arg}[a^2 + (x + I\ y)^2]}{2}\right]\right) \Big/$$

$$\left.\left(8\ \text{Abs}[a^2 + (x + I\ y)^2]^{9/2}\right)\right)$$

$$R^2 = (a^2 + x^2 - y^2)^2 + 4x^2 y^2$$

$$(a^2 + x^2 - y^2) \tan\phi = 2xy$$

$$\tan\phi = \frac{2xy}{(a^2 + x^2 - y^2)}$$

$$r^2 = x^2 + y^2$$

$$\tan\theta = \frac{y}{x}$$

$$z_2^? \cdots \quad e^{\cdots} \cdots \xi \, d\xi$$

$$\int z_2^? \, d\omega = \int_0^a - \frac{e^{-\omega\xi}}{\xi} \, J_0(a\xi) \, d\xi \, .$$

$$\downarrow$$

$$\int \frac{1}{(a^2+\omega^2)^{1/2}} \, d\omega = - \int \frac{e^{-\omega\xi}}{\xi} \, J_0(a\xi) \, d\xi$$

From Mathematica

$$- \int \frac{e^{-\omega\xi}}{\xi} \, J_0(a\xi) \, d\xi = Log \left[\omega + (a^2+\omega^2)^{1/2} \right]$$

$$- Z_1^0 = Log \left[x + R^{1/2} \cos \frac{\phi}{2} + i \left(y + R^{1/2} \sin \frac{\phi}{2} \right) \right]$$

$$= Log \left[r\cos\theta + R^{1/2}\cos\frac{\phi}{2} + i \left(r\sin\theta + R^{1/2} \sin \frac{\phi}{2} \right) \right]$$

$$Z_1^0 = -\ln r_0 - i\theta$$

$$\boxed{S_1^0 = \Theta = \tan^{-1} \left[\frac{r\sin\theta + R^{1/2} \sin \frac{\phi}{2}}{r\cos\theta + R^{1/2}\cos\frac{\phi}{2}} \right]}$$

$$\boxed{C_1^0 = -\ln r_0 = -\frac{1}{2} Ln \left[r^2 + R + 2r R^{1/2} \cos\left(\frac{\phi}{2} - \theta\right) \right]}$$

$$Z_3^0 = \int_{0}^{\infty} ? \ldots ?|| e^{-?(x+iy)} \, d?$$

$$\Xi_3^0 = \frac{x+iy}{\left[a^2 + (x+iy)^2\right]^{3/2}}$$

$$Z_3^0 = \left[\frac{x\cos\left(\frac{3}{2}\theta\right)}{R^{3/2}} + \frac{y\sin\left(\frac{3}{2}\theta\right)}{R^{3/2}}\right] -$$

$$i\left[\frac{-y\cos\left(\frac{3\theta}{2}\right)}{R^{3/2}} + \frac{x\sin\left(\frac{3\theta}{2}\right)}{R^{3/2}}\right]$$
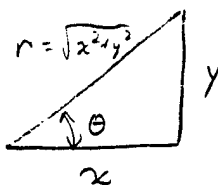
$$r = \sqrt{x^2+y^2} \qquad x = r\cos\theta$$
$$\qquad\qquad y = r\sin\theta$$

$$C_3^0 = \left[r\cos\frac{3\theta}{2}\cos\theta + r\sin\theta\sin\frac{3\theta}{2}\right]/R^{3/2}$$

$$C_3^0 = r\left[\cos\left(\frac{3\theta}{2}-\theta\right)\right]/R^{3/2}$$

$$\boxed{C_3^0 = r\,R^{-3/2}\cos\left(\frac{3\theta}{2}-\theta\right)}$$

$$S_3^0 = R^{-3/2}\left[-r\sin\theta\cos\frac{3\theta}{2} + r\cos\theta\sin\frac{3\theta}{2}\right]$$

$$\boxed{S_3^0 = r\,R^{-3/2}\sin\left(\frac{3\theta}{2}-\theta\right)}$$

$$Z_4^0 = \int_0 \xi^2 \, J_0(a\xi) \, e^{-\xi(x+iy)} \, d\xi$$

$$Z_4^0 = \frac{-1}{\left[a^2 + (x+iy)^2\right]^{3/2}} \quad + \quad \frac{3(x+iy)^2}{\left[a^2 + (x+iy)^2\right]^{5/2}}$$

$$Z_4^0 = \frac{\left(2x^2 - 2y^2 - a^2\right)}{R^{5/2}} \cos\left(5\phi/2\right) \quad +$$

$$\frac{4xy}{R^{5/2}} \sin\left(5\phi/2\right) \quad +$$

$$i\left[\frac{4xy}{R^{5/2}} \cos\left(5\phi/2\right) - \frac{\left(2x^2 - 2y^2 - a^2\right)}{R^{5/2}} \sin\left(5\phi/2\right)\right]$$

$$\boxed{C_4^0 = \frac{\left(2x^2 - 2y^2 - a^2\right)}{R^{5/2}} \cos 5\phi/2 \quad + \quad \frac{4xy}{R^{5/2}} \sin 5\phi/2}$$

$$\boxed{S_4^0 = \frac{4xy}{R^{5/2}} \cos 5\phi/2 \quad - \quad \frac{2x^2 - 2y^2 - a^2}{R^{5/2}} \sin 5\phi/2}$$

$$\zeta_5^0 \cdots$$

$$Z_5^0 = \frac{\Gamma(3+0+)}{\left[a^2 + (x+iy)^2\right]^{9/2}} \quad f_2^0\left(\frac{x+iy}{a^2+(x+iy)^2}\right)$$

$$Z_5^0 = \frac{\Gamma(4)}{\left[a^2+(x+iy)^2\right]^2}\left\{-\frac{3}{2}\frac{x+iy}{\left[a^2+(x+iy)^2\right]^{1/2}} + \frac{5}{2}\frac{(x+iy)^3}{\left[a^2+(x+iy)^2\right]^{3/2}}\right\}$$

$$\zeta_5^0 = -\frac{3}{2}\Gamma(4)\frac{x+iy}{\left[a^2+(x+iy)^2\right]^{5/2}} + \frac{5}{2}\Gamma(4)\frac{(x+iy)^3}{\left[a^2+(x+iy)^2\right]^{7/2}}$$

$$Z_5^0 = \frac{\Gamma(4)\left[-3a^2(x+iy) + 2(x+iy)^3\right]}{2\left[a^2+(x+iy)^2\right]^{7/2}}$$

$$C_5^0 = \frac{\Gamma(4)(2x^3 - 6xy^2 - 3a^2x)\cos\left(\frac{7\phi}{2}\right)}{2R^{7/2}} +$$

$$\frac{\Gamma(4)(6x^2y - 2y^3 - 3a^2y)\sin\left(\frac{7\phi}{2}\right)}{2R^{7/2}}$$

$$S_5^0 = \frac{\Gamma(4)\left(6x^2y - 2y^3 - \frac{3}{a^2}y\right)\cos\left(\frac{7\phi}{2}\right)}{2R^{7/2}} -$$

$$\frac{\Gamma(4)(2x^3 - 6xy^2 - 3a^2x)\sin\left(\frac{7\phi}{2}\right)}{2R^{7/2}}$$

$$Z_6^0 = \int_0^\infty \{ \xi^4 J_0(a\xi)\, e^{-\xi(...)} \}\, d\xi$$

$$P_4(x) = \tfrac{1}{4}\left[(3(3)+1) x\, P_3(x) - 3 P_2(x) \right]$$

$$P_4(x) = \tfrac{7}{4} x \left[\tfrac{5x^3}{2} - \tfrac{3x}{2} \right] - \tfrac{1}{4}\left[\tfrac{9x^2}{2} - \tfrac{3}{2} \right]$$

$$P_4(x) = \frac{35x^4}{8} - \frac{21x^2}{8} - \frac{9x^2}{8} - \frac{3}{8}$$

$$P_4(x) = \frac{35x^4}{8} - \frac{30x^2}{8} - \frac{3}{8}$$

$$C_6^0 = \frac{\Gamma(5)}{8R^{9/2}}\left[3a^4 - 24a^2(x^2-y^2) + 8(x^4 - 6x^2 y^2 + y^4)\right]\cos\frac{9\varnothing}{2}$$

$$+ \frac{\Gamma(5)}{8R^{9/2}}\left[-48a^2 xy + 8(4x^3 y - 4xy^3)\right]\sin\frac{9\varnothing}{2}$$

$$S_6^0 = \frac{\Gamma(5)}{8R^{9/2}}\left[-48a^2 xy + 8(4x^3 y - 4xy^3)\right]\cos\frac{9\varnothing}{2}$$

$$+ \frac{\Gamma(5)}{8R^{9/2}}\left[3a^4 - 24a^2(x^2-y^2) + 8(x^4 - 6x^2 y^2 + y^4)\right]\sin\frac{9\varnothing}{2}$$

```
Z11=((a^2+(x+I y)^2)^(1/2)-(x+I y))/a
```

$$-x + \text{Sqrt}[a^2 + (x + I\ y)^2] - I\ y$$
$$\overline{\phantom{-x + \text{Sqrt}[a^2}}\ a\ }$$

```
ComplexExpand[Expand[Z11]]
```

$$-\left(\frac{x}{a}\right) + \frac{(4\ x^2\ y^2 + (a^2 + x^2 - y^2)^2)^{1/4}\ \text{Cos}\left[\dfrac{\text{Arg}[a^2 + x^2 + 2\ I\ x\ y - y^2]}{2}\right]}{a} +$$

$$I\ \left(-\left(\frac{y}{a}\right) + \frac{(4\ x^2\ y^2 + (a^2 + x^2 - y^2)^2)^{1/4}\ \text{Sin}\left[\dfrac{\text{Arg}[a^2 + x^2 + 2\ I\ x\ y - y^2]}{2}\right]}{a}\right)$$

```
Z12=1/a-(x+I y)/(a*(a^2+(x+I y)^2)^(1/2))
```

$$\frac{1}{a} - \frac{x + I\ y}{a\ \text{Sqrt}[a^2 + (x + I\ y)^2]}$$

```
ComplexExpand[Expand[Z12]]
```

$$\frac{1}{a} - \frac{x\ \text{Cos}\left[\dfrac{\text{Arg}[a^2 + x^2 + 2\ I\ x\ y - y^2]}{2}\right]}{a\ (4\ x^2\ y^2 + (a^2 + x^2 - y^2)^2)^{1/4}} -$$

$$\frac{y\ \text{Sin}\left[\dfrac{\text{Arg}[a^2 + x^2 + 2\ I\ x\ y - y^2]}{2}\right]}{a\ (4\ x^2\ y^2 + (a^2 + x^2 - y^2)^2)^{1/4}} +$$

$$I\ \left(-\left(\frac{y\ \text{Cos}\left[\dfrac{\text{Arg}[a^2 + x^2 + 2\ I\ x\ y - y^2]}{2}\right]}{a\ (4\ x^2\ y^2 + (a^2 + x^2 - y^2)^2)^{1/4}}\right) + \right.$$

$$\left. \frac{x\ \text{Sin}\left[\dfrac{\text{Arg}[a^2 + x^2 + 2\ I\ x\ y - y^2]}{2}\right]}{a\ (4\ x^2\ y^2 + (a^2 + x^2 - y^2)^2)^{1/4}}\right)$$

```
Z13=a/(a^2+(x+I y)^2)^(3/2)
```

$$\frac{a}{(a^2 + (x + I\ y)^2)^{3/2}}$$

```
ComplexExpand[Expand[Z13]]
```

$$
\frac{a \cos\left[\dfrac{3 \operatorname{Arg}[a^2 + x^2 + 2 I x y - y^2]}{2}\right]}{(4 x^2 y^2 + (a^2 + x^2 - y^2)^2)^{3/4}} -
$$

$$
\frac{I a \sin\left[\dfrac{3 \operatorname{Arg}[a^2 + x^2 + 2 I x y - y^2]}{2}\right]}{(4 x^2 y^2 + (a^2 + x^2 - y^2)^2)^{3/4}}
$$

```
Z14=3(x+I y)((x+I y)+(a^2+(x+I y)^2)^(1/2))/(a^2+(x+I y)^2)^(5/2)*
    a/((x+I y)+(a^2+(x+I y)^2)^(1/2))
```

$$
\frac{3 a (x + I y)}{(a^2 + (x + I y)^2)^{5/2}}
$$

```
ComplexExpand[Expand[Z14]]
```

$$
\frac{3 a x \cos\left[\dfrac{5 \operatorname{Arg}[a^2 + x^2 + 2 I x y - y^2]}{2}\right]}{(4 x^2 y^2 + (a^2 + x^2 - y^2)^2)^{5/4}} +
$$

$$
\frac{3 a y \sin\left[\dfrac{5 \operatorname{Arg}[a^2 + x^2 + 2 I x y - y^2]}{2}\right]}{(4 x^2 y^2 + (a^2 + x^2 - y^2)^2)^{5/4}} +
$$

$$
I \left(\frac{3 a y \cos\left[\dfrac{5 \operatorname{Arg}[a^2 + x^2 + 2 I x y - y^2]}{2}\right]}{(4 x^2 y^2 + (a^2 + x^2 - y^2)^2)^{5/4}} - \frac{3 a x \sin\left[\dfrac{5 \operatorname{Arg}[a^2 + x^2 + 2 I x y - y^2]}{2}\right]}{(4 x^2 y^2 + (a^2 + x^2 - y^2)^2)^{5/4}} \right)
$$

P15=LegendreP[3,-1,z]

$$-\frac{(1 - 5\,z^2)\,\text{Sqrt}[1 - z^2]}{8}$$

z=(x+I y)/(a^2+(x+I y)^2)^(1/2)

$$\frac{x + I\,y}{\text{Sqrt}[a^2 + (x + I\,y)^2]}$$

Z15=24/(a^2+(x+I y)^2)^2*P15

$$\frac{-3\,\left(1 - \dfrac{5\,(x + I\,y)^2}{a^2 + (x + I\,y)^2}\right)\,\text{Sqrt}\left[1 - \dfrac{(x + I\,y)^2}{a^2 + (x + I\,y)^2}\right]}{(a^2 + (x + I\,y)^2)^2}$$

PowerExpand[%]

$$\frac{3\,a\,(-a^2 + 4\,x^2 + 8\,I\,x\,y - 4\,y^2)}{(a^2 + x^2 + 2\,I\,x\,y - y^2)^{7/2}}$$

ComplexExpand[Simplify[%]]

$$\frac{3\,a\,(-a^2 + 4\,x^2 - 4\,y^2)\,\text{Cos}\left[\dfrac{7\,\text{Arg}[a^2 + x^2 + 2\,I\,x\,y - y^2]}{2}\right]}{(4\,x^2\,y^2 + (a^2 + x^2 - y^2)^2)^{7/4}} +$$

$$\frac{24\,a\,x\,y\,\text{Sin}\left[\dfrac{7\,\text{Arg}[a^2 + x^2 + 2\,I\,x\,y - y^2]}{2}\right]}{(4\,x^2\,y^2 + (a^2 + x^2 - y^2)^2)^{7/4}} +$$

$$I\,\left(\frac{24\,a\,x\,y\,\text{Cos}\left[\dfrac{7\,\text{Arg}[a^2 + x^2 + 2\,I\,x\,y - y^2]}{2}\right]}{(4\,x^2\,y^2 + (a^2 + x^2 - y^2)^2)^{7/4}} - \right.$$

$$\left.\frac{3\,a\,(-a^2 + 4\,x^2 - 4\,y^2)\,\text{Sin}\left[\dfrac{7\,\text{Arg}[a^2 + x^2 + 2\,I\,x\,y - y^2]}{2}\right]}{(4\,x^2\,y^2 + (a^2 + x^2 - y^2)^2)^{7/4}}\right)$$

```
Z16=(p^2+a^2)^(-5/2)*Gamma[4+1+1]*LegendreP[4,-1,p/(p^2+a^2)^(1/2)]
```

$$-15 \, \sqrt{\frac{a^2}{a^2 + p^2}} \, \frac{(3 \, a^2 \, p - 4 \, p^3)}{(a^2 + p^2)^4}$$

```
p=(x+I y)
```

$$x + I \, y$$

```
Simplify[%]
```

$$\frac{-15 \, I \, a \, (-I \, x + y) \, (3 \, a^2 - 4 \, x^2 - 8 \, I \, x \, y + 4 \, y^2)}{(a^2 + x^2 + 2 \, I \, x \, y - y^2)^{9/2}}$$

`ComplexExpand[%]`

$$8\,x\,y\,\left(\frac{-15\,a\,y\,\cos\left[\dfrac{9\,\text{Arg}[a^2 + x^2 + 2\,I\,x\,y - y^2]}{2}\right]}{(4\,x^2\,y^2 + (a^2 + x^2 - y^2)^2)^{9/4}}\right.$$

$$\left.+\frac{15\,a\,x\,\sin\left[\dfrac{9\,\text{Arg}[a^2 + x^2 + 2\,I\,x\,y - y^2]}{2}\right]}{(4\,x^2\,y^2 + (a^2 + x^2 - y^2)^2)^{9/4}}\right) +$$

$$(3\,a^2 - 4\,x^2 + 4\,y^2)\,\left(\frac{-15\,a\,x\,\cos\left[\dfrac{9\,\text{Arg}[a^2 + x^2 + 2\,I\,x\,y - y^2]}{2}\right]}{(4\,x^2\,y^2 + (a^2 + x^2 - y^2)^2)^{9/4}}\right.$$

$$\left.-\frac{15\,a\,y\,\sin\left[\dfrac{9\,\text{Arg}[a^2 + x^2 + 2\,I\,x\,y - y^2]}{2}\right]}{(4\,x^2\,y^2 + (a^2 + x^2 - y^2)^2)^{9/4}}\right) +$$

$$I\,\left((3\,a^2 - 4\,x^2 + 4\,y^2)\,\left(\frac{-15\,a\,y\,\cos\left[\dfrac{9\,\text{Arg}[a^2 + x^2 + 2\,I\,x\,y - y^2]}{2}\right]}{(4\,x^2\,y^2 + (a^2 + x^2 - y^2)^2)^{9/4}}\right.\right.$$

$$\left.+\frac{15\,a\,x\,\sin\left[\dfrac{9\,\text{Arg}[a^2 + x^2 + 2\,I\,x\,y - y^2]}{2}\right]}{(4\,x^2\,y^2 + (a^2 + x^2 - y^2)^2)^{9/4}}\right) -$$

$$8\,x\,y\,\left(\frac{-15\,a\,x\,\cos\left[\dfrac{9\,\text{Arg}[a^2 + x^2 + 2\,I\,x\,y - y^2]}{2}\right]}{(4\,x^2\,y^2 + (a^2 + x^2 - y^2)^2)^{9/4}}\right.$$

$$\left.\left.-\frac{15\,a\,y\,\sin\left[\dfrac{9\,\text{Arg}[a^2 + x^2 + 2\,I\,x\,y - y^2]}{2}\right]}{(4\,x^2\,y^2 + (a^2 + x^2 - y^2)^2)^{9/4}}\right)\right)$$

$$z_1' = \dots \frac{1}{z} \dots (0.) \dots$$

$$z_1' = \frac{\left[a^2 + (a+y)^2\right]^{\frac{1}{2}} - (x+iy)}{a}$$

$$z_1' = -\frac{x}{a} + \frac{R^{\frac{1}{2}}}{a}\cos\left(\frac{\phi}{2}\right) -$$

$$i\left[+\frac{y}{a} - \frac{R^{\frac{1}{2}}}{a}\sin\left(\frac{\phi}{2}\right)\right]$$

$$\boxed{C_1' = -\frac{x}{a} + \frac{R^{\frac{1}{2}}}{a}\cos\left(\frac{\phi}{2}\right)}$$

$$\boxed{S_1' = \frac{y}{a} - \frac{R^{\frac{1}{2}}}{a}\sin\left(\frac{\phi}{2}\right)}$$

$$Z_2' = \int_0^\infty \cdots d^2$$

$$\Xi_2' = \int_0^\infty \sim_1(o') \, e^{-(x+y)} \, d\cdots$$

$$\Xi_2' = \frac{1}{a} - \frac{x - \cdots}{a(a^2 + x \cdots)^2)^{1/2}}$$

$$Z_2' = \frac{1}{a} - \frac{x \cos \frac{\phi}{2}}{a R^{1/2}} - \frac{y \sin \frac{\phi}{2}}{a R^{1/2}}$$

$$- i \left[\frac{y \cos \frac{\phi}{2}}{a R^{1/2}} - \frac{x \sin \frac{\phi}{2}}{a R^{1/2}} \right]$$

$$Z_2' = \frac{1}{a} - \frac{R^{1/2}}{a} \left[r \cos\theta \cos\frac{\phi}{2} + r \sin\theta \sin\frac{\phi}{2} \right]$$

$$- i \left[\frac{r \sin\theta \cos\frac{\phi}{2} - r \cos\theta \sin\frac{\phi}{2}}{a R^{1/2}} \right]$$

$$\boxed{C_2' = \frac{1}{a} - \frac{r R^{1/2}}{a} \cos\left(\theta - \frac{\phi}{2}\right)}$$

$$\boxed{S_2' = \frac{r R^{1/2}}{a} \sin\left(\theta - \frac{\phi}{2}\right)}$$

$$\Xi_3' = \int_0^\infty J_{-1}(a\zeta)\, e^{-\zeta(x+\eta)}\, d\zeta$$

$$\Xi_3' = \frac{a}{[a^2 + (x+\eta)^2]^{3/2}}$$

$$\boxed{C_3' = a R^{-3/2} \cos \tfrac{3\phi}{2}}$$

$$\boxed{S_3' = a R^{-3/2} \sin \tfrac{3\phi}{2}}$$

$$Z_4' = \int_0^\infty \zeta^2 J_1(a\zeta)\, e^{-\zeta(x+\eta)}\, d\zeta \qquad \text{From Bateman Proj.}$$

$$\Xi_4' = \frac{3(x+iy)\left[(x+iy) + [a^2+(x+\eta)^2]^{1/2}\right]}{[a^2+(x+iy)^2]^{5/2}} \left\{ \frac{a}{(x+iy) + (a^2 + \eta^2 \cdots)} \right.$$

$$Z_4' = \frac{3a(x+iy)}{[a^2 + (x+iy)^2]^{5/2}}$$

$$Z_4' = \frac{3ax}{R^{5/2}} \cos \tfrac{5\phi}{2} + \frac{3ay \sin \tfrac{5\phi}{2}}{R^{5/2}} +$$

$$\qquad - i\left[\frac{3ax}{R^{5/2}} \sin \tfrac{5\phi}{2} - \frac{3ay}{R^{5/2}} \cos \tfrac{5\phi}{2} \right]$$

$$\boxed{C_4' = \frac{3a}{R^{5/2}}\left[x\cos \tfrac{5\phi}{2} + y\sin \tfrac{5\phi}{2} \right]}$$

$$\boxed{S_4' = \frac{3a}{R^{5/2}}\left[x\sin \tfrac{5\phi}{2} - y\cos \tfrac{5\phi}{2} \right]}$$

$$Z_5' = \int_0^\infty t^3 J(at) \, e^{i(\dots)} \, dt$$

Bateman Prj.

$$Z_5' = \frac{\Gamma(3+1+1)}{a^2+(x+iy)^2]^{4/2}} \quad P_3^{-1}\left[\frac{x+y}{a^2+(x+iy)^2)^{\frac{1}{2}}}\right]$$

$$P_3^{-1}(x) = (x^2-1)^{-1/2} \frac{1}{2^{3/2}3!} \frac{d^2}{dz^2}\left[(x^2-1)^3\right]$$

$$P_3^{-1}(x) = \frac{1}{8\cdot6} \frac{1}{(x^2-1)^{1/2}} \left[6(x^2-1)(2x^2) + 6(x^2-1)^2\right]$$

$$\frac{d}{dx}\left[(x^2-1)^3\right] = 3(x^2-1)^2(2x)$$

$$\frac{d^2}{dx^2}\left[(x^2-1)^3\right] = 6(x^2-1)(4x^2) + 3\cdot3(x^2-1)^2$$

$$P_3^{-1}(x) = \frac{1}{2}x^2(x^2-1)^{1/2} + \frac{1}{8}(x^2-1)^{3/2}$$

$$P_3^{-1}(x) = \frac{1}{8}(x^2-1)^{1/2}\left[4x^2 + x^2 - 1\right] = \frac{1}{8}(x^2-1)^{1/2}(5x^2-1)$$

$$Z_5' = \frac{3a(4x^2-4y^2-a^2)}{R^{7/2}}\cos\frac{7\phi}{2} + \frac{24axy}{R^{7/2}}\sin\frac{7\phi}{2}$$

$$- i\left[\frac{-24axy}{R^{7/2}}\cos\frac{7\phi}{2} + \frac{3a(4x^2-4y^2-a^2)}{R^{7/2}}\sin\frac{7\phi}{2}\right]$$

$$\boxed{C_5' = \frac{3a(4x^2-4y^2-a^2)}{R^{7/2}}\cos\frac{7\phi}{2} + \frac{24axy}{R^{7/2}}\sin\frac{7\phi}{2}}$$

$$\boxed{S_5' = \frac{3a(4x^2-4y^2-a^2)}{R^{7/2}}\sin\frac{7\phi}{2} - \frac{24axy}{R^{7/2}}\cos\frac{7\phi}{2}}$$

$$Z_6 = \int_6^\infty \; \gamma(a^2) \; e^{-k(x+y)} \; dy$$

$$Z_6' = \frac{\Gamma(4+1+1)}{\left[a^2+(x+y)^2\right]^{5/2}} \quad P_4^{-1}\left[\frac{x+y}{\left[a^2+(x+y)^2\right]}\right]^4$$

$$P_4^{-1} = (x^2-1)^{-1/2} \; \frac{1}{2^4(4!)} \; \frac{d^3}{dx^3}\left[(x^2-1)^4\right]$$

$$\frac{d}{dx}\left[(x^2-1)^4\right] = 4(x^2-1)^3(2x)$$

$$\frac{d^2}{dx^2}\left[(x^2-1)^4\right] = 12(x^2-1)^2(2x^2) + 8(x^2-1)^3$$

$$\frac{d^3}{dx^3}\left[(x^2-1)^4\right] = 48x^2(x^4-2x^2+1) + 8(x^2-1)^3$$

$$= 48(6)x^5 - 96(4)x^3 + 48(3)x$$
$$+ 24(x^2-1)^2(2x)$$

$$= 48(6)x^5 - 96(4)x^3 + 96x +$$
$$48(x^5 - 2x^3 + x)$$

$$= 48(7)x^5 - 96(5)x^3 + 144x$$
$$= 336x^5 - 480x^3 + 144x$$

$$P_4^{-1} = (x^2-1)^{1/2}(7x^5 - 10x^3 + 3)/8$$

$$P_4^{-1} = \frac{7}{8}(1-x^2)^{1/2}(3x - 7x^3)$$

Define:
$$\delta = a^2 + x^2 - y^2$$

$$Z_6{}' = \int_0^\infty \zeta^4 J_1(a\zeta) e^{-\zeta(x+iy)} \, d\zeta$$

$$Z_0{}' = \frac{\Gamma(4i \cdots)}{\left[a^2 + (x+iy)^2\right]^{\cdots}} \qquad P_1{}' \left[\frac{x+y}{\left[a^2+(x+iy)^2\right]^{1/2}}\right]$$

$$C_6{}' = \frac{-15a\left[3a^2 x - 4(x^3 - 3xy^2)\right]}{R^{9/2}} \cos\frac{9\varphi}{2}$$

$$- \frac{15a\left[3a^2 y - 4(3x^2 y - y^3)\right]}{R^{9/2}} \sin\frac{9\varphi}{2}$$

$$\bar{=}_6{}' = \frac{15a\left[3a^2 y - 4(3x^2 y - y^3)\right]}{R^{9/2}} \cos\frac{9\varphi}{2}$$

$$- \frac{15a\left[3a^2 x - 4(x^3 - 3xy^2)\right]}{R^{9/2}} \sin\frac{9\varphi}{2}$$

Appendix D

I. A copy of the user instructions from Zienkiewicz [7] is included.

II. Additional macro commands are also given.

III. Example Problems

Fig. 15.7   Mesh for circular disk problem

by coalescing the shape functions of two nodes; hence in this case only one element routine need be used.[11]

After a sketch of the mesh has been made the elements and nodes are numbered in consecutive order. The order of numbering nodes is crucial for the profile solution method, whereas the order of numbering the elements is crucial for the frontal method. As a general rule, numbering the elements and nodes along the same directions in the mesh will produce both a minimum front and a minimum profile. Indeed, numbering nodes in the order that a minimum effort front solution would eliminate the unknowns will also produce an efficient profile solution scheme (e.g., see reference 12 where it is shown that the effort in both solution methods is identical). A numbering can usually be improved in some sense by using an automatic renumbering scheme.[13-15] The method in reference 15 produces a near-optimal numbering for the number of terms under the profile—which will give maximum efficiency in a resolve mode. The coding to implement this method is very compact and executes rapidly.

---

method it is necessary to know beforehand the profile of the equations, and this is determined by first numbering the active equations as described above and then using the element connection array, IX, together with the equation number and boundary condition array, ID, to determine the maximum column height of each equation. Finally the equations are compacted into a vector and the column heights are used to construct the address of the diagonal elements in the storage vector. The programming steps for the profile determination are given in subroutine PROFIL. The total number of equations is determined by the maximum value of the ID array and is called NEQ. The total storage requirement for either the upper (or lower) half of the matrix profile is given by the address for the diagonal of NEQ [i.e., JDIAG(NEQ)]. Thus the storage requirements in common ADATA must be increased by this amount for each profile matrix required, e.g., by NEQ and JDIAG(NEQ) for linear symmetric steady-state problems.

In the frontal method, the current implementation divides the available storage into two parts: one part stores the coefficient terms and right-hand size of the active frontal equations and the other is used as a buffer area to store equations that have already been reduced. Only when the buffer is full will writes to the disk be performed. This minimizes costly input/output operations on the disk and greatly improves efficiency over that of previous implementations (e.g., those in reference 2 or 3). In order to make this division it is necessary to know beforehand how large the front will become during the solution process. This computation is performed by subprogram PREFRT and stored in the variable MAXF.

15.3   User instructions for computer program

The solution of a finite element problem using the program given at the end of this chapter begins with a sketch of a mesh covering the region to be analysed. The user must select a consistent set of units to define the numerical values for data. If boundaries are curved the mesh will only approximate the shape of the region (e.g., see Fig. 15.7). In sketching the mesh the type and order (linear, quadratic, etc.) of elements must be taken into consideration: for triangular elements in two dimensions the mesh is described by a net of triangles, whereas for quadrilateral isoparametric four-noded elements the region can be described by a net of quadrilaterals. The user may wish to use both triangles and quadrilaterals. In this case two element routines may be necessary, one for triangles and one for quadrilaterals. The shape function routine, SHAPE, for quadrilaterals given in this chapter includes the three-noded triangle
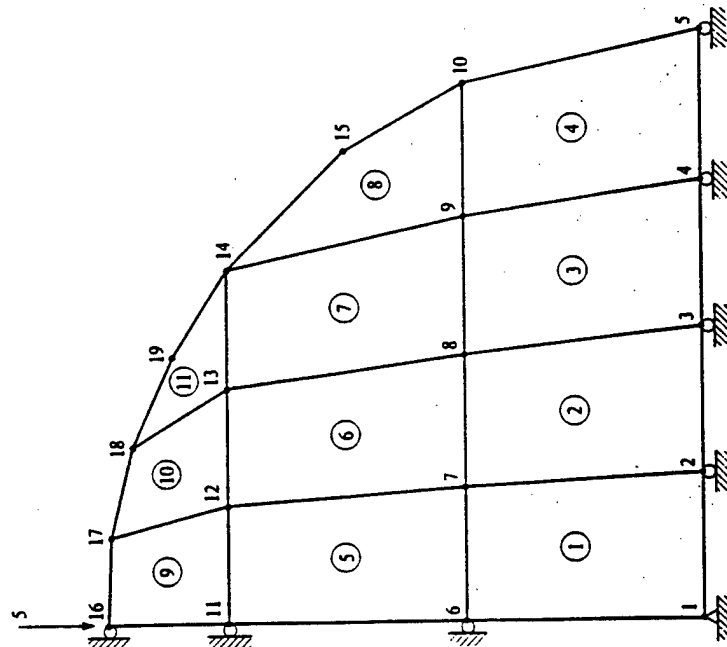
TABLE 15.4
TITLE AND CONTROL INFORMATION FORMATS

TITLE—FORMAT (20A4)
The title also serves as a start of problem record. The first four (4) columns must contain the start word FEAP.

Columns	Description	Variable
1 to 4	Must contain FEAP	TITL(I)
5 to 80	Alphanumeric information for header in output file	TITL(I) I = 2, 20

CONTROL DATA—FORMAT (7I5)

Columns	Description	Variable
1 to 5	Number of nodes	NUMNP
6 to 10	Number of elements	NUMEL
11 to 15	Number of material sets	NUMMAT
16 to 20	Spatial dimension (≤3)	NDM
21 to 25	Number of unknowns per node (≤6)	NDF
26 to 30	Number of nodes/element	NEN
31 to 35	Added size to element matrices, in excess of NDF*NEN	NAD

Once the sketch and numbering of the mesh is completed the user can proceed to the preparation of data for the program. The first step consists of specifying problem title and control information given in Table 15.4, which is used during subsequent data input and also is used to allocate memory in the program.

In addition to the input data formats, Table 15.4 gives the variable names used in the program. The variables NDF, NEN, and NAD are used to calculate the size of the element arrays, NST. Normally for displacement formulations NDF*NEN is the size of the element array; however, if nodeless variables or mixed methods are used it may be desirable to increase the size of the element array NAD (note that the NAD variables are not assembled as global parameters).

Once the control data is supplied the program expects the data records for the mesh description, e.g., nodal coordinates, element connections, etc. Each problem or problem class may require different types and amounts of data; consequently, the flow of data to the program is controlled by a set of *macro* commands. The available macro commands are given in Table 15.5; others may be added by suitably modifying the data list WD in subroutine PMESH. The macro commands PRIN† and NOPRint allow the user to output and suppress output to the screen or the 'output' file, respectively, of any data which is input subsequently.

† Only capital characters are data. In the program, text may be input in upper or lower case. A free format parser is included in PCFEAP which permits input of text and numerical fields to be separated by a comma (,). This avoids the need to keep count of columns.

TABLE 15.5
DATA INPUT: MACRO CONTROL STATEMENTS

INPUT MACRO CONTROL—FORMAT (A4)
The input of each data segment is controlled by the value assigned to CC. The following values are admissible and each CC record must be immediately followed by the appropriate data (described in Tables 15.6 to 15.14).

CC value	Data to be input
COOR	Coordinate data
ELEM	Element data
MATE	Material data
BOUN	Boundary condition data
FORC	Prescribed nodal force data
TEMP	Temperature data
BLOC	Node and element data
POLA	Convert polar coordinates to cartesian form
ANGL	Angle of sloping two-dimensional boundaries
PRIN	Print subsequent mesh data (default mode)
NOPR	Do not print subsequent mesh data
END	Must be last record in mesh data, terminates mesh input

Except for END and POLA the data segments can be in any order. If the values of ANGL, BOUN, FORC, or TEMP are zero, no input data is required.

Thus, once a mesh has been fully checked and subsequent analyses are desired it is not necessary to reprint all the mesh data.

An analysis will require at least:

(a) coordinate data which follows the macro command COOR and is prepared as described in Table 15.6;

TABLE 15.6
COORDINATE DATA

COORDINATE DATA—FORMAT (2I10, 6F10.0)—must immediately follow a COOR macro. The coordinate data contains the node number N and the value of the coordinates for the node. Only the values of (XL(I), I = 1,NDM) are used, where NDM is the value input on the control record.

Nodal coordinates can be generated along a straight line described by the values input on two successive records. The value of the node number is computed using the N and NG on the first record to compute the sequence N, N + NG, N + 2NG, etc. NG may be input as a negative number; if it has incorrect sign the sign will be changed. Nodes need not be in order.

Columns	Description	Variable
1 to 10	Node number	N
10 to 20	Generator increment	NG
21 to 30	X1 coordinate	XL(1) → X(1,N)
31 to 40	X2 coordinate	XL(2) → X(2,N)
41 to 50	X3 coordinate	XL(3) → X(3,N)

Note: terminate with blank record(s).

THE FINITE ELEMENT METHOD

TABLE 15.7
ELEMENT DATA

ELEMENT DATA—FORMAT (16I5)—must immediately follow an ELEM record
The element data contains the element number, material set number (which also selects the element type, see Table 15.8), and the sequence of nodes connected to the element. If there are less than NEN nodes (see Table 15.1 for input of NEN) either leave the appropriate fields blank or zero.

Elements must be in order. If element records are omitted the element data will be generated from the previous element with the same material number and the nodes all incremented by the LX on the previous element. Generation to the maximum element number occurs where a blank record is encountered.

Columns	Description	Variable
1 to 5	Element number	L
6 to 10	Material set number	IX(NEN1,L)
11 to 15	Node 1 number	IX(1,L)
16 to 20	Node 2 number	IX(2,L)
etc.		...
etc.	Node NEN number	IX(NEN,L)
etc.	Generation increment	LX

(b) element data which follows the macro command ELEM and is prepared according to Table 15.7; and

(c) material data which follows the macro command MATE and is prepared according to Table 15.8 and the data required for each particular element (see Sec. 15.8.3).

TABLE 15.8
MATERIAL PROPERTY DATA

MATERIAL DATA SETS—must immediately follow a MATE macro
Each material property set also selects the element type that will be used for the material property data.
RECORD 1). FORMAT (8I10)

Columns	Description	Variable
1 to 10	Property set number	MA
11 to 20	Element type (1 to 4)	IEL
21 to 30	Global DOF number for local DOF 1	IDL (1)
31 to 40	Global DOF number for local DOF 2	IDL (2)
	etc. to NDF	

The IDL(I) may be used to reassign element local variable degree-of-freedom numbers to global degree-of-freedom numbers. The default values are IDL(I) = I. If input values are IDL(1) = 2 and IDL(2) = 1 then element DOF 1 will be assigned to global DOF 2 and element DOF 2 to global DOF 1 (switched). If any IDL is non-zero a zero value of other IDL will not be assembled. Thus, it is easily possible to restrain two-dimensional problems to respond with a one-dimensional solution.

Each material Record 1.) must be followed immediately by the material property data required for the element type IEL being used, e.g., see Sec. 15.8.3.

TABLE 15.9
BOUNDARY RESTRAINT DATA

BOUNDARY CONDITIONS—FORMAT (16I5)—must immediately follow a BOUN macro
For each node that has at least one degree of freedom with a specified displacement, a boundary condition must be input. The convention used for boundary restraints is
= 0 no restraint, force specified
≠ 0 restrained, displacement specified

Values of force or displacement input in FORC (Table 15.10):

Columns	Description	Variable
1 to 5	Node number	N
6 to 10	Generation increment	NX
11 to 15	DOF 1 boundary code	IDL(1) → IDL(1,N)
16 to 20	DOF 2 boundary code	IDL(2) → IDL(2,N)
etc.		
etc.	DOF NDF boundary code	IDL(NDF) → ID(NDF,N)

Note: when generating boundary condition codes for subsequent nodes IDL is set to zero if it was input ≥0, and is set to −1 if input negative. All degrees of freedom with non-zero codes are assumed fixed. Terminate with blank record(s).

In addition, most analyses will require specification of nodal boundary restraint conditions, macro BOUN, and the corresponding nodal force or displacement value, macro FORC, which are specified according to Tables 15.9 and 15.10 respectively. The program permits the specification of sloping boundaries in two dimensions using the macro command ANGL. The anticlockwise angle, in degrees, that the transformed 1-axis makes with the $X(1, 1)$ direction is input. Subsequently, FORC and BOUN values are interpreted with respect to the rotated direction. Some analyses may have auxiliary nodal quantities that specify a loading. For example, in the analysis of elasticity problems, temperature may provide loading. The program provides a capability of specifying a temperature

TABLE 15.10
NODAL FORCED BOUNDARY VALUE DATA

FORCE CONDITIONS—FORMAT (2I10, 7F10.0)—must immediately follow a FORC macro
For each node that has a non-zero nodal force or displacement a force record must be input or generated. Generation is the same as for coordinate data (see Table 15.6). The value specified is a force if the corresponding restraint code is zero and a displacement if the corresponding restraint code is non-zero.

Columns	Description	Variable
1 to 10	Node number	N
11 to 20	Generation increment	NG
21 to 30	DOF 1 Force (Displ.)	XL(1) → F(1,N)
31 to 40	DOF 2 Force (Displ.)	XL(2) → F(2,N)
etc.		
etc.	DOF NDF Force (Displ.)	XL(NDF) → F(NDF,N)

Note: terminate with a blank record(s).

TABLE 15.11
NODAL TEMPERATURE DATA

TEMPERATURE DATA—FORMAT (2I10, F10.0)—must immediately follow a TEMP macro For each node that has a non-zero temperature the value must be input. Generation of values can be performed as described for coordinates (see Table 15.6).

Columns	Description	Variable
1 to 10	Node number	N
10 to 20	Generation increment	NG
21 to 30	Nodal temperature	XL(I)→T(N)

Note: terminate with blank record(s).

TABLE 15.12
BLOCK MESH DATA

BLOCK DATA—must immediately follow a BLOC macro record Generates a 'block' of nodes and elements. A superelement is described by a four- to nine-noded quadrilateral whose supernodes are numbered as shown in Fig. 15.25 (page 560). The block data is specified as:

RECORD 1). FORMAT 8I10

Columns	Description	Variable
1 to 10	Number of supernodes	NN
11 to 20	Number of spaces along 1-2 side of superelement	NR
21 to 30	Number of spaces along 1-4 side of superelement	NS
31 to 40	First node number on block at supernode 1	NI
41 to 50	First element in block adjacent to supernode 1	NE
51 to 60	Property set number for block	MA
61 to 70	Node increment between lines	NODINC
71 to 80	Block type: 0 = 4-noded quadrilaterals 8 = 8-noded quadrilaterals 9 = 9-noded quadrilaterals	NTYP

Notes: (1) Nodes increment along the 1-2 side of the superelement then skip NODINC nodes before starting next line.
(2) If NE is zero no elements are generated.
(3) NR and NS must be even for NTYP of 8 or 9.
(4) Eight-noded quadrilateral elements have a centre node generated but this is not connected to the element (should be zero with BOUN restraints).

RECORD 2 TO NN + 1. FORMAT I10,3F10.0

Columns	Description	Variables
1 to 10	Supernode number	L
11 to 20	X1 coordinate of supernode	R
21 to 30	X2 coordinate of supernode	S
31 to 40	X3 coordinate of supernode	T

Note: only NDM supernode coordinates are used.

TABLE 15.13
POLAR COORDINATE DATA

POLAR DATA—FORMAT 3I10,2F10.0—must immediately follow a POLA macro record Each node that has previously been input in a polar coordinate form r, θ (or $r, 0, z$), where θ is in degrees measured anticlockwise from the X1 axis, is converted to cartesian components X1, X2 (or X1, X2, X3).

Columns	Description	Variable
1 to 10	First node number	NI
11 to 20	Last node number	NE
21 to 30	Increment between nodes	INC
31 to 40	X1 coordinate for centre of polar coordinates	XO
41 to 50	X2 coordinate for centre	YO

Note: coordinates are computed as:

$$X(1,I) = XO + r \cos \theta$$
$$X(2,I) = YO + r \sin \theta$$
$$X(3,I) = X(3,I)$$

where r is X(1,I) and θ is X(2,I) input by COOR or BLOC.

(or corresponding nodal loading) using the TEMP macro followed by data prepared according to Table 15.11.

The end of any mesh data is indicated by use of an END macro. The use of the macro command cards allows the user to specify only those data items actually needed for each analysis. The END macro signifie... the end of mesh data input. The use of macro cards also reduces th... chance of data input errors due to extraneous blank records. Stric... record sequencing is necessary only within each macro segment. Severa... blank records may exist after actual data without affecting the executio... of the program.

Once all necessary mesh data is supplied the user can select to solv... the problem or not. If only a check of the mesh is desired, insert either the STOP macro command to stop execution or start a new problem a... described in Table 15.1. If a solution to the problem is desired, addi... tional data is required, as discussed in the next section.

TABLE 15.14
ANGLE DATA

ANGLE DATA—FORMAT 2I10,F10.0—must immediately follow an ANGL macro record The angle data contains the node number N and the value of the angle, in degree... measured anticlockwise from the X1 axis. The nodal angles may be generated using NG... in the same way as for coordinate data.

Column	Description	Variable
1 to 10	Node number	N
11 to 20	Generator increment	NG
21 to 30	Angle in degrees	ANG

TABLE 15.15

DATA INPUT CARD IMAGES FOR DISK PROBLEM

```
FEAP**QUADRANT OF A CIRCULAR DISK (EXAMPLE PROBLEM)
 19  11   1   2   2   4
COOR
   1   1   0.       0.
   5   0   5.       0.
   6   1   0.       2.
  10   0   4.5828   2.
  11   1   0.       4.
  14   0   3.0      4.
  15   0   4.0      3.
  16   0   0.       5.
  17   0   0.75     4.9434
  18   0   1.5      4.7697
  19   0   2.25     4.4651
ELEM
   1   1   1   2   7   6        1
   5   6   6   7  12  11        1
   9  11  11  12  17  16        1
BOUN
   1   1   1  -1                1
   5   0   0  -1                1
   6   5  -1   0                1
  16   0   0   0                1
FORC
  16   0   0.      -5.
MATE
   1   1              0.0    2   1   1
 100.  0.3
END
```

or in free-format form using the parser and lower case text:

```
feap * * Quadrant of a circular disk (example problem)
19,11,1,2,2,4
coord
1,1,0,0.
5,,5.
6,1,2.
10,,4.5828,2.
etc. to
end
interactive
stop
```

As an example of the data input required to describe a mesh consider the mesh shown in Fig. 15.7 for the quadrant of a circular disk. The input data card images for this problem are shown in Table 15.15.

15.4 Solution of finite element problems—the macro programming language

At the completion of data input and any checks on the mesh we are prepared to initiate a problem solution. It is at this stage that the particular type of solution mode must be available to the user in the program. In many existing programs only a small number of fixed algorithm solution modes are available to the user. For example, the program may only be able to solve linear steady-state problems, or, in addition, it may be able to solve linear transient problems. In practical engineering problems fixed algorithm programs are often too restrictive and the user must continually modify the program to solve a given problem—often at the expense of another user! For this reason it is desirable to have a program that has modules for variable algorithm capabilities and, if necessary, can be modified without interrupting other users' capabilities. The program that we discuss here is basic and the reader can undoubtedly see many ways to improve and extend the program for other classes of problems. One important extension would be to include a matrix interpretive language so that individual terms or equations can be modified for specific needs.

The macro programming concept described in this section has been used by the authors for more than 10 years and, to date, has not inhibited our research activities by becoming outmoded. Applications are routinely conducted on personal computers, minicomputers, and mainframe computers with the same program. Only the equation solution subprograms are changed in different environments.

15.4.1 Linear steady-state problems. The basic aspect of the variable algorithm program is a macro instruction language which can be used to construct modules for specific algorithms as needed. The user only needs to learn the mnemonics of the language to use it. For example, if one wishes to form the global stiffness matrix the program instruction TANG is used (TANG is the mnemonic for a tangent stiffness matrix and for non-linear, elements would form and assemble into the global stiffness matrix the element tangent stiffness computed about the current displacement state; for linear elements this is just the linear stiffness matrix). If one wishes to form the right-hand side of the equations modified for specified displacements one uses the program instruction FORM. The resulting equations are solved using the instruction SOLV. Printed

Additional Macro Statements

TABLE 1
CRACK DEFINITION

CRACK DEFINITION - Format(i10,4f10.4) - must immediately follow a CRAC macro.
The crack type is as follows: kedge(ncrac)-> crack type (1=edge; 0 or 2=embedded; 3 symm)
Example: 2x2crac.inp

Columns	Descriptions	Variable
1-10	Crack Type	kedge(ncrac)
10-20	X-Coord. - 1	xyck(1,1,ncrac)
20-30	Y-Coord. - 1	xyck(2,1,ncrac)
30-40	X-Coord. - 2	xyck(1,2,ncrac)
40-50	Y-Coord. - 2	xyck(2,2,ncrac)

TABLE 2
SYMMETRY

SYMMETRY - Format(4i10) - must immediately follow a SYMM macro.
The variables SYM1A and SYM1B give any two nodes on the X axis of symmetry. Likewise the variables SYM2A and SYM2B give those on the Y axis of symmetry. Note that the axes of symmetry can only be parallel to X and/or Y axes but need not be the X and Y axis.

Columns	Descriptions	Variable
1-10		SYM1A
10-20		SYM2A
20-30		SYM1B
30-40		SYM2B

TABLE 3
DISTRIBUTED LOAD

DISTRIBUTED LOAD - Format(3i10,4f10.0), Format(5f10.0) - must immediately follow a DIST macro.
Two lines that give the element N, the generator increment NG, the Gaussian Rule LS, and the remaining parts give the loads at each gauss point. If only one load is given, it is assumed to be evenly distributed over the element. Note: TWO LINES MUST ALWAYS BE USED Example: PLATESS.INP

Columns	Descriptions	Variable
1-10	Element Number	N
10-20	Generator Increment	NG
20-30	Gaussian Rule	LS
30-40	Gauss pt #1	ld(1)
40-50	Gauss pt #2	ld(2)
50-60	Gauss pt #3	ld(3)
60-70	Gauss pt #4	ld(4)
10-20	Gauss pt #5	ld(5)
20-30	Gauss pt #6	ld(6)
30-40	Gauss pt #7	ld(7)
40-50	Gauss pt #8	ld(8)
60-70	Gauss pt #9	ld(9)

TABLE 4
BOUNDARY MOMENT

BOUNDARY MOMENT - Format(4i10,9f10.0), Format(5f10.0) - must immediately follow a MOME macro. Distributed moment along boundary edge at specified gauss points. Example: 2x2cracb.inp

Columns	Descriptions	Variable
1-10	Node Number 1	N1
10-20	Node Number 2	N2
20-30	Generator Increment	NG
30-40	Gaussian Rule	LS
40-50	Mx - Pt. #1	ld(1)
50-60	Mx - Pt. #2	ld(2)
60-70	Mx - Pt. #3	ld(3)
10-20	My - Pt. #1	ld(4)
20-30	My - Pt. #2	ld(5)
30-40	My - Pt. #3	ld(6)
40-50	Mxy - Pt. #1	ld(7)
60-70	Mxy - Pt. #2	ld(8)
70-80	Mxy - Pt. #3	ld(9)

TABLE 6
POINT MOMENT LOAD

POINT MOMENT LOAD - Format(2f10.5,f10.2) - must immediately follow a MOMP macro.

Columns	Descriptions	Variable
1-10	X Coord.	XC
10-20	Y Coord.	YC
20-30	Mx	LD(1)
30-40	My	LD(2)

TABLE 7
DISTRIBUTED SHEAR LOAD

DISTRIBUTED SHEAR LOAD - Format(4i10,6f10.0) - must immediately follow a DISQ macro. Distributed shear load between nodes N1 and N2 at up to 6 gauss points. Example: plateldq.inp

Columns	Descriptions	Variable
1-10	Node Number 1	N1
10-20	Node Number 2	N2
20-30	Generator Increment	NG
30-40	Gaussian Rule	LS
40-50	Gauss pt #1	ld(1)
50-60	Gauss pt #2	ld(2)
60-70	Gauss pt #3	ld(3)
70-80	Gauss pt #4	ld(4)
80-90	Gauss pt #5	ld(5)
90-100	Gauss pt #6	ld(6)

TABLE 8
POINT SHEAR LOAD

POINT SHEAR LOAD- Format(2f10.5,f10.2)- must immediately follow a POIN macro.
Example: plateld2.inp

Columns	Descriptions	Variable
1-10	X Coord.	XC
10-20	Y Coord.	YC
20-30	Shear Load	LD

Example Problems

All the example problems that follow are done on the same simple mesh shown in Figure 1. All element lengths are 1.0, therefore, each side has a length of 2.0
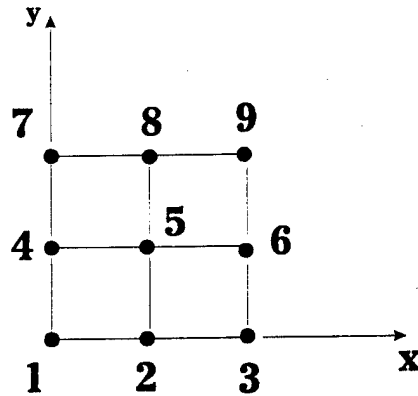

Figure 1. Simple mesh used in all examples (all elements lengths = 1.0)

File Name	*Description*
example2.inp	Force in X and Y direction at Node 9
2x2plate.inp	My moments between 1-3 and 7-9
2x2crac.inp	2D alternating method example
2x2cracb.inp	Alternating method for bending example
platess.inp	Simply supported plate with distributed shear load
plateldq.inp	Cantilever example with boundary shear load
plateld2.inp	Point shear load example

example2.inp

feap** Example Problem
9,4,1,2,2,4,0

coord
1,1,0,0
3,0,2,0
4,1,0,1
6,0,2,1
7,1,0,2
9,0,2,2

elem
1,1,1,2,5,4,1
3,1,4,5,8,7,1

boun
1,1,1,-1
3,0,0,1
4,0,1,0
7,0,1,0

forc
9,0,5,5

mate
1,1
100,.3,1.0,3,3,1

end
macr
tang
form
solv
disp
stre
end
stop

2x2plate.inp

feap** Example Problem
9,4,1,2,3,4,0

coord
1,1,0,0
3,0,2,0
4,1,0,1
6,0,2,1
7,1,0,2
9,0,2,2

elem
1,1,1,2,5,4,1
3,1,4,5,8,7,1

boun
1,0,1,0,0
2,0,1,0,0
3,0,1,0,0
7,0,1,0,0
8,0,1,0,0
9,0,1,0,0

mome
1,2,0,3,0,0,0
10,10,10,0,0,0
2,3,0,3,0,0,0
10,10,10,0,0,0
9,8,0,3,0,0,0
10,10,10,0,0,0
8,7,0,3,0,0,0
10,10,10,0,0,0

crac
2,.8,1.,1.2,1.

mate
1,2
1000000,.3,0.04,2,2,1

end
macr
tang
form
solv
disp
stre,node
end
stop

2x2crac.inp

feap** Example Problem
9,4,1,2,2,4,0

coord
1,1,0,0
3,0,2,0
4,1,0,1
6,0,2,1
7,1,0,2
9,0,2,2

elem
1,1,1,2,5,4,1
3,1,4,5,8,7,1

boun
1,1,1,-1
3,0,0,1

forc
7,0,0,5
8,0,0,10
9,0,0,5

crac
2,.8,1.,1.2,1.

mate
1,1
100,.3,0.04,2,2,1

end
macr
tang
form
solv
disp
stre,node
afem,memb
end

2x2cracb.inp

feap** Example Problem
9,4,1,2,3,4,0

coord
1,1,0,0
3,0,2,0
4,1,0,1
6,0,2,1
7,1,0,2
9,0,2,2

elem
1,1,1,2,5,4,1
3,1,4,5,8,7,1

boun
1,0,1,0,0
2,0,1,0,0
3,0,1,0,0
7,0,1,0,0
8,0,1,0,0
9,0,1,0,0

mome
1,2,0,3,0,0,0
10,10,10,0,0,0
2,3,0,3,0,0,0
10,10,10,0,0,0
9,8,0,3,0,0,0
10,10,10,0,0,0
8,7,0,3,0,0,0
10,10,10,0,0,0

crac
2,.8,1.,1.2,1.

mate
1,2
1000000,.3,0.04,2,2,1

end
macr
tang
form
solv
disp
stre,node
afem,bend
end

platess.inp

feap** Example Problem
9,4,1,2,3,4,0

coord
1,1,0,0
3,0,2,0
4,1,0,1
6,0,2,1
7,1,0,2
9,0,2,2

elem
1,1,1,2,5,4,1
3,1,4,5,8,7,1

boun
1,0,1,0,0
2,0,1,0,0
3,0,1,0,0
4,0,1,0,0
6,0,1,0,0
7,0,1,0,0
8,0,1,0,0
9,0,1,0,0

dist
1,0,3,100

2,0,3,100

3,0,3,100

4,0,3,100

mate
1,2
10000000,.3,0.04,3,2,1

end
macr
tang
form
solv
disp
stre,node
end
stop

plateldq.inp

feap** Example Problem
9,4,1,2,3,4,0

coord
1,1,0,0
3,0,2,0
4,1,0,1
6,0,2,1
7,1,0,2
9,0,2,2

elem
1,1,1,2,5,4,1
3,1,4,5,8,7,1

boun
1,0,1,1,1
4,0,1,1,1
7,0,1,1,1

disq
3,6,0,3,100.
9,6,0,3,100.

mate
1,2
10000000,.3,0.04,2,2,1

end
macr
tang
form
solv
disp
stre,node
end
stop

plateld2.inp

feap** Example Problem
9,4,1,2,3,4,0

coord
1,1,0,0
3,0,2,0
4,1,0,1
6,0,2,1
7,1,0,2
9,0,2,2

elem
1,1,1,2,5,4,1
3,1,4,5,8,7,1

boun
1,0,1,1,1
2,0,1,1,1
3,0,1,1,1
4,0,1,1,1
7,0,1,1,1

poin
2.,2.,100.

mate
1,2
10000000,.3,0.04,2,2,1

end
macr
tang
form
solv
disp
stre,node
end
stop

Appendix C

I. When Equations (47) and (49) are substituted into the even and odd parts of Equations (30)-(37) and (38)-(45), respectively, the resulting equations are of the form shown in these handwritten notes. You will realize that both parts of each function are not fully written out because the minor differences in the equations may be accounted for by observation.

II. The infinite integrals are solved analytically by a method similar to Sneddon, pp. 496-497 [5]. The derivations and symbols are slightly different than those used in [2].

The following is equivalent to Equation (75), (142), and (143) in [5]:

$$C_n^m(a,x,y) = \int_0^\infty \xi^{n-2} \cos(\xi y) J_m(a\xi) e^{-\xi x} d\xi \tag{75}$$

$$S_n^m(a,x,y) = \int_0^\infty \xi^{n-2} \sin(\xi y) J_m(a\xi) e^{-\xi x} d\xi \tag{142}$$

$$C_n^m(a,x,y) - i S_n^m(a,x,y) = Z_n^m(a, x + iy) \tag{143}$$

NOTE: The Mathematica output is utilized in the handwritten portion. The notation is the same.

```
Z=1/(a^2+w^2)^(1/2)
```

$$\frac{1}{\text{Sqrt}[a^2 + w^2]}$$

```
Integrate[Z,w]
```

$$\text{Log}[w + \text{Sqrt}[a^2 + w^2]]$$

```
Z01=w + Sqrt[a^2+w^2]
```

$$w + \text{Sqrt}[a^2 + w^2]$$

```
w=x+I y
```

$$x + I\,y$$

```
Z01
```

$$x + \text{Sqrt}[a^2 + (x + I\,y)^2] + I\,y$$

```
ComplexExpand[Expand[Z01]]
```

$$x + (4\,x^2\,y^2 + (a^2 + x^2 - y^2)^2)^{1/4}$$

$$\text{Cos}\left[\frac{\text{Arg}[a^2 + x^2 + 2\,I\,x\,y - y^2]}{2}\right] +$$

$$I\,(y + (4\,x^2\,y^2 + (a^2 + x^2 - y^2)^2)^{1/4}$$

$$\text{Sin}\left[\frac{\text{Arg}[a^2 + x^2 + 2\,I\,x\,y - y^2]}{2}\right])$$

```
ro=((r Cos[O]+R^(1/2)Cos[Fe/2])^2+(r Sin[O]+R^(1/2)Sin[Fe/2])^2)^(1/2)
```

$$\text{Sqrt}\left[\left(\text{Sqrt}[R]\,\text{Cos}\left[\frac{Fe}{2}\right] + r\,\text{Cos}[O]\right)^2 + \right.$$

$$\left.\left(\text{Sqrt}[R]\,\text{Sin}\left[\frac{Fe}{2}\right] + r\,\text{Sin}[O]\right)^2\right]$$

```
Simplify[ro]
```

$$\text{Sqrt}\left[r^2 + R + 2\,r\,\text{Sqrt}[R]\,\text{Cos}\left[\frac{Fe}{2} - O\right]\right]$$

```
Zo2=(a^2+(x+I y)^2)^(-1/2)
```

$$\frac{1}{\text{Sqrt}[a^2 + (x + I\,y)^2]}$$

```
ComplexExpand[Expand[Zo2]]
```

$$\frac{\cos\left[\dfrac{\text{Arg}[a^2 + x^2 + 2 I x y - y^2]}{2}\right]}{(4 x^2 y^2 + (a^2 + x^2 - y^2)^2)^{1/4}} -$$

$$\frac{I \sin\left[\dfrac{\text{Arg}[a^2 + x^2 + 2 I x y - y^2]}{2}\right]}{(4 x^2 y^2 + (a^2 + x^2 - y^2)^2)^{1/4}}$$

```
Z03=(x+I y)/(a^2+(x+I y)^2)^(3/2)
```

$$\frac{x + I y}{(a^2 + (x + I y)^2)^{3/2}}$$

```
ComplexExpand[Expand[Z03]]
```

$$\frac{x \cos\left[\dfrac{3\,\text{Arg}[a^2 + x^2 + 2 I x y - y^2]}{2}\right]}{(4 x^2 y^2 + (a^2 + x^2 - y^2)^2)^{3/4}} +$$

$$\frac{y \sin\left[\dfrac{3\,\text{Arg}[a^2 + x^2 + 2 I x y - y^2]}{2}\right]}{(4 x^2 y^2 + (a^2 + x^2 - y^2)^2)^{3/4}} +$$

$$I\left(\frac{y \cos\left[\dfrac{3\,\text{Arg}[a^2 + x^2 + 2 I x y - y^2]}{2}\right]}{(4 x^2 y^2 + (a^2 + x^2 - y^2)^2)^{3/4}} - \frac{x \sin\left[\dfrac{3\,\text{Arg}[a^2 + x^2 + 2 I x y - y^2]}{2}\right]}{(4 x^2 y^2 + (a^2 + x^2 - y^2)^2)^{3/4}}\right)$$

```
Z04=-1/(a^2+(x+I y)^2)^(3/2)+3(x+I y)^2/(a^2+(x+I y)^2)^(5/2)
```

$$-(a^2 + (x + I y)^2)^{-(3/2)} + \frac{3 (x + I y)^2}{(a^2 + (x + I y)^2)^{5/2}}$$

`ComplexExpand[Together[ExpandAll[Z04]]]`

$$\left(\frac{(-a^2 + 2x^2 - 2y^2)\,\cos\!\left[\dfrac{5\,\mathrm{Arg}[a^2 + x^2 + 2\,I\,x\,y - y^2]}{2}\right]}{(4x^2y^2 + (a^2 + x^2 - y^2)^2)^{5/4}} + \right.$$

$$\frac{4xy\,\sin\!\left[\dfrac{5\,\mathrm{Arg}[a^2 + x^2 + 2\,I\,x\,y - y^2]}{2}\right]}{(4x^2y^2 + (a^2 + x^2 - y^2)^2)^{5/4}} +$$

$$I\left(\frac{4xy\,\cos\!\left[\dfrac{5\,\mathrm{Arg}[a^2 + x^2 + 2\,I\,x\,y - y^2]}{2}\right]}{(4x^2y^2 + (a^2 + x^2 - y^2)^2)^{5/4}} - \right.$$

$$\left.\left.\frac{(-a^2 + 2x^2 - 2y^2)\,\sin\!\left[\dfrac{5\,\mathrm{Arg}[a^2 + x^2 + 2\,I\,x\,y - y^2]}{2}\right]}{(4x^2y^2 + (a^2 + x^2 - y^2)^2)^{5/4}}\right)\right)$$

`Z05=-3/2 G (x+I y)/(a^2+(x+I y)^2)^(5/2)+5/2 G (x+I y)^3/(a^2+(x+I y)^2)^`

$$\frac{-3\,G\,(x + I\,y)}{2\,(a^2 + (x + I\,y)^2)^{5/2}} + \frac{5\,G\,(x + I\,y)^3}{2\,(a^2 + (x + I\,y)^2)^{7/2}}$$

`Together[Z05]`

$$(-3\,a^2\,G\,x + 2\,G\,x^3 - 3\,I\,a^2\,G\,y + 6\,I\,G\,x^2\,y - 6\,G\,x\,y^2 -$$

$$2\,I\,G\,y^3)\,/\,(2\,(a^2 + x^2 + 2\,I\,x\,y - y^2)^{7/2})$$

```
ComplexExpand[Together[Z05]]
```

$$((-3 a^2 G x + 2 G x^3 - 6 G x y^2)$$

$$Cos\left[\frac{7 Arg[a^2 + x^2 + 2 I x y - y^2]}{2}\right]) /$$

$$(2 (4 x^2 y^2 + (a^2 + x^2 - y^2)^2)^{7/4}) +$$

$$((-3 a^2 G y + 6 G x^2 y - 2 G y^3)$$

$$Sin\left[\frac{7 Arg[a^2 + x^2 + 2 I x y - y^2]}{2}\right]) /$$

$$(2 (4 x^2 y^2 + (a^2 + x^2 - y^2)^2)^{7/4}) +$$

$$I (((-3 a^2 G y + 6 G x^2 y - 2 G y^3)$$

$$Cos\left[\frac{7 Arg[a^2 + x^2 + 2 I x y - y^2]}{2}\right]) /$$

$$(2 (4 x^2 y^2 + (a^2 + x^2 - y^2)^2)^{7/4}) -$$

$$((-3 a^2 G x + 2 G x^3 - 6 G x y^2)$$

$$Sin\left[\frac{7 Arg[a^2 + x^2 + 2 I x y - y^2]}{2}\right]) /$$

$$(2 (4 x^2 y^2 + (a^2 + x^2 - y^2)^2)^{7/4}))$$

```
Z06=(p^2+a^2)^(-5/2)*G5*LegendreP[4,p/(p^2+a^2)^(1/2)]
```

$$\frac{G5 (3 a^4 - 24 a^2 p^2 + 8 p^4)}{8 (a^2 + p^2)^{9/2}}$$

```
p=x+I y
```

$$x + I y$$

ComplexExpand[Z06]

$$(G5 \; (3 \; a^4 \; - \; 24 \; a^2 \; (x^2 \; - \; y^2) \; +$$

$$8 \; (x^4 \; - \; 6 \; x^2 \; y^2 \; + \; y^4))$$

$$\cos\left[\frac{9 \; \mathrm{Arg}[a^2 \; + \; (x \; + \; I \; y)^2]}{2}\right]) \; /$$

$$(8 \; \mathrm{Abs}[a^2 \; + \; (x \; + \; I \; y)^2]^{9/2}) \; +$$

$$(G5 \; (-48 \; a^2 \; x \; y \; + \; 8 \; (4 \; x^3 \; y \; - \; 4 \; x \; y^3))$$

$$\sin\left[\frac{9 \; \mathrm{Arg}[a^2 \; + \; (x \; + \; I \; y)^2]}{2}\right]) \; /$$

$$(8 \; \mathrm{Abs}[a^2 \; + \; (x \; + \; I \; y)^2]^{9/2}) \; +$$

$$I \; ((G5 \; (-48 \; a^2 \; x \; y \; + \; 8 \; (4 \; x^3 \; y \; - \; 4 \; x \; y^3))$$

$$\cos\left[\frac{9 \; \mathrm{Arg}[a^2 \; + \; (x \; + \; I \; y)^2]}{2}\right]) \; /$$

$$(8 \; \mathrm{Abs}[a^2 \; + \; (x \; + \; I \; y)^2]^{9/2}) \; -$$

$$(G5 \; (3 \; a^4 \; - \; 24 \; a^2 \; (x^2 \; - \; y^2) \; +$$

$$8 \; (x^4 \; - \; 6 \; x^2 \; y^2 \; + \; y^4))$$

$$\sin\left[\frac{9 \; \mathrm{Arg}[a^2 \; + \; (x \; + \; I \; y)^2]}{2}\right]) \; /$$

$$(8 \; \mathrm{Abs}[a^2 \; + \; (x \; + \; I \; y)^2]^{9/2}))$$

Z11=((a^2+(x+I y)^2)^(1/2)-(x+I y))/a

$$\frac{-x + \text{Sqrt}[a^2 + (x + I\ y)^2] - I\ y}{a}$$

ComplexExpand[Expand[Z11]]

$$-\left(\frac{x}{a}\right) + \frac{(4\ x^2\ y^2 + (a^2 + x^2 - y^2)^2)^{1/4}\ \text{Cos}\left[\dfrac{\text{Arg}[a^2 + x^2 + 2\ I\ x\ y - y^2]}{2}\right]}{a} +$$

$$I\ \left(-\left(\frac{y}{a}\right) + \frac{(4\ x^2\ y^2 + (a^2 + x^2 - y^2)^2)^{1/4}\ \text{Sin}\left[\dfrac{\text{Arg}[a^2 + x^2 + 2\ I\ x\ y - y^2]}{2}\right]}{a}\right)$$

Z12=1/a-(x+I y)/(a*(a^2+(x+I y)^2)^(1/2))

$$\frac{1}{a} - \frac{x + I\ y}{a\ \text{Sqrt}[a^2 + (x + I\ y)^2]}$$

ComplexExpand[Expand[Z12]]

$$\frac{1}{a} - \frac{x\ \text{Cos}\left[\dfrac{\text{Arg}[a^2 + x^2 + 2\ I\ x\ y - y^2]}{2}\right]}{a\ (4\ x^2\ y^2 + (a^2 + x^2 - y^2)^2)^{1/4}} -$$

$$\frac{y\ \text{Sin}\left[\dfrac{\text{Arg}[a^2 + x^2 + 2\ I\ x\ y - y^2]}{2}\right]}{a\ (4\ x^2\ y^2 + (a^2 + x^2 - y^2)^2)^{1/4}} +$$

$$I\ \left(-\left(\frac{y\ \text{Cos}\left[\dfrac{\text{Arg}[a^2 + x^2 + 2\ I\ x\ y - y^2]}{2}\right]}{a\ (4\ x^2\ y^2 + (a^2 + x^2 - y^2)^2)^{1/4}}\right) + \right.$$

$$\left. \frac{x\ \text{Sin}\left[\dfrac{\text{Arg}[a^2 + x^2 + 2\ I\ x\ y - y^2]}{2}\right]}{a\ (4\ x^2\ y^2 + (a^2 + x^2 - y^2)^2)^{1/4}}\right)$$

Z13=a/(a^2+(x+I y)^2)^(3/2)

$$\frac{a}{(a^2 + (x + I\ y)^2)^{3/2}}$$

`ComplexExpand[Expand[Z13]]`

$$\frac{a \, \cos\left[\dfrac{3 \, \text{Arg}[a^2 + x^2 + 2\,I\,x\,y - y^2]}{2}\right]}{(4 \, x^2 \, y^2 + (a^2 + x^2 - y^2)^2)^{3/4}} -$$

$$\frac{I \, a \, \sin\left[\dfrac{3 \, \text{Arg}[a^2 + x^2 + 2\,I\,x\,y - y^2]}{2}\right]}{(4 \, x^2 \, y^2 + (a^2 + x^2 - y^2)^2)^{3/4}}$$

`Z14=3(x+I y)((x+I y)+(a^2+(x+I y)^2)^(1/2))/(a^2+(x+I y)^2)^(5/2)*`
`    a/((x+I y)+(a^2+(x+I y)^2)^(1/2))`

$$\frac{3 \, a \, (x + I \, y)}{(a^2 + (x + I \, y)^2)^{5/2}}$$

`ComplexExpand[Expand[Z14]]`

$$\frac{3 \, a \, x \, \cos\left[\dfrac{5 \, \text{Arg}[a^2 + x^2 + 2\,I\,x\,y - y^2]}{2}\right]}{(4 \, x^2 \, y^2 + (a^2 + x^2 - y^2)^2)^{5/4}} +$$

$$\frac{3 \, a \, y \, \sin\left[\dfrac{5 \, \text{Arg}[a^2 + x^2 + 2\,I\,x\,y - y^2]}{2}\right]}{(4 \, x^2 \, y^2 + (a^2 + x^2 - y^2)^2)^{5/4}} +$$

$$I \left(\frac{3 \, a \, y \, \cos\left[\dfrac{5 \, \text{Arg}[a^2 + x^2 + 2\,I\,x\,y - y^2]}{2}\right]}{(4 \, x^2 \, y^2 + (a^2 + x^2 - y^2)^2)^{5/4}} - \right.$$

$$\left.\frac{3 \, a \, x \, \sin\left[\dfrac{5 \, \text{Arg}[a^2 + x^2 + 2\,I\,x\,y - y^2]}{2}\right]}{(4 \, x^2 \, y^2 + (a^2 + x^2 - y^2)^2)^{5/4}}\right)$$

. P15=LegendreP[3,-1,z]

$$-\frac{(1 - 5 z^2)\, \text{Sqrt}[1 - z^2]}{8}$$

z=(x+I y)/(a^2+(x+I y)^2)^(1/2)

$$\frac{x + I\, y}{\text{Sqrt}[a^2 + (x + I\, y)^2]}$$

Z15=24/(a^2+(x+I y)^2)^2*P15

$$\frac{-3\left(1 - \dfrac{5\,(x + I\, y)^2}{a^2 + (x + I\, y)^2}\right) \text{Sqrt}\left[1 - \dfrac{(x + I\, y)^2}{a^2 + (x + I\, y)^2}\right]}{(a^2 + (x + I\, y)^2)^2}$$

PowerExpand[%]

$$\frac{3\, a\,(-a^2 + 4 x^2 + 8 I\, x\, y - 4 y^2)}{(a^2 + x^2 + 2 I\, x\, y - y^2)^{7/2}}$$

ComplexExpand[Simplify[%]]

$$\frac{3\, a\,(-a^2 + 4 x^2 - 4 y^2)\, \text{Cos}\left[\dfrac{7\, \text{Arg}[a^2 + x^2 + 2 I\, x\, y - y^2]}{2}\right]}{(4 x^2 y^2 + (a^2 + x^2 - y^2)^2)^{7/4}} +$$

$$\frac{24\, a\, x\, y\, \text{Sin}\left[\dfrac{7\, \text{Arg}[a^2 + x^2 + 2 I\, x\, y - y^2]}{2}\right]}{(4 x^2 y^2 + (a^2 + x^2 - y^2)^2)^{7/4}} +$$

$$I\left(\frac{24\, a\, x\, y\, \text{Cos}\left[\dfrac{7\, \text{Arg}[a^2 + x^2 + 2 I\, x\, y - y^2]}{2}\right]}{(4 x^2 y^2 + (a^2 + x^2 - y^2)^2)^{7/4}} -\right.$$

$$\left.\frac{3\, a\,(-a^2 + 4 x^2 - 4 y^2)\, \text{Sin}\left[\dfrac{7\, \text{Arg}[a^2 + x^2 + 2 I\, x\, y - y^2]}{2}\right]}{(4 x^2 y^2 + (a^2 + x^2 - y^2)^2)^{7/4}}\right)$$

```
Z16=(p^2+a^2)^(-5/2)*Gamma[4+1+1]*LegendreP[4,-1,p/(p^2+a^2)^(1/2)]
```

$$-15 \sqrt{\dfrac{a^2}{a^2 + p^2}} \; (3 a^2 p - 4 p^3)$$

$$\overline{\hspace{3cm}}$$

$$(a^2 + p^2)^4$$

```
p=(x+I y)
```

$$x + I y$$

```
Simplify[%]
```

$$\dfrac{-15 I a (-I x + y) (3 a^2 - 4 x^2 - 8 I x y + 4 y^2)}{(a^2 + x^2 + 2 I x y - y^2)^{9/2}}$$

`ComplexExpand[%]`

$$8\,x\,y\left(\frac{-15\,a\,y\,\cos\left[\dfrac{9\,\text{Arg}[a^2+x^2+2\,I\,x\,y-y^2]}{2}\right]}{(4\,x^2\,y^2+(a^2+x^2-y^2)^2)^{9/4}}+\frac{15\,a\,x\,\sin\left[\dfrac{9\,\text{Arg}[a^2+x^2+2\,I\,x\,y-y^2]}{2}\right]}{(4\,x^2\,y^2+(a^2+x^2-y^2)^2)^{9/4}}\right)+$$

$$(3\,a^2-4\,x^2+4\,y^2)\left(\frac{-15\,a\,x\,\cos\left[\dfrac{9\,\text{Arg}[a^2+x^2+2\,I\,x\,y-y^2]}{2}\right]}{(4\,x^2\,y^2+(a^2+x^2-y^2)^2)^{9/4}}-\frac{15\,a\,y\,\sin\left[\dfrac{9\,\text{Arg}[a^2+x^2+2\,I\,x\,y-y^2]}{2}\right]}{(4\,x^2\,y^2+(a^2+x^2-y^2)^2)^{9/4}}\right)+$$

$$I\left((3\,a^2-4\,x^2+4\,y^2)\left(\frac{-15\,a\,y\,\cos\left[\dfrac{9\,\text{Arg}[a^2+x^2+2\,I\,x\,y-y^2]}{2}\right]}{(4\,x^2\,y^2+(a^2+x^2-y^2)^2)^{9/4}}+\frac{15\,a\,x\,\sin\left[\dfrac{9\,\text{Arg}[a^2+x^2+2\,I\,x\,y-y^2]}{2}\right]}{(4\,x^2\,y^2+(a^2+x^2-y^2)^2)^{9/4}}\right)-\right.$$

$$\left.8\,x\,y\left(\frac{-15\,a\,x\,\cos\left[\dfrac{9\,\text{Arg}[a^2+x^2+2\,I\,x\,y-y^2]}{2}\right]}{(4\,x^2\,y^2+(a^2+x^2-y^2)^2)^{9/4}}-\frac{15\,a\,y\,\sin\left[\dfrac{9\,\text{Arg}[a^2+x^2+2\,I\,x\,y-y^2]}{2}\right]}{(4\,x^2\,y^2+(a^2+x^2-y^2)^2)^{9/4}}\right)\right)$$

Appendix D

I. A copy of the user instructions from Zienkiewicz [7] is included.

II. Additional macro commands are also given.

III. Example Problems

Appendix E

I. Copy of "A finite element alternating approach fro the bending analysis of thin cracked plates" by Chen
[2]

A finite element alternating approach for the bending analysis of thin cracked plates

JEN-HWA CHEN[1], KUNG-CHUAN YANG[1] and CHENQ-SHYOUNG CHANG[2]

[1] Department of Power Mechanical Engineering, National Tsing Hua University, Hsinchu, Taiwan 30043, Republic of China;

[2] Chung Shan Institute of Science and Technology, Lung-Tan, Taiwan 32526, Republic of China

Abstract. Based on the classical plate theory, the analytical solution for an infinite thin plate containing a crack subjected to arbitrary symmetric bending moments on the crack surfaces is first derived. Using this solution, an efficient and accurate finite element alternating procedure is then devised to deal with symmetric plate bending problems with single or multiple cracks. The interaction effect among cracks and the influence of the geometric boundaries on the calculation of bending stress intensity factors are also presented in detail. Several numerical examples are solved to demonstrate the validity of the approach.

1. Introduction

The analysis of a plate containing cracks subjected to bending type loadings has been investigated extensively during the past two decades because of its significance in various engineering applications. Due to the existence of cracks, the service strength of a cracked plate will be diminished because of the singular characteristics of the stress field near the crack tip. [1]. Hence, the accurate determination of bending stress intensity factors, which indicate the severity of cracks, should receive much attention for the safe design of plate structures.

Unlike the case for the plate subjected to in-plate loadings, the prediction of bending stress intensity factors is different. In the literature, the analytical solutions for bending cracked plates are available only for limited problems with simple geometry and boundary conditions. Williams [1] obtained the stress distribution in the vicinity of the crack tip for plates loaded in bending, and found that the stress was proportional to the inverse of the square root of the radial distance from the crack tip. Sih et al. [2] used Williams' results to define symmetric and anti-symmetric stress intensity factors for cracked plate problems involving bending loads. Incorporated with Reissner's transverse shear theory, the effect of plate thickness on the analysis of cracked plates in bending was then studied by several researchers [3-7]. To deal with more realistic problems, however, numerical approaches such as the finite element methods appear to be imperative. Wilson and Thompson [8] first calculated the bending stress intensity factor for a rectangular plate containing a center crack, subjected to pure cylindrical bending by a conventional finite element method. To account for the singularity of the stress field near the crack tip, various types of singular elements and finite element models were then developed and employed [9-15]. Sosa and Eischen [16] proposed an indirect way to compute the bending stress intensity factor via a path-independent integral.

Among these surveys, the accuracy of the bending stress intensity factors obtained largely depends on mesh size and expensive computer time is consumed especially for solving the

problem with multiple cracks. To compensate for these shortcomings, an efficient technique that combines the advantages of finite element method and Schwarz's alternating method [17] is thus studied in this work. As is known, the so-called finite element alternating method has been successfully applied in solving three dimensional fracture problems [18] and two dimensional fracture problems [19–21]. For the analysis of cracked plates in bending, however, no work has been done. The aim of this work is thus to extend the finite element alternating method to deal with the bending of a thin plate with single or multiple cracks. Based on the classical plate theory [22] and the solution obtained by Sneddon and Elliott [23] for the plate with a crack under symmetric normal pressure, the analytical solution for an infinite thin plate containing a crack for which the crack surfaces are subjected to arbitrary symmetric bending loadings represented by a polynomial of appropriate order is first derived. An iterative superposition procedure is then used to satisfy traction and displacement boundary conditions on the external boundaries of the plate repeatedly until the variation of bending stress intensity factors on each crack is negligible.

To demonstrate the applicability and versatility of the new technique, several numerical examples concerning thin plates with single or multiple cracks subjected to various types of loading and boundary conditions are analyzed. The influence of the boundaries on the computation of bending stress intensity factors and the interaction effect among cracks are also studied in detail.

2. Analytical solution for a cracked thin plate in bending

Based on the classical plate theory [22], in the absence of distributed lateral loading, the governing equation for a thin plate can be written as

$$w_{,xxxx} + 2w_{,xxyy} + w_{,yyyy} = 0. \tag{1}$$

The relations among the lateral deflection w and related variables are

$$m_x = -D(w_{,xx} + \nu w_{,yy}), \tag{2}$$

$$m_y = -D(w_{,yy} + \nu w_{,xx}), \tag{3}$$

$$m_{xy} = -D(1-\nu)w_{,xy}, \tag{4}$$

$$q_x = -D(w_{,xxx} + w_{,xyy}), \tag{5}$$

$$q_y = -D(w_{,xxy} + w_{,yyy}), \tag{6}$$

$$r_x = q_x + m_{xy,y} = -D(w_{,xxx} + (2-\nu)w_{,xyy}) \tag{7}$$

and

$$r_y = q_y + m_{yx,x} = -D(w_{,yyy} + (2-\nu)w_{,xxy}). \tag{8}$$

here (m_x, m_y, m_{xy}), (q_x, q_y) and (v_x, v_y) represent the bending and twisting moments, transverse shear forces, and equivalent shear forces per unit length of the plate, respectively. $D = Eh^3/12(1 - v^2)$ is the flexural rigidity of the plate. E, h and v denote Young's modulus, plate thickness and Poisson's ratio respectively.

To solve (1), one can transform the variables (w, y) into the variables $(\hat{w}, \xi)$ by the Fourier transform technique [24] as:

$$\hat{w}(x, \xi) = \int_{-\infty}^{\infty} w(x, y) e^{i\xi y} \, dy$$

Variable x has not been transformed where $i = \sqrt{-1}$. Then, (1) to (8) become

$$\left[\frac{d^2}{dx^2} - \xi^2 \right]^2 \hat{w}(x, \xi) = 0, \tag{9}$$

$$\hat{m}_x = -D(\hat{w}_{,xx} - v\xi^2\hat{w}), \tag{10}$$

$$\hat{m}_y = -D(v\hat{w}_{,xx} - \xi^2\hat{w}), \tag{11}$$

$$\hat{m}_{xy} = i(1 - v)D\xi\hat{w}_{,x}, \tag{12}$$

$$\hat{q}_x = -D(\hat{w}_{,xxx} - \xi^2\hat{w}_{,x}), \tag{13}$$

$$\hat{q}_y = iD\xi(\hat{w}_{,xx} - \xi^2\hat{w}), \tag{14}$$

$$\hat{v}_x = -D(w_{,xxx} - (2 - v)\xi^2\hat{w}_{,x}) \tag{15}$$

and

$$\hat{v}_y = iD\xi((2 - v)\hat{w}_{,xx} - \xi^2\hat{w}). \tag{16}$$

The solution of (9) is thus obtained as follows:

$$\hat{w}(x, \xi) = (c_1 + c_2 x)e^{-|\xi|x} + (c_3 + c_4 x)e^{|\xi|x}. \tag{17}$$

where the constants c_1, c_2, c_3 and c_4 are functions of the variable ξ and can be determined by the given boundary conditions. The transformed $\hat{w}$ and $(\hat{m}_x, \hat{m}_y, \hat{m}_{xy}, \hat{q}_x, \hat{q}_y, \hat{v}_x, \hat{v}_y)$ are hence determined from (10) to (17). After taking the inverse Fourier transform for these variables, one obtains the analytical solution consistent with thin plate theory.

(1) A semi-infinite thin plate subjected to arbitrary pure bending

To obtain the complete analytical solution for cracked thin plates in bending, the solution to the problem of a semi-infinite plate subjected to an arbitrary edge bending load must be obtained, see Fig. 1. The boundary conditions for this problem are listed below:

(i) $m_x = f(y)$ at $x = 0$,
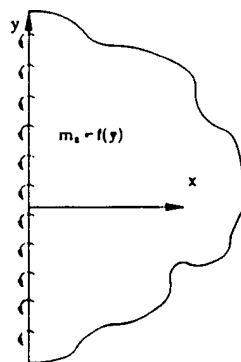(From the equilibrium condition. $\int_{-\infty}^{\infty} m_x \, dy = 0$ is satisfied automatically.) $\left(\begin{smallmatrix} ? \end{smallmatrix} \right)$

Fig. 1. A semi-infinite plate subjected to pure bending

(ii) $v_x = 0$ at $x = 0$ (Shear at x is zero)

and

(iii) $w \to 0$ as $x \to \infty$.

By condition (iii), the constants c_3 and c_4 in (17) must vanish. Thus, (17) can be simplified to:

$$\hat{w}(x, \xi) = (c_1 + c_2 x)e^{-|\xi|x}. \tag{18}$$

Carrying out the Fourier transform on both sides of condition (i) and (ii), we obtain

$$\hat{m}_x = \hat{f}(\xi) \tag{19}$$

and

$$\hat{v}_x = 0 \tag{20}$$

where $\hat{f}(\xi) = \int_{-\infty}^{\infty} f(y)e^{i\xi y}\,dy$. Substituting (18) into Eqns. (10) and (15) and comparing with the variables $\hat{m}_x$ and $\hat{v}_x$ obtained by (19) and (20), the constants c_1 and c_2 are determined and the transformed $\hat{w}(x, \xi)$ in (18) can be thus found as

$$\hat{w}(x, \xi) = \frac{-1}{(3 + v)(1 - v)D|\xi|^2}\hat{f}(\xi)[(1 + v) - (1 - v)|\xi|x]e^{-|\xi|x}. \tag{21}$$

Now, substituting (21) into Eqns. (10)–(16) and taking the inverse Fourier transform respectively, the analytical solution of the bending semi-infinite thin plate is derived as:

$$w(x, y) = \frac{-1}{2\pi(3 + v)(1 - v)D}\int_{-\infty}^{\infty}\frac{\hat{f}(\xi)}{|\xi|^2}[(1 + v) - (1 - v)|\xi|x]e^{-|\xi|x - i\xi y}\,d\xi. \tag{22}$$

$$m_x(x, y) = \frac{1}{2\pi(3 + v)}\int_{-\infty}^{\infty}\hat{f}(\xi)[(3 + v) - (1 + v)|\xi|x]e^{-|\xi|x - i\xi y}\,d\xi. \tag{23}$$

— sin

$$m_y(x, y) = \frac{(1-v)}{2\pi(3+v)} \int_{-\infty}^{\infty} \hat{f}(\xi)[-1 + |\xi|x] \, e^{-|\xi|x - i\xi y} \, d\xi. \tag{24}$$

$$m_{xy}(x, y) = \frac{-i}{2\pi(3+v)} \int_{-\infty}^{\infty} \hat{f}(\xi)\xi\left[\frac{-2}{|\xi|} + (1-v)x\right] e^{-|\xi|x - i\xi y} \, d\xi. \tag{25}$$

$$q_x(x, y) = \frac{-1}{\pi(3+v)} \int_{-\infty}^{\infty} \hat{f}(\xi)|\xi| \, e^{-|\xi|x - i\xi y} \, d\xi. \tag{26}$$

$$q_y(x, y) = \frac{-i}{\pi(3+v)} \int_{-\infty}^{\infty} \hat{f}(\xi)\xi \, e^{-|\xi|x - i\xi y} \, d\xi. \tag{27}$$

$$v_x(x, y) = \frac{-(1-v)x}{2\pi(3+v)} \int_{-\infty}^{\infty} \hat{f}(\xi)|\xi|^2 \, e^{-|\xi|x - i\xi y} \, d\xi \tag{28}$$

and

$$v_y(x, y) = \frac{-i}{2\pi(3+v)} \int_{-\infty}^{\infty} \hat{f}(\xi)\xi[(5-v) - (1-v)|\xi|x] \, e^{-|\xi|x - i\xi y} \, d\xi. \tag{29}$$

Since the function $f(y)$ describing the prescribed bending moment m_x can be divided into two parts, say, even part $f_1(y)$ and odd part $f_2(y)$, Eqns. (22)–(29) can be separated into two succinct groups as follows:

(a) for even function $f_1(y)$

$$w(x, y) = \frac{-1}{\pi(3+v)(1-v)D} \int_0^{\infty} \frac{\hat{f}_1(\xi)}{\xi^2}[(1+v) - (1-v)\xi x] \, e^{-\xi x} \cos(\xi y) \, d\xi. \tag{30}$$

$$m_x(x, y) = \frac{1}{\pi(3+v)} \int_0^{\infty} \hat{f}_1(\xi)[(3+v) - (1+v)\xi x] \, e^{-\xi x} \cos(\xi y) \, d\xi. \tag{31}$$

$$m_y(x, y) = \frac{(1-v)}{\pi(3+v)} \int_0^{\infty} \hat{f}_1(\xi)[-1 + \xi x] \, e^{-\xi x} \cos(\xi y) \, d\xi. \tag{32}$$

$$m_{xy}(x, y) = \frac{-1}{\pi(3+v)} \int_0^{\infty} \hat{f}_1(\xi)[-2 + (1-v)\xi x] \, e^{-\xi x} \sin(\xi y) \, d\xi. \tag{33}$$

$$q_x(x, y) = \frac{-2}{\pi(3+v)} \int_0^{\infty} \hat{f}_1(\xi)\xi \, e^{-\xi x} \cos(\xi y) \, d\xi. \tag{34}$$

$$q_y(x, y) = \frac{-2}{\pi(3+v)} \int_0^{\infty} \hat{f}_1(\xi)\xi \, e^{-\xi x} \sin(\xi y) \, d\xi. \tag{35}$$

$$r_x(x, y) = \frac{-(1-v)x}{\pi(3+v)} \int_0^\infty \hat{f}_1(\xi)\xi^2 e^{-\xi x} \cos(\xi y)\, d\xi \tag{36}$$

and

$$r_y(x, y) = \frac{-1}{\pi(3+v)} \int_0^\infty \hat{f}_1(\xi)\xi[(5-v)-(1-v)\xi x] e^{-\xi x} \sin(\xi y)\, d\xi \tag{37}$$

(b) for odd function $f_2(y)$

$$w(x, y) = \frac{-1}{\pi(3+v)(1-v)D} \int_0^\infty \frac{\hat{f}_2(\xi)}{\xi^3}[(1+v)-(1-v)\xi x] e^{-\xi x} \sin(\xi y)\, d\xi, \tag{38}$$

$$m_x(x, y) = \frac{1}{\pi(3+v)} \int_0^\infty \hat{f}_2(\xi)[(3+v)-(1+v)\xi x] e^{-\xi x} \sin(\xi y)\, d\xi, \tag{39}$$

$$m_y(x, y) = \frac{(1-v)}{\pi(3+v)} \int_0^\infty \hat{f}_2(\xi)[-1+\xi x] e^{-\xi x} \sin(\xi y)\, d\xi, \tag{40}$$

$$m_{xy}(x, y) = \frac{1}{\pi(3+v)} \int_0^\infty \hat{f}_2(\xi)[-2+(1-v)\xi x] e^{-\xi x} \cos(\xi y)\, d\xi, \tag{41}$$

$$q_x(x, y) = \frac{-2}{\pi(3+v)} \int_0^\infty \hat{f}_2(\xi)\xi e^{-\xi x} \sin(\xi y)\, d\xi, \tag{42}$$

$$q_y(x, y) = \frac{2}{\pi(3+v)} \int_0^\infty \hat{f}_2(\xi)\xi e^{-\xi x} \cos(\xi y)\, d\xi, \tag{43}$$

$$r_x(x, y) = \frac{-(1-v)x}{\pi(3+v)} \int_0^\infty \hat{f}_2(\xi)\xi^2 e^{-\xi x} \sin(\xi y)\, d\xi \tag{44}$$

and

$$r_y(x, y) = \frac{1}{\pi(3+v)} \int_0^\infty \hat{f}_2(\xi)\xi[(5-v)-(1-v)\xi x] e^{-\xi x} \cos(\xi y)\, d\xi. \tag{45}$$

In the above, the functions $\hat{f}_1(\xi)$ and $\hat{f}_2(\xi)$ are defined as

$$\hat{f}_1(\xi) = 2 \int_0^\infty f_1(y) \cos(\xi y)\, dy$$

and

$$f_2(\xi) = 2\int_0^t f_2(y)\sin(\xi y)\,dy.$$

(2) *An infinite thin plate containing a crack subjected to arbitrary symmetric bending on crack surfaces*

As seen in Fig. 2, consider an infinite thin plate with a crack for which a crack of length $2a$ is located $x = 0$, $|y| \leq a$. The crack surfaces are subjected to an arbitrary symmetric distributed bending moment $m_x = f(y)$ which can be represented by a polynomial of order N. The boundary conditions follow (In general, when sufficient extensional stress exists in the plate, no crack closure on the compression side is observed.):

(i) $m_x = f(y) = \displaystyle\sum_{n=0}^{N} C_n\left(\frac{y}{a}\right)^n$ at $x = 0, |y| \leq a$.

(ii) $\dfrac{\partial w}{\partial x} = 0$ at $x = 0, |y| > a$.

(iii) $v_x = 0$ at $x = 0$

and

(iv) $w \to 0$ as $x \to \pm \infty$.

Due to the symmetry of the bending moment m_x, only the region $x \geq 0$ needs to be analyzed. Furthermore, since the bending moment m_x is represented by a polynomial as shown in condition (i), the complete analytical solution can be expressed as the combination of the solutions for even n and/or odd n, respectively.
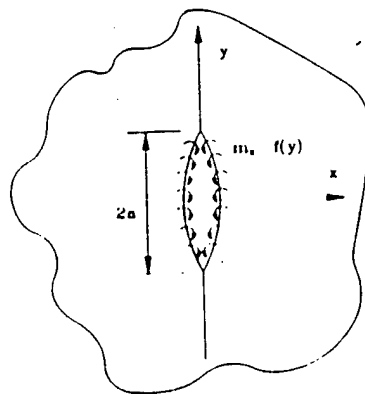

Fig. 2. An infinite plate containing a crack subjected to arbitrary symmetric bending

(a) For even order n

Let $f_1(r) = \sum_{n=0,2,...}^{N} C_n(r/a)^n$. Upon substituting the boundary conditions (i) and (ii) into (31) and (30), a pair of dual integral equations result:

$$\left. \begin{array}{ll} \dfrac{1}{\pi} \displaystyle\int_0^{\infty} \hat{f}_1(\xi) \cos(\xi r) \, d\xi = f_1(r) & a > r > 0 \\[4mm] \displaystyle\int_0^{\infty} \hat{f}_1(\xi) \cos(\xi r) \, \dfrac{d\xi}{\xi} = 0 & r > a \end{array} \right\} \tag{46}$$

Define the following parameters:

$$\xi = \frac{\rho}{a}$$

$$\eta = \frac{r}{a}$$

$$g_1(\eta) = a \left(\frac{\pi}{2\eta} \right)^{1/2} f_1(r).$$

$$\hat{f}_1(\xi) = 2\rho^{1/2} F_1(\rho)$$

and

$$\cos(\rho\eta) = \left[\frac{\pi\rho\eta}{2} \right]^{1/2} J_{-(1/2)}(\rho\eta).$$

where J_r denotes the Bessel function of the first kind with order r (here $r = -\frac{1}{2}$). Equation (46) can be rewritten as:

$$\left. \begin{array}{ll} \displaystyle\int_0^{\infty} \rho F_1(\rho) J_{1/2}(\rho\eta) \, d\rho = g_1(\eta) & 1 \geqslant \eta \geqslant 0 \\[4mm] \displaystyle\int_0^{\infty} F_1(\rho) J_{1/2}(\rho\eta) \, d\rho = 0 & \eta > 1 \end{array} \right\}.$$

The solution of $F_1(\rho)$ can be obtained from Sneddon [24] as:

$$F_1(\rho) = \left(\frac{2\rho}{\pi} \right)^{1/2} \left[J_0(\rho) \int_0^1 y^{1/2} (1 - y^2)^{1/2} g_1(y) \, dy \right.$$

$$\left. + \rho \int_0^1 u^{1/2} (1 - u^2)^{1/2} \left[\int_0^1 g_1(vu) v^{3/2} J_1(\rho v) \, dv \right] du \right].$$

Hence, from the definition as stated above, one obtains:

$$\hat{f}_1(\xi) = \tfrac{1}{2} a^2 \pi^{1/2} \xi \sum_{n=0,2,\dots}^{K} \frac{\Gamma\left(\frac{n}{2}+\frac{1}{2}\right)}{\Gamma\left(\frac{n}{2}+2\right)} C_n\left[J_0(a\xi) + a\xi \int_0^1 y^{n+2} J_1(a\xi y)\,dy \right].$$ (47)

where $\Gamma(\cdot)$ represents the Gamma function. Substituting (47) into Eqns. (30)–(37), analytical solutions for w, m_x, m_y, m_{xy}, q_x, q_y, v_x and v_y due to moment loading with even order n are thus found.

(b) For odd order n

Similarly, let $f_2(y) = \sum_{n=1,3,\dots}^{N} C_n (y/a)^n$, and substitute the boundary conditions (i) and (ii) into (39) and (38), a pair of dual integral equations are obtained as:

$$\left.\begin{aligned} \frac{1}{\pi}\int_0^\infty \hat{f}_2(\xi)\sin(\xi y)\,d\xi &= f_2(y) & a \geqslant y \geqslant 0\\[2mm] \int_0^\infty \hat{f}_2(\xi)\sin(\xi y)\,\frac{d\xi}{\xi} &= 0 & y > a \end{aligned}\right\}.$$ (48)

Define the functions $g_2(\eta)$, $\hat{f}_2(\xi)$ and $\sin(\rho\eta)$ as follows:

$$g_2(\eta) = a\left(\frac{\pi}{2\eta}\right)^{1/2} f_2(y),$$

$$\hat{f}_2(\xi) = 2\rho^{1/2} F_2(\rho)$$

and

$$\sin(\rho\eta) = \left[\frac{\pi\rho\eta}{2}\right]^{1/2} J_{1/2}(\rho\eta).$$

Equation (48) can be rewritten as:

$$\left.\begin{aligned} \int_0^\infty \rho F_2(\rho) J_{1/2}(\rho\eta)\,d\rho &= g_2(\eta) & 1 \geqslant \eta \geqslant 0\\[2mm] \int_0^\infty F_2(\rho) J_{1/2}(\rho\eta)\,d\rho &= 0 & \eta > 1 \end{aligned}\right\}.$$

From Sneddon [24], $F_2(\rho)$ is derived as

$$F_2(\rho) = \left(\frac{2\rho}{\pi}\right)^{1/2}\left[J_1(\rho)\int_0^1 y^{1/2}(1-y^2)^{1/2} g_2(y)\,dy \right.$$

$$\left. + \rho\int_0^1 u^{3/2}(1-u^2)^{1/2}\left[\int_0^1 g_2(yu) y^{3/2} J_2(\rho y)\,dy\right]du \right]$$

and $\bar{f}_2(\xi)$ is thus observed as:

$$f_2(\xi) = \tfrac{1}{2}a^2\pi^{1.2}\xi \sum_{n=1,3,\ldots}^{N} \frac{\Gamma\left(\frac{n}{2}+1\right)}{\Gamma\left(\frac{n}{2}+\frac{5}{2}\right)} C_n\left[J_1(a\xi) + a\xi\int_0^1 y^{n+2}J_2(a\xi y)dy\right]. \tag{49}$$

Substituting (49) into Eqns. (38)–(45), the analytical solutions for w, m_x, m_y, m_{xy}, q_x, q_y, r_x and r_y due to moment loading with odd order n are thus obtained.

3. Computation of bending stress intensity factor

In general, deformations near a crack tip occur in three different modes, namely, opening mode (mode I), sliding mode (mode II) and tearing mode (mode III). The severity of the crack-tip stress/displacement field is described by three corresponding parameters (K_1, K_2, K_3), which are known as stress intensity factors [25]. For a cracked plate in bending, however, the fracture behavior is described by the symmetric and anti-symmetric stress intensity factors as defined by Sih et al. [2]. Since only the symmetric type problem is considered in this work, the symmetric bending stress intensity factor which is actually the mode I stress intensity factor K_1 is therefore studied. From the definition by Erdogan [25] and the relation between the stress component σ_x and moment m_x in plate theory [22], K_1 can be expressed as

$$K_1 = \lim_{y\to a} \frac{6}{h^2}\sqrt{2(y-a)}m_x(0, y).$$

Substituting the aforementioned analytical solution of m_x into the above expression, and performing tedious manipulations, K_1 is obtained as:

(a) for even order n

$$K_1 = \sum_{n=0,2,\ldots}^{N} \frac{6}{h^2} C_n\sqrt{a}\ \frac{n!}{2^n[(n/2)!]^2};$$

(b) for odd order n

$$K_1 = \sum_{n=1,3,\ldots}^{N} \frac{6}{h^2} C_n\sqrt{a}\ \frac{(n+1)!}{2^{n+1}[[(n/2)/2]!]^2};$$

The complete expression for K_1 is thus:

$$K_1 = \sum_{n=0,2,\ldots}^{N} \frac{6}{h^2} C_n\sqrt{a}\ \frac{n!}{2^n[(n/2)!]^2} + \sum_{n=1,3,\ldots} \frac{6}{h^2} C_n\sqrt{a}\ \frac{(n+1)!}{2^{n+1}[[(n/2)/2]!]^2};$$

Substituting (47) and (49) into Eqns. (30) (37) and (38) (45) respectively, the analytical solutions for $w, m_x, m_y, m_{xy}, q_x, q_y, v_x, v_y$ and K_1 due to moment loading with order n are obtained. They can be expressed in terms of the coefficients $C_n (n = 0, 1, 2, ...)$ in matrix form as:

$$\{Q\} = [T]\{C\}, \tag{50}$$

$$\{K\} = [S]\{C\}, \tag{51}$$

where the column vectors $\{Q\}$, $\{K\}$ and $\{C\}$ are defined as:

$$\{Q\} = [w, m_x, m_y, m_{xy}, q_x, q_y, v_x, v_y]^T$$
$$\{K\} = [K_{1,1}, K_{1n}]^T$$

and

$$\{C\} = [C_0, C_1, ..., C_N]^T.$$

$([T], [S])$ are the matrix of relation function between the analytical solution vectors $\{Q\}$ and $\{K\}$ for $w, m_x, m_y, m_{xy}, q_x, q_y, v_x, v_y$ and K_1 and the coefficient vector $\{C\}$. Both $[T]$ and $[s]$ are functions of crack length. In addition, $[T]$ is also a function of space. As a result, once the coefficient vector $\{C\}$ is determined, the vector $\{Q\}$ at any location of the infinite plate and the bending stress intensity factor $\{K\}$ can be calculated from (50) and (51).

4. Finite element alternating procedure

The finite element alternating procedure employed by Chen and Chang [19 21] for two dimensional problems is extended to solve the present cracked plate problems in bending. Accordingly, finite cracked plate problems can be superposed by finite domain problems without cracks and infinite domain problems with a crack subjected to suitable bending moments on crack surfaces. Furthermore, multiple crack problems can be superposed by single cracked problems successively in the similar manner. The fast decaying nature and self-equilibrating condition of the residual bending moments on the crack surfaces and resultant residual traction/displacement on the external boundary show the great advantage of the method in obtaining convergent solutions. For completeness, these procedures are described briefly as follows:

⟨1⟩ Input geometry and boundary conditions of the bounded cracked plate to be analyzed.

⟨2⟩ Evaluate the residual bending moment m_{xk}^f at the location of fictitious crack $k(k = 1, 2, ..., Nc)$ by a conventional finite element method (The crack need not lie along element boundaries.). Nc is the total number of cracks existing in the plate.

⟨3⟩ Since the crack surfaces are free of tractions, reverse the sign of the residual bending moment m_{xk}^f and fit it with a polynomial of appropriate order. The fitted residual bending moment m_{xk}^0 can be expressed as $m_{xk}^0 = \{L\}^T \{C\}_k^0$, where $\{C\}_k^0$ is the polynomial coefficient vector for crack k and $\{L\}$ is the vector composed of $(y/a_k)^n (n = 0, 1, 2, ..., N)$ in which a_k is the

half length of the kth crack. For better accuracy, $\{C\}_k^0$ can be determined by a least-squares method through the minimization of the integral,

$$\int_{a_k}^{a_k} (m_{xk}^f - m_{xk}^0)^2 \, ds \quad (k = 1, 2, \ldots, Nc),$$

thus

$$\{C\}_k^0 = [H]_k^{-1} \{R\}_k,$$

where

$$[H]_k = \int_{-a_k}^{a_k} \{L\}\{L\}^T \, ds$$

and

$$\{R\}_k = \int_{-a_k}^{a_k} \{L\} m_{xk}^f \, ds.$$

⟨4⟩ Since the symmetric bending type problems are solved, the interaction effect among cracks is induced from the bending moment m_x only. From $\{C\}_k^0$ in step (3) and (50), the reversed residual interaction coefficient vectors induced by crack k at fictitious crack $l(l = 1, 2, \ldots, Nc, l \neq k)$ $\{A\}_{lk}$ can be evaluated. If $l > k$, add $\{A\}_{lk}$ to $\{C\}_l^0$ and compute the updated $\{C\}_l^0$. Thus the coefficient vector $\{C\}_k^1$ of the residual bending moment for crack k needed to be released for the next computation is found to be $\{C\}_k^1 = \sum_{l=k+1}^{Nc} \{A\}_{kl}$. Repeat all measures as mentioned above until the cumulative residual bending moments on each crack are negligible. As a result, the resultant coefficient vector for crack $k\{C\}_k = \{C\}_k^0 + \{C\}_k^1 + \cdots$ for the current iteration is obtained.

⟨5⟩ Substituting the resultant coefficient vector for crack $k\{C\}_k$ into (50) and (51), the parameters $w, m_x, m_{xy}, q_x, q_y, r_x, r_y$ and K_1 can be computed and updated.

⟨6⟩ Once the variation of the bending stress intensity factor K_1 for all crack tips is smaller than a small value γ, say,

$$\frac{|K_1(\text{current iteration}) - K_1(\text{previous iteration})|}{K_1(\text{current iteration})} < \gamma,$$

the iteration is finished. Here, γ is taken as 0.005.

⟨7⟩ To satisfy loading conditions on the external boundary, the resultant residual equivalent nodal force $\{Q\}_x^*$ on the external boundary at the xth element is computed from (50) by the sum of the contribution of each crack $\{Q\}_{xk}$ as

$$\{Q\}_x^* = \sum_{k=1}^{Nc} \{Q\}_{xk}.$$

where

$$\{Q\}_{ak} = [G]_{ak}\{C\}_k$$

and

$$[G]_{ak} = \int_{s_a} [N]^T[U]_{ak}[T]_k \, ds.$$

$[G]_{ak}$ denotes the relation matrix and s_a is the boundary where loading conditions applied. $[N]$ represents the shape function, $[U]_{ak}$ is the transformation matrix and $[T]_k$ is the matrix of relation function for the kth crack as defined in (50). To satisfy the displacement boundary condition on the external boundary, the resultant residual nodal displacements $\{u\}_\beta^*$ in the external displacement boundary at node β are computed from (50) by the sum of the contribution of each crack $\{u\}_{\beta k}$ as:

$$\{u\}_\beta^* = \sum_{k=1}^{Nc} \{u\}_{\beta k}.$$

where

$$\{u\}_{\beta k} = [Z]_{\beta k}\{C\}_k$$

and

$$[Z]_{\beta k} = [M]_{\beta k}[T]_k,$$

$[M]_{\beta k}$ is the transformation matrix and $[T]_k$ is defined in (50).

⟨8⟩ Reverse the resultant residual equivalent nodal force $\{Q\}_\beta^*$ and resultant residual nodal displacement $\{u\}_\beta^*$ calculated in step (7) and consider those as new loading and displacement conditions acting on the external boundaries. Repeat all the iteration steps ⟨2⟩ to ⟨7⟩ until the variation of bending stress intensity factor K_1 on each crack tip is negligible.

5. Results and discussions

To verify the validity of the new proposed method, several plate bending problems with single or double cracks under different moment and displacement boundary conditions are solved. The effect of interaction between cracks and the influence of boundaries on the computation of bending stress intensity factors are also studied. As for finite element modeling, the simple four-node plate element (each node has four degrees of freedom $w, w_{,x}, w_{,y}$ and $w_{,xy}$) is employed in all analyses.

Example 1: A square center cracked thin plate subjected to uniform bending

As seen in Fig. 3 and Fig. 4, a square center cracked plate subjected to uniform bending moment along the boundary at $y = \pm H$ is first solved. The geometry and its finite element mesh with 9
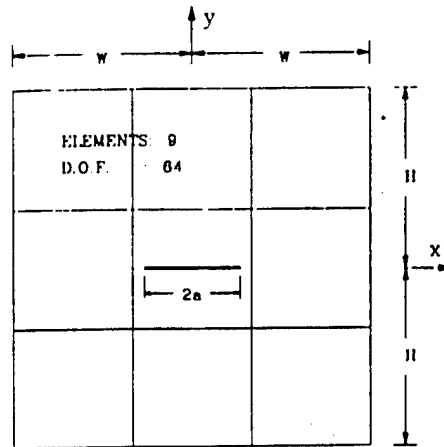
Fig. 3. Finite element mesh for a center-cracked plate.
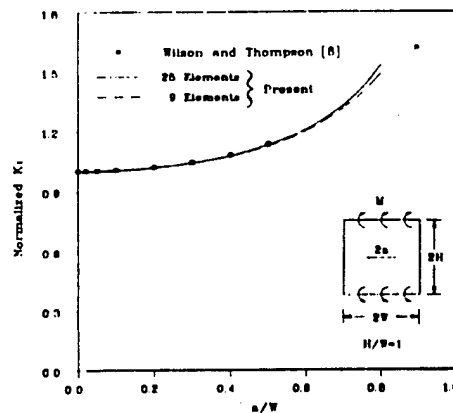

Fig. 4. Variation of normalized symmetric bending stress intensity factors for crack lengths (Example 1).

elements are also shown. The variation of symmetric bending stress intensity factors K_1 normalized by the value of $6M\sqrt{a}/h^2$ versus the crack length is displayed in Fig. 4. The results are compared with the solution obtained by Wilson and Thompson [8]. Good agreement is observed. To evaluate the accuracy of the finite element model developed, meshes with both 9 and 25 elements were tested and very little difference was found. Hence, without using any singular elements or special finite element models, a simple mesh with 9 elements is sufficiently accurate for this case even as the ratio of a/W reaches 0.8.

The rapid convergence of the bending stress intensity factor computed can be seen in Table 1. Usually, only two or three iterations are needed to obtain acceptable results. Table 2 presents the comparison of the polynomial order N taken for fitting the bending moment on crack surfaces. It is concluded that $N = 1$ or 2 is sufficient for these cases.

Example 2: A rectangular center-cracked thin plate subjected to uniform pressure with various boundary conditions

The geometry and finite element mesh are similar to those of Example 1, except that the aspect ratio of the plate H/W is taken as 1.2. Three different boundary conditions, i.e., all edges simply supported (SSSS), two edges simply supported and the other two edges clamped (SCSC), and all edges clamped (CCCC) are solved respectively. The variation of computed symmetric bending stress intensity factors versus crack lengths for the SSSS case is shown in Fig. 5. For comparison purposes, the analytical solution derived by Keer and Sve [26] and hybrid displacement finite element solution computed by Chen and Chen [13] are also shown.

Table 1. Convergence of normalized bending stress intensity factor K_1

iteration	a/W	0.3	0.5	0.8
1		1.0384	1.1108	1.3392
2		1.0398	1.1228	1.4436
3			1.1241	1.4757
4				1.4856
5				1.4886

Table 2. Comparison of order N of the polynomial fitted

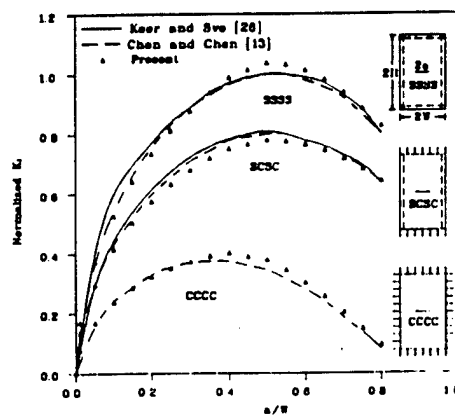| order N	a/W	0.3	0.5	0.8
1		1.0397	1.1224	1.4634
2		1.0398	1.1241	1.4886
3		1.0398	1.1241	1.4886
4		1.0398	1.1244	1.4913

Fig. 5. Variation of normalized symmetric bending stress intensity factors versus crack lengths under various boundary conditions (Example 2).

Example 3: A rectangular thin plate with two collinear cracks subjected to uniform bending

To examine the interaction effect among cracks and geometrical boundaries, the problem of a thin rectangular plate containing two collinear internal cracks subjected to uniform bending at $y = \pm H$ is shown in Fig. 6. The dimensions are: $H = 3W$, $W = 10h$ and $h = a$. Figure 7 displays the variation of symmetric bending stress intensity factors normalized by the value of $6M\sqrt{a}/h^2$ versus the ratio of c/a, where c is the half distance between two cracks. A finite element mesh with 9 elements was again adopted for this case. However, as cracks approach the boundaries (e.g. $c/a > 7$), the residual stress near the boundaries becomes more complex and more elements need to be included.
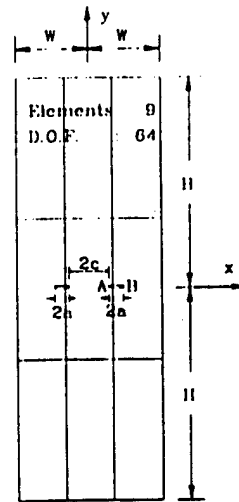

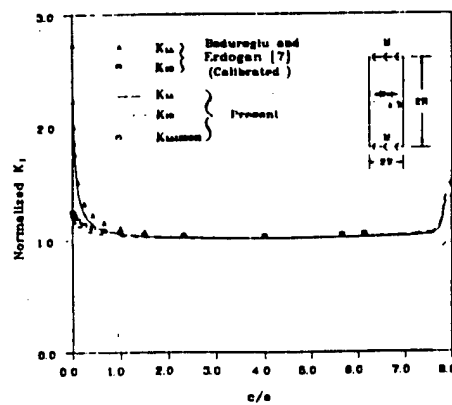Fig. 6. Finite element mesh for a plate with two collinear cracks.

Fig. 7. Variation of normalized symmetric bending stress intensity factors versus the ratio c/a (Example 3).

As is known, the stress distribution in the vicinity of the crack tip and the bending stress intensity factor depend on the plate thickness and the specific plate theory [3 5]. From the work of Hartranft and Sih [4], it is found that the present computed symmetric bending stress intensity factor K_1 based on the classical plate theory can be deduced from that derived by Reissners' theory after dividing by a factor $\phi(1)$, which is a function of v and h/a. The value of the factor $\phi(1)$ used here is 0.744578313 for $v = 0.3$ and $h/a = 1$ [4]. Thus, for comparison purposes, the results based on Reissner's theory obtained by Boduroglu and Erdogan [7] for a plate unbounded in y-direction are calibrated and shown in Fig. 7.

The interaction effect between cracks can be seen for the ratio $c/a < 1.0$. The bending stress intensity factor for crack tip $A(K_{1A})$ is larger than that for crack tip $B(K_{1B})$. As $1.0 < c/a < 7.5$, as would be expected, the plate with two collinear cracks behaves like nothing but an infinite plate containing one crack. That is, neither the interaction effect between cracks nor the boundary influence is noted. When the value c/a is greater than 7.5, both values of K_{1A} and K_{1B} increase rapidly (K_{1B} is slightly larger than K_{1A}) due to the influence of the boundary. As c/a reaches 8.0, the plate becomes equivalent to having two collinear edge cracks. The present finite element alternating method can also be modified to deal with such problem by extending a fictitious crack which is the same as the original crack to the outside of the plate. Again, as seen in Fig. 7, the calculated result by this modified procedure is also in good agreement with the calibrated data by Boduroglu and Erdogan [7].

6. Conclusions

Based on the analytical solutions derived for a thin cracked plate subjected to symmetric arbitrary bending on crack surfaces, an efficient and accurate finite element alternating procedure has been successfully developed to deal with plate bending problems with single or multiple cracks. Using only a simple conventional finite element mesh, excellent solutions for symmetric bending stress intensity factors can be computed. The interaction effect among cracks and the influence of the geometric boundaries on the calculation of the bending stress intensity factor can be evaluated accurately.

By the technique developed, the computation can also be performed to analyze the cases with more cracks (e.g. more than two cracks) without any difficulty. This work can be further extended to deal with thick or moderate thick cracked plate under arbitrary bending type loadings. This will be presented in a subsequent report.

References

1. M.L. Williams, *ASME Journal of Applied Mechanics* 28 (1961) 78 82.
2. G.C. Sih, P.C. Paris and F. Erdogan, *ASME Journal of Applied Mechanics* 29 (1962) 306 312.
3. J.K. Knowles, and N.M. Wang, *Journal of Mathematics and Physics* 39 (1960) 223 236.
4. R.J. Hartranft and G.C. Sih, *Journal of Mathematics and Physics* 47 (1968) 279 291.
5. N.M. Wang, *Journal of Mathematics and Physics* 47 (1968) 371 390.
6. M.V.V. Murthy, K.N. Raju and S. Viswanath, *International Journal of Fracture* 17 (1981) 537 552.
7. H. Boduroglu and F. Erdogan, *ASME Journal of Applied Mechanics* 50 (1983) 621 629.
8. W.K. Wilson and D.G. Thompson, *Engineering Fracture Mechanics* 3 (1971) 97 102.
9. R.S. Barsoum, *International Journal for Numerical Methods in Engineering* 10 (1976) 551 564.
10. G. Yagawa and T. Nishioka, *International Journal for Numerical Methods in Engineering* 14 (1979) 727 740.

TA409 E5